Planning and Operation of Active Smart Grids

by

Mohammad Ghasemi Damavandi

B.Sc., University of Tehran, 2008
M.Sc., University of Tehran, 2011

A THESIS SUBMITTED IN PARTIAL FULFILLMENT OF
THE REQUIREMENTS FOR THE DEGREE OF

DOCTOR OF PHILOSOPHY

in

The Faculty of Graduate and Postdoctoral Studies

(Electrical and Computer Engineering)

THE UNIVERSITY OF BRITISH COLUMBIA

(Vancouver)

January 2017

Abstract

Future smart grids will be operated actively in the presence of distributed generators and topological reconfigurations. Distributed Storage Systems (DSS) will also become a viable solution for balancing the load and the intermittent generation of renewable energy sources. The DSS can also provide the smart grid operator with various other benefits including peak load shaving, resilience enhancement, power loss reduction, and arbitrage gain.

The active nature of future smart grids calls for an accurate state estimation mechanism to serve as a building block for many operational tasks. To that end, the first part of the present thesis leverages the concept of submodularity to solve the problem of robust meter placement for state estimation in reconfigurable smart grids. Next, the thesis proposes a methodology for optimal planning of DSS in smart grids with high penetration of renewable sources. The presented methodology accounts for various advantages of energy storage in smart grids and seeks the optimal trade-off between the investment cost and the expected discounted reward of DSS installation. Finally, the thesis focuses on the problem of Volt-VAR Optimization (VVO) in active smart grids. The optimal joint operation of reconfiguration switches, energy storage units, under load tap changers, and shunt capacitors is investigated in the presented VVO methodology. The proposed methodologies in this thesis have been tested on sample distribution systems and their effectiveness is validated using real data of smart meters and renewable energy sources.

Preface

The work presented in this thesis is based on the research conducted by the author with assistance and guidance of Prof. Vikram Krishnamurthy and Prof. José R Martí. The problem formulations, algorithmic solutions, numerical simulations, and writeup of all chapters and papers is done by the author. For all these works, Prof. Krishnamurthy and Prof. Martí guided the author with their useful suggestions, technical discussions, supervisory comments, and editorial feedbacks.

The following articles are derived from the research conducted in the present thesis.

- M. Ghasemi Damavandi, V. Krishnamurthy, and J. R. Martí, *Robust meter placement for state estimation in active distribution systems, IEEE Trans. Smart Grid, vol. 6, no. 4, pp. 1972-1982, Jul. 2015.* [Related to chapter 2 of the thesis]

- M. Ghasemi Damavandi, J. R. Martí, V. Krishnamurthy, *A methodology for optimal distributed storage planning in smart distribution grids, submitted.* [Related to chapter 3 of the thesis]

- M. Ghasemi Damavandi, V. Krishnamurthy, and J. R. Martí, *A comprehensive methodology for volt-VAR optimization in active smart grids, submitted.* [Related to chapter 4 of the thesis]

Table of Contents

List of Tables

List of Figures

List of Abbreviations

AAE Average Angle Error.

ACPF AC Power Flow.

AME Average Magnitude Error.

AMI Advanced Metering Infrastructure.

CAIDI Customer Average Interruption Duration Index.

CRLB Cramér-Rao Lower Bound.

DG Distributed Generators.

DOD Depth of Discharge.

DSS Distributed Storage Systems.

FIM Fisher Information Matrix.

GA Genetic Algorithm.

LLN Law of Large Numbers.

MAE Maximum Angle Error.

MC Markov Chain.

MLE Maximum Likelihood Estimate.

MME Maximum Magnitude Error.

MV Medium Voltage.

NLE Normalized Loss Error.

PMU Phasor Measurement Units.

SAIFI System Average Interruption Frequency Index.

SGO Smart Grid Operator.

SLEM Second Largest Eigenvalue Modulus.

ToU Time of Use.

TVE Total Vector Error.

ULTC Under Load Tap Changers.

VMM Voltage Magnitude Meters.

VVO Volt-VAR Optimization.

WLS Weighted Least Squares.

Acknowledgments

First and foremost, my sincerest gratitudes go to my advisor, Prof. Vikram Krishnamurthy, for his great academic guidance and invaluable intellectual support during this research. His deep knowledge and remarkable insights profoundly improved the quality of this thesis. I also want to thank Prof. Krishnamurthy specifically for the enormous encouragement and enthusiasm that he brought to this research. His amazing concentration and incredible dedication to his job has definitely become an unforgettable lesson for my life.

Also, I would like to express my deep gratitude to my co-advisor, Prof. José R Martí for his huge support during preparation of this thesis. Prof. Martí spent an enormous amount of time on discussions about this research and provided strategic insights, novel ideas, and invaluable feedbacks about the power engineering side of this thesis. Nonetheless, engineering is not the only area in which I learned a lot from Prof. Martí. He symbolizes a true man of science who teaches his students how to think critically about all aspects of life.

I feel deeply honored for having had the opportunity of working with Prof. Krishnamurthy and Prof. Martí without whom this research could have never been done.

Dedication

To my parents.

Chapter 1

Introduction

1.1 Active Smart Grids: An Overview

The next generation power grids are envisioned to operate in an active manner. They can benefit from high penetration of renewable energy sources distributed throughout the grid. Parts of the future distribution systems are even envisioned to work as microgrids where during the islanded mode the demand power should be completely supplied by local Distributed Generators (DG) [1]. These DGs are often highly intermittent and can cause dramatic changes in the demand/generation of the nodes. They can also cause bidirectional flow of power in the feeder and even from distribution level to the sub-transmission system [2].

In addition, the topological configuration of active smart grids can be dynamically optimized using remotely controllable tie line switches. In fact, use of remotely controllable switches enables the SGO to reconfigure the distribution system even in daily or hourly intervals [3–7]. In practice, feeder reconfiguration can be done for a variety of goals including load balancing [8], reliability improvement [9], service restoration [10], voltage profile improvement and power loss minimization [11], [12]. In systems with high penetration of non-dispatchable sources, the reconfiguration routine can also be employed to mitigate the effect of intermittent renewable generation. Traditionally, the topological configurations of the distribution grid have been radial to reduce the short circuit current under fault conditions and to facili-

tate protection of the system [13]. However, in the future systems the topological configurations may no longer be limited to radial and can possibly include weakly meshed ones [14, 15].

The active nature of future smart grids calls for an online monitoring of the system for state estimation and situational awareness. State estimation in present distribution systems mostly relies on substation measurements and pseudo-measurements (historical data). However, in future grids new data from Voltage Magnitude Meters (VMM), smart meters and Phasor Measurement Units (PMU) can be incorporated in the state estimation process [16–18]. The data reported by these meters will also increase the visibility of the secondary network for monitoring power losses and electricity thefts. Note that the reporting rate of the smart meters is expected to be every 15 to 60 minutes in the future smart grid. The residential meters of some utilities currently transmit their measurements even a few times a day due to concerns about privacy and exposure to frequency radiation. Hence, the smart metering data may not be adequate for a real-time, highly accurate monitoring of the future distribution systems. Therefore, VMMs and PMUs can play an important role for state estimation as they provide highly accurate synchronized information about different parts of the system [19]. The PMUs can be specifically useful in monitoring the distribution system for islanding/reconnection [2], bidirectional flow of power [20], and power quality [21, 22]. Moreover, they provide capabilities for fault detection in radial and weakly meshed distribution systems [23]. Furthermore, synchronized measurements are a major candidate for parallel monitoring of the energy distribution and communication sub-systems of the smart grid [24]. It is expected that for some critical applications in the future distribution grids, a time synchronization of $1\mu s$ between multiple devices (possibly in different sub-systems) will be needed [24]. In a 60-Hz distribution system, this amount of time synchronization requires

a maximum phase error less than 3.77×10^{-4} rad [20].

As much as the active smart grids can benefit from the renewable energy sources, the intermittent nature of those sources requires careful operation and control. For example, when the amount of non-dispatchable renewable energy generation is forecast to violate a system constraint, the Smart Grid Operator (SGO) may have to curtail the excess power. In addition, when the amount of total non-dispatchable generation is higher than the total demand, the excess power has to flow to the transmission system. If the amount of excess power is less than the allowable reverse power limit of the substations, this will not cause any problem. However, if the amount of excess power is greater than the allowable reverse power limit, the SGO or the private DG owner will have to curtail some non-dispatchable sources. In contrast, if the system is equipped with Distributed Storage Systems (DSS), the SGO will have the option to store the excess generation in storage units [25]. Similarly, when one part of the smart grid is to work as a microgrid in an islanded mode, the mismatch between the load and power generation of local DGs can be smoothed out using DSS [26]. An islanded mode occurs when the microgrid is disconnected from the Medium Voltage (MV) grid due to faults or planned switching actions [27, 28]. On the other hand, when the microgrid is connected back to the MV grid, the SGO can exploit the installed DSS to improve some metric of the system performance such as voltage profile or power loss.

Fig. 1.1 illustrates the schematic of an active smart grid with a distributed storage unit. In this figure, the smart meters, distributed solar cells, distributed wind turbines, and DSS are symbolically shown on a radial distribution system. The smart grid shown in Fig. 1.1, is also topologically reconfigurable as represented by a schematic dotted branch.

In virtue of DSS, the SGO will also be able to buy the excess energy from DG

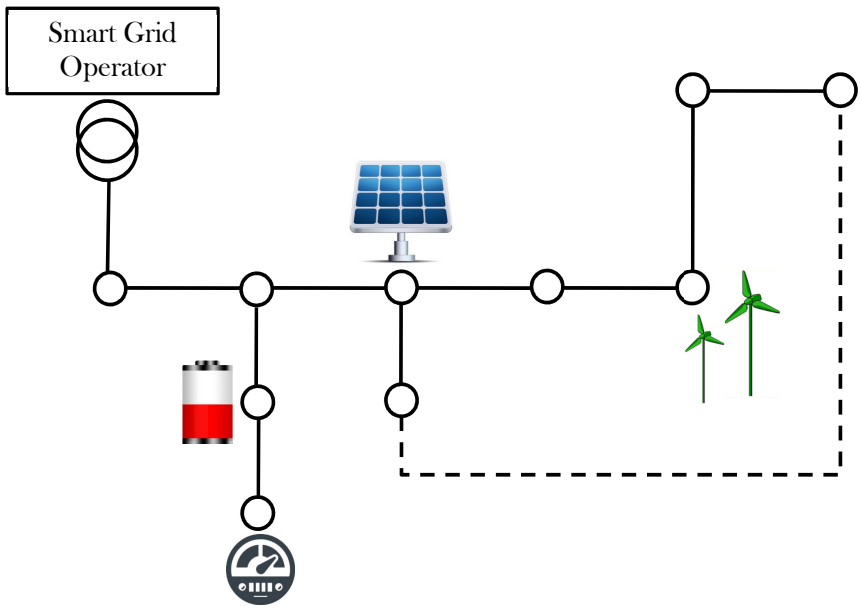

Figure 1.1: Schematic of an active smart grid with smart meters, DGs, and DSS.

owners and sell it back to the network when the demand is higher. In markets with dynamic energy pricing where the price of energy is proportional to the total demand, that naturally translates into an arbitrage gain for the SGO. Likewise, the DG owner will be able to gain some profit by selling to the SGO the excess energy that would be spilled otherwise [25]. If the system undergoes a fault, the SGO will also have the degree of freedom to take advantage of these DSS during system restoration [29] to minimize the energy-not-supplied. More importantly, use of DSS can shave the peak load which constantly increases in distribution systems [30]. Shaving the peak load of the system can in turn defer the inevitable upgrade of the feeders and substations which, depending on the size of the system, can result in substantial financial gains [31, 32]. Other applications of DSS in distribution systems include voltage control [33, 34], ancillary services, feeder load management and congestion control, and power smoothing for solar arrays [35, 36].

Storage units can also be deployed at the very low-voltage end of the power

system. Recently, some authors have considered the use of DSS at the household level [37]. Also, Tesla Motors recently introduced a 10 kWh home battery, called Powerwall, for smart homes. The concept of community energy storage also deploys 120/240-Volt storage units to protect the same group of houses that share a common secondary transformer [38].

In addition to possible generation-demand mismatches in smart grids with high penetration of renewable energy sources, the nodes of the system can also be subject to sever voltage fluctuations. For example, when the instantaneous generation of the renewable sources is high but the load is low the nodes of the system may undergo over-voltage problems [39]. Another potential problem is the violation of feeder ampacities at times when the renewable generation is considerably high. Due to the high variability of non-dispatchable sources, the Volt-VAR Optimization (VVO) problem will be a very important issue in active smart grids. The VVO problem, in the classical sense, is the optimal operation of the capacitor banks and Under Load Tap Changers (ULTC). The objective of the VVO techniques has conventionally been to optimize some metric of the system performance such as active power loss or voltage profile. In practice, the stochasticity of renewable energy sources requires the VVO problem to optimize the *expected* performance of the system. Furthermore, in modern smart grids, the VVO technique should take advantage of the DSS and remotely controllable switches as additional degrees of freedom on top of classical VVO equipment. The incorporation of DSS and reconfiguration routine into the VVO procedure can improve various performance metrics of the system including the voltage profile and power losses.

1.2 Research Goals

This research is dedicated to the optimal planning and operation of active smart grids with high penetration of renewable energy sources. Various aspects of active smart grids including monitoring and state estimation, feeder reconfiguration, DSS planning and operation, wind and solar power stochasticity, and VVO have been studied. The main goal of the research has been to come up with mathematical formulations and algorithmic solutions that can be implemented efficiently for smart distribution systems. In particular, three major problems have been considered in this thesis which include the following:

- Robust meter placement in reconfigurable distribution systems
- Optimal DSS planning in smart distribution grids
- VVO in active smart grids considering feeder reconfiguration and DSS operation

For each problem mentioned above, a mathematical formulation is presented in such a way that the resulting optimization problem can be solved in an efficient way. The effectiveness of the proposed methodologies has been studied and validated on different test systems using real data from smart meters and renewable energy sources.

1.3 Related Works

This section provides a review of the existing literature related to the three major problems studied in this thesis.

1.3.1 Robust Meter Placement

As the first part of this thesis, the problem of meter placement for state estimation in reconfigurable distribution systems is considered. In what follows, a summary of the existing works related to the optimal meter placement problem in distribution systems is provided.

The meter placement problem for single configuration distribution systems has been considered in [17, 18, 40]. In [41] and [42], the joint placement of PMUs and smart metering peripherals for reconfigurable distribution systems has been presented. Several authors have also considered the installation of PMUs in the distribution system [43]. For example, a multiphase state estimator is proposed in [44] which relies on the synchronized voltage and current measurements of the feeder. Also in [20] and [45], a linear distribution system state estimator is presented which incorporates synchronized phasor measurements along with the smart metering data. A branch-current-based distribution system state estimator is also presented in [46] which takes advantage of PMU measurements and handles radial and weakly meshed networks. In [47], the performance of various state estimators for distribution system has been compared where data from optimally located PMUs is incorporated as real measurements. The application of synchronized meters for distribution system monitoring is also suggested in [48] as the data from smart meters will not be sufficient for full observability of the system. Use of one or few PMUs in the distribution system is also an enabler of the multilevel state estimation paradigm proposed in [49]. In this paradigm, the state estimation of the system is done at different levels (feeder level, substation level, transmission level, and regional level) and the results are integrated together in a synchronized fashion to provide a very large scale monitoring of the power system.

1.3.2 Distributed Storage Planning

As part of this research, the problem of DSS placement in distribution systems with high penetration of wind and solar energy sources is considered. This section provides a review of the existing literature on the optimal DSS planning problem.

The optimal DSS planning has been considered in several recent works [39, 50–56]. In [25], a framework is presented which optimizes the capacity and power rating of DSS to ensure that the renewable energy generated by DGs never spill. Nonetheless, this work does not consider various other advantages that the DDS introduce to the system. In [57], the potential of DSS in the low-voltage distribution grid for deferring upgrades needed to increase the solar penetration level is investigated. In [58], the optimal allocation of DSS in distribution systems using a multi-objective optimization approach is considered. However, [57, 58] do not consider the role of DSS in improving the resilience of the system. In [59], a methodology for DSS allocation in distribution systems is proposed which which aims at cost-effective improvement of the system reliability. In, [60], the optimal planning of DSS using the point estimate method is considered. In [61], the problem of DSS allocation is solved using Bender's decomposition and a scenario tree for wind power simulation. In [31, 32, 62], the optimal placement of DSS considering the benefits due to system upgrade deferral is investigated. Nevertheless, none of the aforementioned papers includes a complete and comprehensive consideration of the technical and financial aspects of distributed storage planning using mixed-integer convex formulation.

1.3.3 Volt-VAR Optimization in Active Smart Grids

The third part of this research is focused on the VVO problem in active smart grids. Below, we review the recent literature on the VVO problem in distribution systems.

Several works in the literature have considered the VVO problem for distribution

systems [63–67]. In [68], a VVO technique using oriented discrete coordinate descent method for minimization of power loss or the number of control actions is proposed. In [69], a VVO methodology is presented which minimizes the total reactive power supplied by the DGs. In [70], a scenario-based multiobjective method for daily VVO is presented which considers renewable energy sources. However, [68–70] do not consider feeder reconfiguration as a tool for VVO. Voltage control and VAR optimization methodologies are also presented in [71] and [72] that consider feeder reconfiguration in addition to classical VVO devices. However, these papers do not consider the DSS and the stochasticity of wind power generation in their VVO methodologies. In [73], the integration of energy storage systems into the voltage control mechanisms of distribution systems is proposed. Nonetheless, none of the aforementioned works provides a mixed-integer convex program formulation of the VVO problem that takes care of the operation of all the available equipment and treats the stochasticity of wind power generation in a statistically rigorous way.

1.4 Contributions

The main theme of the thesis is to propose comprehensive mathematical formulations and algorithmic solutions for some important planning and operational problems in active smart grids. The concepts of submodularity and convexity have been employed in mathematical formulations such that the resulting problems can be solved efficiently. The mathematical formulations presented in this thesis are comprehensive in that various relevant aspects of the problem have been taken into account. The stochasticity of the renewable power generation and loads has also been addressed in a statistically rigorous way.

In what follows, the three major contributions of the thesis are briefly introduced.

1.4.1 Robust Meter Placement

The first part of the present thesis is focused on the formulation and solving the optimal meter placement problem in reconfigurable distribution systems. In the following, we summarize our contributions in this part of the thesis.

In this thesis, the near-optimal placement of a limited number of VMMs and PMUs for state estimation in reconfigurable distribution systems is considered. The trace (sum of diagonal entires) of the inverse of the Fisher Information Matrix (FIM) is proposed as the estimation accuracy criterion. Under some conditions, the reduction in the trace of the inverse of the FIM is a submodular function [74] which lends itself for a greedy algorithm for a near-optimal meter placement in a single configuration distribution system. For a given number of meters, the greedy algorithm also provides a $(1-1/e)$ approximation guarantee for the meter placement problem [74, 75] in single configuration distribution systems. The meter placement problem in reconfigurable distribution systems, however, should take into account the topological reconfigurations of the system [41, 42]. Therefore, the problem should be formulated in a robust way so as to optimize the worst case estimation accuracy among all the possible configurations of the system. To that end, a robust submodular optimization algorithm, called submodular saturation algorithm [76], is proposed in this thesis which outperforms the greedy algorithm and the Genetic Algorithm (GA) in most cases and provides competitive results in other cases.

1.4.2 Distributed Storage Planning

The second contribution of the present thesis is a comprehensive formulation of the optimal DSS placement problem in smart grids. This section provides a summary of the contributions on the optimal DSS planning problem.

This thesis presents a comprehensive methodology for optimal DSS planning in

smart distribution systems. The optimal DSS placement problem is formulated as a mixed-integer quadratic program to be solved using branch-and-bound methods. Various financial gains due to price arbitrage, reduction in the system losses, reduction in the renewable energy curtailed, system resilience enhancement, and system upgrade deferral have been considered in the presented methodology. The stochasticity of the loads and renewable energy sources are accounted for by evaluating the expected discounted gains using the Law of Large Numbers (LLN). Simulation results on a radial distribution test system and with real data from smart meters and renewable energy sources are presented and discussed. The present thesis is the first work that provides a mixed-integer convex formulation that comprehensively accounts for all the technical and financial aspects of distributed storage planning as well as the stochasticity of load and renewable energy sources.

1.4.3 Volt-VAR Optimization in Active Smart Grids

The third contribution of this research is a comprehensive formulation of the VVO problem for smart distribution grids. In what follows, we review our contributions in this part of the thesis.

This thesis provides a comprehensive formulation of the VVO problem in active smart grids. The formulation provided in the thesis is comprehensive in that it jointly considers wind turbines, DSS, capacitor banks, ULTCs, and feeder reconfiguration. The VVO problem presented is formulated as a mixed-integer, quadratic program which can be solved efficiently using commercial softwares. The formulation provided for the VVO problem tries to minimize the expected power loss of the system. In order to address the stochasticity of the wind power generation in evaluating the expected power loss of the system, a first-order Markov Chain (MC) model [77] is employed. Simulation results on a 33-node, 12.66 kV active smart grid

using real data from wind turbines and smart meters are also presented and discussed. Various test cases are considered in the simulations to compare the impact of different VVO equipment on the system loss and voltage profile.

1.5 Thesis Structure

In this section, the structure of this thesis is presented.

Chapter 2 is devoted to the problem of robust meter placement in single-configuration and reconfigurable smart grids. This chapter takes the reduction in the trace of the inverse of the FIM as the metric of the state estimation accuracy and provides a formulation of the meter placement based on the concept of submodularity and diminishing returns. Numerical results of robust meter placement on three different active distribution systems are presented and discussed in this chapter.

Chapter 3 is the dedicated to the problem of optimal DSS planning in smart distribution grids. This chapter formulates various economic gains of the DSS as a function of the amount and location of storage units in the system. Based on the real data from smart meters and renewable energy sources, the methodology presented in this chapter evaluates and optimizes the total expected discounted gain due to installation of DSS. In order to come up with a mixed-integer convex programming[1] formulation of the optimal DSS planning problem, the chapter utilizes the linearized power flow equations in rectangular coordinates [78–80]. Numerical results for optimal DSS placement and sizing on a test system are also provided in this chapter.

Chapter 4 is devoted to a comprehensive formulation of the VVO problem in active smart grids. This chapter considers various VVO equipment and provides

[1]With slight abuse of terminology, the term mixed-integer convex programming is used in this thesis to refer to the problems that are non-convex merely due to the integrality of some variables. Therefore, these problems become convex if the integrality constraint is relaxed.

a mixed-integer convex formulation of the problem to be solved using branch-and-bound methods. To that end, the chapter uses the linearized DistFlow equations for radial distribution systems [8, 81] and extends them to accommodate the DGs and bi-directional flow of power. Also, an MC model is utilized in this chapter to model the stochasticity of the wind power generation. The chapter also presents simulation results for VVO on an active smart grid and compares them for various test cases.

Finally, chapter 5 concludes the thesis and provides some insights about the possible future lines of research.

It should be pointed out that the formulations provided throughout the thesis assume that the systems are balanced. However, in practice, the distribution systems are often unbalanced. For an unbalanced distribution system, the formulations presented in this thesis should be modified to include a full 3-phase power flow solution. Nonetheless, the rest of the formulations remain the same.

Chapter 2

Robust Meter Placement in Reconfigurable Smart Grids

The active nature of future smart grids requires an online state estimation procedure for system monitoring and situational awareness. The state estimation procedure can be viewed as a building block of virtually all operational tasks in distribution systems. That is because optimization of the system against any objective function would require up-to-date knowledge about the current state of the system. State estimation in current distribution systems mostly relies on substation measurements and historical data. In future smart grids, however, the measurements from VMMs, PMUs, and smart meters will also be used for state estimation. Although the reporting rate of the smart metering data may be around 15 to 60 minutes in the future smart grids, the current reporting rate is often much less (e.g. twice a day). This is because of concerns about customer privacy, exposure to frequency radiation, and communications bandwidth. This concept is schematically illustrated in Fig. 2.1. As a result, the smart metering data is currently insufficient for an accurate monitoring of the smart grid. Therefore, it would make sense to install a limited number of VMMs and/or PMUs in the distribution system to increase the grid visibility. As such, optimal meter placement in the system plays an important role in finding the best trade-off between the upgrade costs and the state estimation accuracy. This chapter presents a methodology for robust meter placement in reconfigurable smart

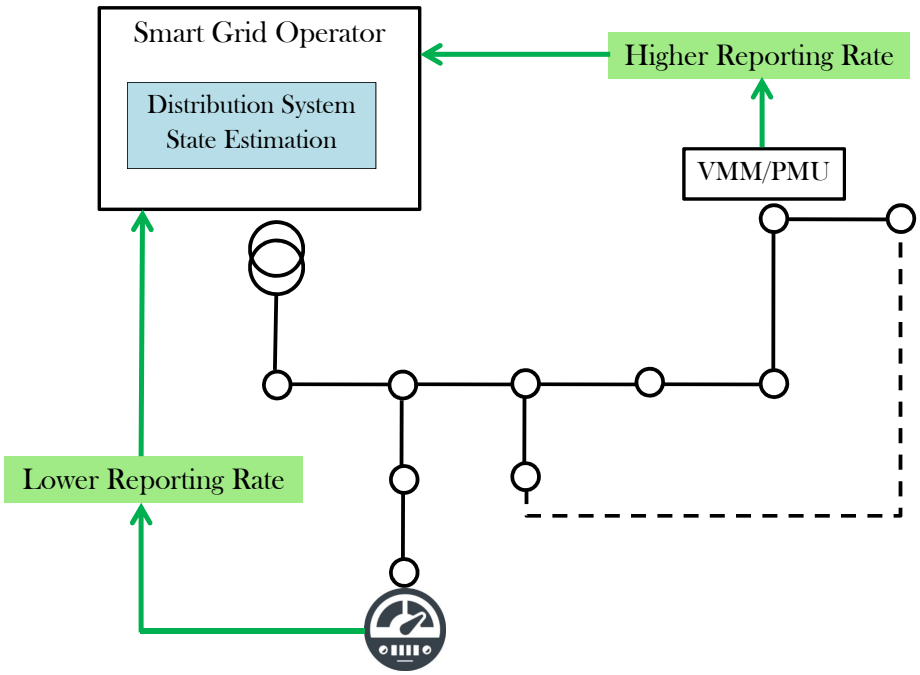

Figure 2.1: Schematic of a reconfigurable distribution system with smart meters, VMMs, and PMUs.

grids [82].

It should be pointed out that in distribution systems, the voltage angles with respect to the slack node are typically small. However, the possibility of installation of PMUs in distribution systems is included in this chapter for completeness. Even though the differences in the bus angles in distribution systems is small, a new generation of PMUs is under development that can measure these differences. Therefore, it is worthwhile to explore how much more accuracy in the state estimation is achievable if PMUs were to be placed in the system.

This chapter is organized as follows. Sec. 2.1 describes the state estimation of the distribution systems using non-linear measurements. An expression for the corresponding FIM is also provided in this section. Sec. 2.2 reviews the linearized power flow equations and the corresponding formulations for the meter placement

problem. Sec. 2.3 reviews the greedy algorithm for meter placement in a single configuration distribution system. Sec. 2.4 considers the problem of meter placement in reconfigurable distribution systems. The submodular saturation algorithm is presented in this section. Sec. 2.5 presents the numerical results and discussions. Finally, Sec. 2.6 concludes this chapter.

2.1 State Estimation Using Non-Linear Measurements and the FIM

This section describes the state estimation of distribution systems using nonlinear measurements including substation measurements and smart metering data. An expression for the corresponding FIM is also provided.

Consider a distribution system with N nodes, each having a voltage phasor $v_n = |v_n|e^{j\theta_n}, n = 1, 2, \ldots, N$. Let $\mathbf{v} = [|v_1|, |v_2|, \ldots, |v_N|, \theta_1, \theta_2, \ldots, \theta_N]'$ be the state of the system comprising the magnitudes and phases of all the voltages in the system. Here, $[\cdot]'$ denotes transposition. The conventional substation measurements and the measurements provided by smart meters are related to $\mathbf{v}$ through a nonlinear model as follows

$$\mathbf{z}_i = \mathbf{h}_i(\mathbf{v}) + \boldsymbol{\eta}_i, \quad i = 1, 2, \ldots, M \tag{2.1}$$

where $\boldsymbol{\eta}_i \sim \mathcal{N}(\mathbf{0}, \mathbf{R}_i)$ is the Gaussian noise in the ith measurement and M is the total number of non-linear measurements. The Maximum Likelihood Estimate (MLE) of the voltages, denoted by $\hat{\mathbf{v}}$, can be found through the famous Weighted Least Squares (WLS) method as follows

$$\hat{\mathbf{v}} = \arg\min_{\mathbf{v}} \sum_{i=1}^{M} [\mathbf{z}_i - \mathbf{h}_i(\mathbf{v})]' \mathbf{R}_i^{-1} [\mathbf{z}_i - \mathbf{h}_i(\mathbf{v})]. \tag{2.2}$$

For state estimation of the system one has to solve (2.2) using an iterative Newton-based algorithm.

Let $\mathbf{Z}$ be the vector of all available data from substation measurements and smart meters. The FIM matrix for the model in (2.1) is defined as

$$\mathbf{J}(\mathbf{v}) = \mathbb{E}_{\mathbf{p}(\mathbf{Z}|\mathbf{v})}\{[\nabla_{\mathbf{v}} \ln \mathbf{p}(\mathbf{Z}|\mathbf{v})]'[\nabla_{\mathbf{v}} \ln \mathbf{p}(\mathbf{Z}|\mathbf{v})]\}, \tag{2.3}$$

where $\mathbf{p}(\mathbf{Z}|\mathbf{v})$ is the conditional probability density function of $\mathbf{Z}$ given $\mathbf{v}$. Note that in the literature of the power system state estimation, the FIM evaluated at $\mathbf{v} = \hat{\mathbf{v}}$ is usually referred to as the *gain matrix*. One can expand the FIM as follows (see [83] for this derivation)

$$\mathbf{J}(\mathbf{v}) = \sum_{i=1}^{M} [\nabla_{\mathbf{v}} \mathbf{h}_i(\mathbf{v})]' \mathbf{R}_i^{-1} [\nabla_{\mathbf{v}} \mathbf{h}_i(\mathbf{v})]. \tag{2.4}$$

Eq. (2.4) shows that the FIM is the sum of M symmetric positive semi-definite matrices. We further assume that the system is fully observable such that $\mathbf{J}$ is indeed a positive definite, and hence, invertible matrix.

The Cramér-Rao Lower Bound (CRLB) establishes a bound on the conditional covariance matrix of the estimates based on the FIM. More precisely, $\mathbf{C}(\hat{\mathbf{v}}|\mathbf{v}) - \mathbf{J}^{-1}$ is guaranteed to be a positive semi-definite matrix. As a result, the diagonal entries of $\mathbf{J}^{-1}$ establish a lower bound on the conditional estimation variances. To verify this, let $\mathbf{u}_r$ be a unit vector whose elements are zero except for the rth element which is equal to one. It follows directly from CRLB that

$$\mathbf{u}_r'[\mathbf{C}(\hat{\mathbf{v}}|\mathbf{v})]\mathbf{u}_r \geq \mathbf{u}_r'[\mathbf{J}(\mathbf{v})]^{-1}\mathbf{u}_r. \tag{2.5}$$

Because (2.5) holds for all r, the total conditional estimation variance is lower

bounded by trace of the inverse of the FIM. Therefore, one can design the meter places for minimization of the trace of $\mathbf{J}^{-1}$. However, the FIM depends on the actual state of the system, especially when the variance of the measurement noises are proportional to the actual measured values. Therefore, a robust meter placement method should consider the worst case estimation variance among all possible states of the system. If the variances of the measurement noises are proportional to the measured values, it will be shown in the following that the worst estimation variance approximately corresponds to the peak loads. Hence, we design the meter places for peak loads.

2.2 Meter Placement Using Linearized Power Flow Equations

Although the FIM of the nonlinear model (2.1) depends on the actual state of the system, the dependency of the functions

$$H_i(\mathbf{v}) = \nabla_{\mathbf{v}} \mathbf{h}_i(\mathbf{v}), \tag{2.6}$$

on $\mathbf{v}$ is very minimal, as mentioned in [84]. That is, the change in $H_i(\mathbf{v})$ is very small as we start from the initial flat voltage point and iterate through the Newton's method. One way of interpreting this phenomenon is by considering the linearized power flow equations in rectangular coordinates.

2.2.1 Linearized Power Flow Equations In Rectangular Coordinates

Let the voltage of the nth node be represented in rectangular coordinates as $v_n = 1 + \tilde{v}_n = 1 + \mathrm{e}_n + j\mathrm{f}_n$. Without loss of generality, assume the first node is the slack

node with a given voltage of 1 p.u.. Let $\tilde{\mathbf{v}} = [\tilde{v}_2, \tilde{v}_3, \ldots, \tilde{v}_N]'$ denote the vector of deviations from the flat voltage profile at the remaining nodes of the system. Also, let $\mathbf{e} = [\mathrm{e}_2, \mathrm{e}_3, \ldots, \mathrm{e}_N]'$ and $\mathbf{f} = [\mathrm{f}_2, \mathrm{f}_3, \ldots, \mathrm{f}_N]'$ represent the real and imaginary parts of $\tilde{\mathbf{v}}$. These vectors can be approximated by linearized power flow equations in rectangular coordinates provided that their elements are small [79]. For real distribution systems it is a known fact that the elements of $\mathbf{f}$ are very small (i.e., the voltage angles with respect to the slack node are very small.) The operational constraints of distribution systems also require that the elements of $\mathbf{e}$ remain small (e.g., within ± 0.06 p.u.) at peak hours. At off-peak hours, the elements of $\mathbf{e}$ and $\mathbf{f}$ are even smaller which make the linearized power flow equations more accurate.

Let $\mathbf{Y}_{N\times N} = \mathbf{G} + j\mathbf{B}$ be the bus admittance matrix of the system where $\mathbf{G}$ and $\mathbf{B}$ are the bus conductance and bus susceptance matrices, respectively. Since $\mathbf{G}$ is a symmetric matrix, by separating its first row and column, we can partition it as follows:

$$\mathbf{G} = \begin{bmatrix} \mathrm{g}_{11} & \mathbf{g}_1' \\ \mathbf{g}_1 & \tilde{\mathbf{G}} \end{bmatrix} \tag{2.7}$$

where $\tilde{\mathbf{G}}_{(N-1)\times(N-1)}$ is a submatrix of the bus conductance matrix corresponding to the non-slack nodes and $(\cdot)'$ denotes transposition. The same partitioning can also be applied to the matrices $\mathbf{Y}$ and $\mathbf{B}$ to obtain the symmetric submatrices $\tilde{\mathbf{Y}}$ and $\tilde{\mathbf{B}}$, respectively. Using these matrices and assuming that no shunt capacitor is installed in the system, the linearized power flow in rectangular coordinates can be written as [79]:

$$\begin{bmatrix} \mathbf{p} \\ \mathbf{q} \end{bmatrix} - \begin{bmatrix} \mathbf{p}_{\mathrm{DG}} \\ \mathbf{q}_{\mathrm{DG}} \end{bmatrix} = \mathbf{A}^{-1} \begin{bmatrix} \mathbf{e} \\ \mathbf{f} \end{bmatrix} \tag{2.8}$$

where $\mathbf{p} = [p_2, p_3, \ldots, p_N]'$ and $\mathbf{q} = [q_2, q_3, \ldots, q_N]'$ are the vector of active and

reactive power consumptions of the nodes, respectively. Similarly,

$$\mathbf{p}_{\mathrm{DG}} = [p_{\mathrm{DG},2}, p_{\mathrm{DG},3}, \ldots, p_{\mathrm{DG},N}]',$$
$$\mathbf{q}_{\mathrm{DG}} = [q_{\mathrm{DG},2}, q_{\mathrm{DG},3}, \ldots, q_{\mathrm{DG},N}]'$$

are the vector of active and reactive power generation by local DGs, respectively. Moreover, $\mathbf{A}$ is defined as:

$$\mathbf{A} = \begin{bmatrix} \tilde{\mathbf{G}} & -\tilde{\mathbf{B}} \\ -\tilde{\mathbf{B}} & -\tilde{\mathbf{G}} \end{bmatrix}^{-1}. \tag{2.9}$$

Rearranging the matrix form of the linearized power flow equations, (3.1) reads as:

$$\begin{aligned}(\mathbf{p} - j\mathbf{q}) - (\mathbf{p}_{\mathrm{DG}} - j\mathbf{q}_{\mathrm{DG}}) &= (\tilde{\mathbf{G}}\mathbf{g} - \tilde{\mathbf{B}}\mathbf{f}) + j(\tilde{\mathbf{B}}\mathbf{g} + \tilde{\mathbf{G}}\mathbf{f}) \\ &= (\tilde{\mathbf{G}} + j\tilde{\mathbf{B}})(\mathbf{g} + j\mathbf{f}),\end{aligned} \tag{2.10}$$

or, equivalently,

$$\mathbf{s}^* - \mathbf{s}^*_{\mathrm{DG}} = \tilde{\mathbf{Y}}\tilde{\boldsymbol{v}}, \tag{2.11}$$

where $\mathbf{s} = \mathbf{p} + j\mathbf{q}$ is the vector of complex power consumption of the nodes, $\mathbf{s}_{\mathrm{DG}} = \mathbf{p}_{\mathrm{DG}} + j\mathbf{q}_{\mathrm{DG}}$ is the vector of complex power injections by local DGs, and $(\cdot)^*$ denotes complex conjugation. Eq. (2.11) is the complex form of the linearized equations derived in [78] with appropriate modifications to account for DGs. In [78], the authors have used this complex form to theoretically bound the approximation error of the linearized power flow equations in rectangular coordinates.

2.2.2 The Linearized Measurement Model

From (2.8) one can see that the gradients of the power consumptions with respect to $\mathbf{g}$ and $\mathbf{f}$ are constant (independent of the actual state of the system.) In addition, because the elements of $\mathbf{f}$ are very small, the magnitude of the voltages measured by VMMs are quite close to the real part of the voltages. Therefore, the magnitude of the voltage v_n is approximately a linear function of g_n whose gradient is equal to one.

Even though the gradient of the nonlinear measurements is approximately independent of the actual state of the system, the variance of the measurement noise could depend on the actual state of the system. This will happen if the measurement error is a constant percentile of the measured values, as widely assumed in the literature [17, 18, 20, 41, 47]. To see how this can impact the FIM, assume that the measurement noises of different measured values are independent. Therefore, the covariance matrices $\mathbf{R}_i$ are diagonal. Also, let $H_i(\mathbf{v})$ be approximately independent of $\mathbf{v}$. The FIM can now be expanded as

$$\mathbf{J} = \sum_i \sum_r \frac{1}{\sigma_{i,r}^2} h_{i,r} h_{i,r}', \tag{2.12}$$

where $\sigma_{i,r}^2$ is the rth diagonal element of $\mathbf{R}_i$ and $h_{i,r}$ is the rth column of H_i. It is seen from (2.12) that the FIM is a weighted sum of a series of Hermitian positive definite matrices. When $\sigma_{i,r}^2$ increases, the single non-zero eigenvalue of the matrix $\frac{1}{\sigma_{i,r}^2} h_{i,r} h_{i,r}'$ decreases and all the zero eigenvalues remain the same. It follows then from Weyl's inequality that all the eigenvalues of $\mathbf{J}$ decrease as well. As a result, all the eigenvalues of $\mathbf{J}^{-1}$ increase. Consequently, the total estimation variance which is equal to the sum of the eigenvalues of $\mathbf{J}^{-1}$ increases as well. This shows that the maximum value of the total estimation variance corresponds to the maximum

measurement noises. If the variance of the measurement noises is proportional to the measured values, then the maximum total estimation variance corresponds to the peak loads. That is because in the peak hours the consumption powers can be several times bigger than those of off-peak hours whereas the reduction in the voltages is limited. Our simulations also verify that $\mathbf{h}_i(\mathbf{v})$ is approximately independent of $\mathbf{v}$ and the maximum estimation variance corresponds to peak hours. Finally, note that the same conclusions can be made if $\mathbf{R}_i$ are not diagonal. In that case, one has to exploit the eigenvalue decomposition of $\mathbf{R}_i$. For the sake of brevity we omit the details of this case.

Mathematically, designing the meter places for peak loads is equivalent to linearizing the measurement model given in (2.1) around $\mathbf{v}_{\text{peak}}$ as follows

$$\mathbf{z}_i = \mathbf{h}_i(\mathbf{v}_{\text{peak}}) + H_i(\mathbf{v} - \mathbf{v}_{\text{peak}}) + \boldsymbol{\eta}_i, \tag{2.13}$$

where

$$H_i = \nabla_{\mathbf{v}} \mathbf{h}_i(\mathbf{v}_{\text{peak}}), \tag{2.14}$$

and $\mathbf{v}_{\text{peak}}$ is the vector of nodal voltages at peak hours. To realize this equivalence, define $\tilde{\mathbf{z}}_i$ as follows:

$$\tilde{\mathbf{z}}_i = \mathbf{z}_i - \mathbf{h}_i(\mathbf{v}_{\text{peak}}) + H_i \mathbf{v}_{\text{peak}}. \tag{2.15}$$

Then the linearized model can be rewritten as:

$$\tilde{\mathbf{z}}_i = H_i \mathbf{v} + \boldsymbol{\eta}_i. \tag{2.16}$$

It is readily seen that the FIM corresponding to the measurement model in (2.16) is equal to the FIM in (2.4) evaluated at $\mathbf{v} = \mathbf{v}_{\text{peak}}$, i.e., $\mathbf{J}(\mathbf{v}_{\text{peak}})$. In fact, in this linearized model the conditional covariance matrix is independent of $\mathbf{v}$ and achieves

the CRLB. That is,

$$\mathbf{C}_{\text{lin}}(\hat{\mathbf{v}}) = [\mathbf{J}(\mathbf{v}_{\text{peak}})]^{-1}, \tag{2.17}$$

where $\mathbf{C}_{\text{lin}}(\hat{\mathbf{v}})$ is the unconditional covariance matrix of the linearized model.

2.3 Meter Placement in Single Configuration Distribution Systems

In this section the problem of optimal meter placement for minimization of the total estimation variance of nodal voltages in a single configuration distribution system is formulated. This formulation is identical to the one presented in [74] for optimal placement in transmission networks. The greedy algorithm [74, 75] is then reviewed as a near-optimal meter placement scheme. Although the greedy algorithm is presented here for meter placement in single configuration distribution systems, it can also be used as a suboptimal algorithm for meter placement in active distribution systems. Throughout the rest of the chapter a meter refers to a VMM or a PMU.

2.3.1 Formulation of the Meter Placement Problem

A PMU measures the magnitude and the phase of the voltage of a node with high accuracy [2, 19, 41]. The measurement model of the data provided by a PMU installed at the bus $j \in \{1, 2, \ldots, N\}$ is as follows:

$$\mathbf{y}_j = P_j \mathbf{v} + \mathbf{q}_j, \tag{2.18}$$

where

$$P_j = \begin{bmatrix} \mathbf{e}_j' & \mathbf{0} \\ \mathbf{0} & \mathbf{e}_j' \end{bmatrix}, \tag{2.19}$$

$\mathbf{e}_j$ is a unit vector with a one as its jth element, and $\mathbf{q}_j \sim \mathcal{N}(\mathbf{0}, \mathbf{Q}_j)$ is the measurement noise.

Similarly, a VMM measures the magnitude of the voltage of a node. Therefore, one should consider the same measurement model as in (2.18) for a VMM placed in node j with the following regression matrix:

$$P_j = \begin{bmatrix} \mathbf{e}_j' & \mathbf{0} \\ \mathbf{0} & \mathbf{0} \end{bmatrix}. \tag{2.20}$$

Let $\mathcal{A}$ be the set of nodes equipped with a meter (PMU or VMM). The MLE of the node voltages given substation measurements and the measurements provided by VMMs, smart meters and PMUs is found as follows:

$$\hat{\mathbf{v}} = \arg\min_{\mathbf{v}} \left\{ \sum_{i=1}^{M} [\mathbf{z}_i - \mathbf{h}_i(\mathbf{v})]' \mathbf{R}_i^{-1} [\mathbf{z}_i - \mathbf{h}_i(\mathbf{v})] + \sum_{j \in \mathcal{A}} [\mathbf{y}_j - P_j \mathbf{v}]' \mathbf{Q}_j^{-1} [\mathbf{y}_j - P_j \mathbf{v}] \right\}. \tag{2.21}$$

For distribution system state estimation the MLE of the voltages should be computed according to (2.21). However, the meter placement will be done so as to optimize the trace of the inverse of the FIM at $\mathbf{v} = \mathbf{v}_{\text{peak}}$. As explained in Sec. 2.1, this is equivalent to linearizing the non-linear measurement models as in (2.16). For the linearized model, the MLE of the voltages is given by the following equation

$$\hat{\mathbf{v}}_{\text{lin}} = \mathbf{J}_{\text{lin}}^{-1} \left[\sum_{i=1}^{M} H_i' \mathbf{R}_i^{-1} \tilde{\mathbf{z}}_i + \sum_{j \in \mathcal{A}} P_j' \mathbf{Q}_j^{-1} \mathbf{y}_j \right], \tag{2.22}$$

where H_i and $\tilde{\mathbf{z}}_i$ are as defined in (2.14) and (2.15), respectively, and

$$\mathbf{J}_{\text{lin}} = \sum_{i=1}^{M} H_i' \mathbf{R}_i^{-1} H_i + \sum_{j \in \mathcal{A}} P_j' \mathbf{Q}_j^{-1} P_j \tag{2.23}$$

is the FIM corresponding to the linearized model.

The accuracy of the PMUs and VMMs is considerably higher than the historical data (pseudo-measurements) and smart metering data with relatively low reporting rates. Therefore, as in [74], we can assume that the MLE of the voltages of the meter-equipped nodes is equal to the actual measurements reported by the meter of those nodes. That is, if a node is equipped with a VMM, the estimate of the magnitude of the voltage of that node can be considered to be equal to the measured value. Similarly, if a node is equipped with a PMU, the magnitude and the phase of the voltage of that node can be considered to be equal to the measured values. Denote by $\mathbf{Y}$ the vector of all magnitude and phase measurements reported by the placed meters. Also, denote by $\mathcal{A}^c$ the complement of the set $\mathcal{A}$ with respect to the set $\{1, 2, \ldots, N\}$. Let H_i be decomposed as $[H_{i,\mathcal{A}} | H_{i,\mathcal{A}^c}]$. In the case of VMM placement, $H_{i,\mathcal{A}}$ corresponds to the magnitudes of the voltages of the VMM-equipped nodes and $H_{i,\mathcal{A}^c}$ corresponds to the remaining magnitudes and phases. In the case of PMU placement, $H_{i,\mathcal{A}}$ and $H_{i,\mathcal{A}^c}$ correspond to the columns of H_i associated with the magnitudes and phases of the PMU and non-PMU nodes, respectively. With these notations and for the linearized model in (2.16), the MLE of the voltages at the non-meter nodes can be computed as:

$$\hat{\mathbf{v}}_{\text{lin}}[\mathcal{A}^c] \;=\; \left[\sum_{i=1}^{M} H_{i,\mathcal{A}^c}' \mathbf{R}_i^{-1} H_{i,\mathcal{A}^c} \right]^{-1} \times \left[\sum_{i=1}^{M} H_{i,\mathcal{A}^c}' \mathbf{R}_i^{-1} \left(\tilde{\mathbf{z}}_i \;-\; H_{i,\mathcal{A}} \mathbf{Y} \right) \right]. \tag{2.24}$$

It is shown in [74] that for $\mathbf{Q}_i = \sigma^2 I$, the estimates obtained from this approach are

equal to those given in (2.22) as σ^2 goes to zero.

The FIM corresponding to the estimates in (2.24), which now coincides with the unconditional covariance matrix $\mathbf{C}(\hat{\mathbf{v}}_{\text{lin}}[\mathcal{A}^c])$, is given by

$$\mathbf{J}_{\text{lin}}[\mathcal{A}^c] = \sum_{i=1}^{M} H'_{i,\mathcal{A}^c}\mathbf{R}_i^{-1}H_{i,\mathcal{A}^c}. \tag{2.25}$$

According to (2.25), the total variance reduction due to installing meters at nodes $j \in \mathcal{A}$ is given by

$$F(\mathcal{A}) \quad = \quad \text{tr}\left(\left[\sum_{i=1}^{M} H'_i\mathbf{R}_i^{-1}H_i\right]^{-1}\right) \; - \; \text{tr}\left(\left[\sum_{i=1}^{M} H'_{i,\mathcal{A}^c}\mathbf{R}_i^{-1}H_{i,\mathcal{A}^c}\right]^{-1}\right), \tag{2.26}$$

where $\text{tr}(\cdot)$ denotes the trace of the matrix. Therefore, the meter placement problem for minimization of the total estimation variance (maximization of the reduction in total estimation variance) can be formulated as

$$\mathcal{A}^* = \arg\max_{|\mathcal{A}|\leq K} F(\mathcal{A}), \tag{2.27}$$

where K is the number of available meters. It should be pointed out that the above approach is only adopted for formulation of the meter placement problem and the actual task of state estimation will still be done according to (2.21).

Problem (2.27) is an NP-hard, combinatorial optimization problem. The complexity of finding the optimal solution to this problem is exponential in the number of nodes. Since the distribution systems usually have a large number of nodes, one has to resort to low complexity algorithms for finding suboptimal solutions to this problem. In the next subsection, a simple greedy algorithm for solving this problem is presented.

2.3.2 Submodularity and the Greedy Algorithm

As stated above, the meter placement problem (2.27) is an NP-hard problem. However, due to the *submodularity* of the set function $F(\mathcal{A})$, a simple greedy algorithm can provide a near-optimal solution to this problem.

Formally, a set function $F : 2^{\{1,2,\ldots,N\}} \to \mathbb{R}$ is defined to be submodular if for any two sets $\mathcal{A}, \mathcal{B} \subseteq 2^{\{1,2,\ldots,N\}}$ the following inequality holds:

$$F(\mathcal{A} \cup \mathcal{B}) + F(\mathcal{A} \cap \mathcal{B}) \leq F(\mathcal{A}) + F(\mathcal{B}). \tag{2.28}$$

Also, F is called monotonic if for any two sets $\mathcal{A}, \mathcal{B} \subseteq 2^{\{1,2,\ldots,N\}}$ such that $\mathcal{A} \subseteq \mathcal{B}$ we have $F(\mathcal{A}) \leq F(\mathcal{B})$. A set function $F(\mathcal{A})$ is called antitonic, if $-F(\mathcal{A})$ is monotonic.

By expanding the FIM as in (2.4) it can be shown that the trace of $\mathbf{J}^{-1}$ is an antitonic function of the set of available measurements and, hence, the reduction in the total estimation variance is monotonic. To see this, first note that all eigenvalues of the FIM are greater than zero because it is positive-definite. Now, let $\mathbf{J}_M$ and $\mathbf{J}_{M+1}$ be the FIM when there exist M and $M+1$ measurement vectors in the system, respectively. Here, the FIM may include terms corresponding to both linear and nonlinear measurements. Let $H(\mathbf{v}) = [\nabla_{\mathbf{v}} \mathbf{h}_{M+1}(\mathbf{v})]$. From (2.4) we can write

$$\mathbf{J}_{M+1} = \mathbf{J}_M + H'(\mathbf{v}) \mathbf{R}_{M+1}^{-1} H(\mathbf{v}), \tag{2.29}$$

where $\mathrm{tr}(\cdot)$ denotes the trace of the matrix. It follows from the structure of the second term in the right-hand side of (2.29) that it is a positive-definite matrix. Therefore, based on Weyl's inequality for the sum of two positive-definite Hermitian matrices, the eigenvalues of the $\mathbf{J}_{M+1}$ are greater than the corresponding eigenvalues of $\mathbf{J}_M$. As a result, the eigenvalues of $\mathbf{J}_{M+1}^{-1}$ are smaller than the corresponding

eigenvalues of $\mathbf{J}_M^{-1}$. Therefore, we have

$$\mathrm{tr}\Big(\mathbf{J}_{M+1}^{-1}\Big) \leq \mathrm{tr}\Big(\mathbf{J}_M^{-1}\Big). \tag{2.30}$$

Now consider the case where the estimate of the voltages measured by VMMs or PMUs are considered to be equal to the actual measurements. Let $\mathbf{J}$ be the FIM where no measurements from VMMs or PMUs are available. Also, let $\tilde{\mathbf{J}}$ be the FIM corresponding to estimation of the remaining voltages when some voltages (magnitudes and/or angles) are measured. It then follows from Cauchy's interlacing theorem that the eigenvalues of $\tilde{\mathbf{J}}$ are greater than the corresponding eigenvalues of $\mathbf{J}$ (note that the number of eigenvalues of $\tilde{\mathbf{J}}$ is less than that of $\mathbf{J}$). Therefore, we can conclude that

$$\mathrm{tr}\Big(\tilde{\mathbf{J}}^{-1}\Big) \leq \mathrm{tr}\Big(\mathbf{J}^{-1}\Big). \tag{2.31}$$

For a monotonic, submodular function satisfying $F(\emptyset) = 0$, a classical result by Nemhauser *et. al.* [75] shows that the greedy algorithm shown in Algorithm 1 achieves a $(1-1/e)$ approximation to the problem (2.27). That is, if $\mathcal{A}^*$ is the optimal solution to the problem (2.27) and $\mathcal{A}_G$ is the solution returned by Algorithm 1, then

$$F(\mathcal{A}_G) \geq (1 - 1/e)F(\mathcal{A}^*). \tag{2.32}$$

Algorithm 1 *Greedy*

```
Specify the number of meters K
Initialize A = ∅
while |A| < K do
    a* = arg max_{a∈A^c} { F(A ∪ {a}) − F(A) }
    A ← A ∪ {a*}
end while
return A
```

From (2.26), it is obvious based on the structure of the total variance reduction

function, $F(\mathcal{A})$, that $F(\emptyset) = 0$. Furthermore, if the columns of the matrix

$$\mathbf{H} = \begin{bmatrix} H_1 \\ H_2 \\ \vdots \\ H_M \end{bmatrix} \tag{2.33}$$

are nearly orthogonal, $F(\mathcal{A})$ is a submodular function (see [74]). If the submodularity of $F(\mathcal{A})$ holds, then the greedy algorithm results in a $(1 - 1/e)$ approximation to the meter placement problem (2.27) [74]. Moreover, there exists no polynomial time algorithm for a better approximation guarantee [85].

2.4 Meter Placement in Reconfigurable Distribution Systems

In this section the problem of meter placement for minimization of total estimation variance of the magnitudes and phases of the voltages in a reconfigurable distribution system is considered. Unlike the meter placement problem for single configuration distribution systems, the meter placement problem for active distribution systems does not admit any approximation guarantee. Therefore, a robust algorithm for meter placement in reconfigurable distribution systems is proposed which outperforms the greedy algorithm and GA in most cases and provides competitive results in other cases.

2.4.1 Formulation of the Robust Meter Placement Problem

In an active distribution system, the configuration of the system may change due to opening/closing some tie line switches. Therefore, the meter placement problem

should be formulated in a robust fashion to take these changes into account. In the following, we formulate the robust meter placement problem for reconfigurable distribution systems.

The model for the ith measurement in the lth configuration of the system is given by

$$\mathbf{z}_i^l = \mathbf{h}_i^l(\mathbf{v}) + \boldsymbol{\eta}_i^l. \tag{2.34}$$

Denote by $\mathbf{v}_{\text{peak}}^l$ the vector of nodal voltages corresponding to peak load of the lth configuration of the system. Let

$$H_i^l = \nabla_{\mathbf{v}} \mathbf{h}_i^l(\mathbf{v}_{\text{peak}}^l) \tag{2.35}$$

be the gradient of $\mathbf{h}_i^l(\mathbf{v})$ evaluated at $\mathbf{v} = \mathbf{v}_{\text{peak}}^l$. Decompose H_i^l as $[H_{i,\mathcal{A}}^l | H_{i,\mathcal{A}^c}^l]$, where $H_{i,\mathcal{A}}^l$ and $H_{i,\mathcal{A}^c}^l$ correspond to the columns of H_i^l associated with the magnitudes and/or phases of the meter-equipped and non-meter nodes, respectively. The minimization of the worst case total estimation variance is equivalent to maximizing the reduction in total estimation variances compared to the worst initial configuration. With the above-mentioned notations, the reduction in the total estimation variance of the lth configuration of the system with respect to the worst initial configuration is given by the following expression:

$$F_l(\mathcal{A}) = \max_{0 \le l \le L} \left\{ \text{tr}\left(\left[\sum_{i=1}^{M} [H_i^l]' \mathbf{R}_i^{-1} [H_i^l] \right]^{-1} \right) \right\} - \text{tr}\left(\left[\sum_{i=1}^{M} [H_{i,\mathcal{A}^c}^l]' \mathbf{R}_i^{-1} [H_{i,\mathcal{A}^c}^l] \right]^{-1} \right), \tag{2.36}$$

where $\text{tr}(\cdot)$ denotes the trace of the matrix. We further assume that the columns of

$$\mathbf{H}^l = \begin{bmatrix} H_1^l \\ H_2^l \\ \vdots \\ H_M^l \end{bmatrix} \tag{2.37}$$

are nearly orthogonal such that $F_l(\mathcal{A})$ is a submodular function [74].

Finally, the robust meter placement problem for minimization of the total estimation variance (maximization of the reduction in total estimation variance) in a reconfigurable distribution system can be formulated as follows:

$$\mathcal{A}^* = \arg \max_{|\mathcal{A}| \leq K} \min_{0 \leq l \leq L} F_l(\mathcal{A}), \tag{2.38}$$

where K is the number of available meters and L is the total number of possible configurations of the system. Observe that by defining the functions in a specific way as in (2.36), the optimization problem in (2.38) is equivalent to minimizing the worst case total estimation variance of the system.

Remark 2.1 *An alternative way of formulating the meter placement problem in a reconfigurable distribution system is to assign probabilities to the configurations and optimize the expected reduction in the total estimation variance. Let λ_l be the probability that the system will have the lth configuration, where $\sum_{l=1}^{L} \lambda_l = 1$. Then, the expected reduction in total estimation variance of the system is given by:*

$$\mathbb{E}\{F(\mathcal{A})\} = \sum_{l=1}^{L} \lambda_l F_l(\mathcal{A}), \tag{2.39}$$

where $F_l(\mathcal{A})$, defined in (2.36), is the reduction in the total estimation variance of the lth configuration of the system when meters are placed in the set $\mathcal{A}$. Since submodular functions are closed under convex combinations, it follows from the sub-

modularity of the functions $F_l(\mathcal{A})$ that the expected reduction in the total estimation variance is also a submodular function in $\mathcal{A}$. Therefore, the $(1-1/e)$ performance guarantee will be provided by the greedy algorithm. However, in this chapter we consider the robust meter placement problem where the objective is to optimize the worst configuration.

2.4.2 The Submodular Saturation Algorithm

In this part, the submodular saturation algorithm for robust submodular optimization problems is presented. In [76], this algorithm has been successfully used for robust sensor placement and observation selection over various temperature and precipitation data sets. In this chapter, this algorithm is employed for robust meter placement in reconfigurable distribution systems.

The minimum of a set of submodular functions is not submodular in general. Therefore, the application of the greedy algorithm for the robust meter placement problem (2.38) does not provide the $(1-1/e)$ approximation guarantee. More importantly, it is shown in [76] that problem (2.38) does not admit *any* approximation guarantee. Therefore, we consider the following relaxed problem:

$$\mathcal{A}^* = \arg \max_{|\mathcal{A}| \leq \alpha K} \min_{0 \leq l \leq L} F_l(\mathcal{A}), \tag{2.40}$$

where $\alpha \geq 1$ is a fixed parameter. The objective in (2.40) is to maximize the reduction in the total estimation variance with respect to the worst initial configuration, where the number of available meters is increased with a factor of α. It is obvious that for $\alpha = 1$, (2.40) reduces to (2.38). Problem (2.40) can be reformulated in the

following equivalent form

$$\begin{aligned} &\max\ t \\ s.t.\quad &\min_{0\le l\le L} F_l(\mathcal{A}) \ge t \\ &|\mathcal{A}| \le \alpha K \end{aligned} \tag{2.41}$$

Now suppose there exists an algorithm that for any t solves the following related problem

$$\begin{aligned} &\min |\mathcal{A}| \\ s.t.\quad &\min_{0\le l\le L} F_l(\mathcal{A}) \ge t. \end{aligned} \tag{2.42}$$

Problem (2.42) seeks the minimum number of meters to be installed in the system such that the reduction in the total estimation variances is greater than a threshold t for all the configurations. If the solution to this problem satisfies the constraint $|\mathcal{A}| \le \alpha K$, then t is a feasible solution to the problem (2.41). On the other hand, if the the solution to the problem (2.42) has more elements than αK, then t is not a feasible solution to the problem (2.41). Our task is then to find the largest t for which problem (2.41) is feasible. It is evident that such a t is indeed the solution to the problem. Now consider the following two extreme values for t:

$$\begin{aligned} t_{max} &= \min_{0\le l\le L} F_l(\{1,2,\ldots,N\}) \\ t_{min} &= 0 \end{aligned} \tag{2.43}$$

It is obvious that the solution to the problem (2.42) with $t = t_{min}$ (which is $\mathcal{A}^* = \emptyset$) is a feasible solution to the problem (2.41). If the solution to the problem (2.42)

with $t = t_{max}$ is also a feasible solution to the problem (2.41), then the optimal solution of the problem (2.41) is found. Otherwise, we need to do a binary search between t_{min} and t_{max} to find the largest feasible t. This is the main idea of the submodular saturation algorithm [76].

According to the above discussion, for solving (2.40) and (2.41), it remains to find an algorithm to solve (2.42). The main difficulty with (2.42) is that it contains a non-submodular constraint. However, this constraint can be reformulated to be in a submodular form. The trick is to define a set of truncated functions as follows

$$F_l'(\mathcal{A}) = \min\{F_l(\mathcal{A}), t\}. \tag{2.44}$$

Note that if $F_l(\mathcal{A})$ is monotonic and submodular, $F_l'(\mathcal{A})$ will be monotonic and submodular, too. Now define the following average truncated function

$$\bar{F}'(\mathcal{A}) = \frac{1}{L}\sum_{l=1}^{L} F_l'(\mathcal{A}). \tag{2.45}$$

Since submodular functions are closed under convex combinations, $\bar{F}'(\mathcal{A})$ is submodular. Using above definitions, problem (2.42) can be written as

$$\begin{aligned} &\min |\mathcal{A}| \\ s.t.\ \ &\bar{F}'(\mathcal{A}) \geq t. \end{aligned} \tag{2.46}$$

One can easily verify that problems (2.42) and (2.46) are equivalent. Problem (2.46), if feasible, is a submodular set covering problem as it is equivalent to the following

problem:

$$\min |\mathcal{A}| \tag{2.47}$$
$$s.t. \quad \bar{F}'(\mathcal{A}) = \bar{F}'(\{1, 2, \ldots, N\}).$$

Submodular set covering problems are NP-hard in general. However, a near-optimal solution can be found by a greedy algorithm which starts with the empty set and iteratively adds elements with the best increment until $\bar{F}'(\mathcal{A}) = \bar{F}'(\{1, 2, \ldots, N\})$. If the functions $F_l(\mathcal{A}), l = 1, 2, \ldots, L$, are integral-valued, a famous result due to Wolsey shows that the solution obtained by greedy algorithm has a logarithmic performance guarantee [86]. In practice, the greedy algorithm usually performs very well even if the functions are not integral-valued.

Having the greedy algorithm for solving problem (2.42), or its equivalent form (2.47), we are now ready to solve problem (2.40). The pseudo-code provided in the next page presents the submodular saturation algorithm for solving this problem.

If α is greater than a certain lower bound and the initial estimation accuracy is the same for all the configurations, Algorithm 2 provides approximation guarantees for the relaxed problem (2.40), see [76]. If the initial estimation accuracy is not equal for all configurations, the performance guarantee provided in [76] requires a slight modification in the definition of the submodular functions. It is also shown in [76] that it is very unlikely that any other algorithm provides the same performance guarantee with a less restricting condition on α. Note, however, that the performance guarantee provided by Algorithm 2 requires the functions $F_l(\mathcal{A})$ to be integral-valued. In our application for meter placement in active distribution systems, the total reduction in variances is not an integral-valued function. However, one can round the functions with an arbitrary number of high order bits and then run Algorithm 2 for these approximate functions. Although the approximate func-

Algorithm 2 *Submodular Saturation*

Initialize:

$t_{min} = 0$

$t_{max} = \min_{0 \leq l \leq L} F_l(\{1, 2, \ldots, N\})$

$\mathcal{A} = \emptyset$

Specify:

A small non-negative tolerance δ

The number of meters K

The number of configurations L

while $t_{max} - t_{min} \geq \delta$ **do**

  $t \leftarrow \frac{t_{max}+t_{min}}{2}$

  Define $\bar{F}'(\mathcal{A}) = \frac{1}{L} \sum_{l=1}^{L} \min\{F_l(\mathcal{A}), t\}$

  Let $\hat{\mathcal{A}} = \emptyset$

  while $|\hat{\mathcal{A}}| < \alpha K + 1$ **do**

    $a^* = \arg\max_{a \in \hat{\mathcal{A}}^c} \left\{ \bar{F}'(\hat{\mathcal{A}} \cup \{a\}) - \bar{F}'(\hat{\mathcal{A}}) \right\}$

    $\hat{\mathcal{A}} \leftarrow \hat{\mathcal{A}} \cup \{a^*\}$

  end while

  if $|\hat{\mathcal{A}}| \leq \alpha K$ **then**

    $\mathcal{A} \leftarrow \hat{\mathcal{A}}$

    $t_{min} \leftarrow t$

  else

    $t_{max} \leftarrow t$

  end if

end while

return $\mathcal{A}$

tions do not necessarily remain submodular in this case, the corresponding error in the theoretical guarantees can be bounded as explained in [76] and [87]. In addition, observe that Algorithm 1 can also be used for meter placement in an active distribution system. In this case, Algorithm 1 considers the minimum of all the submodular functions as a submodular function and greedily finds the meter places. In order to fairly compare Algorithm 2 with Algorithm 1 for such a case, we need to run Algorithm 2 for $\alpha = 1$. Even though the performance guarantee of the Algorithm 2 does not hold in this case, numerical results show that in most cases it outperforms Algorithm 1 even for $\alpha = 1$ and without rounding.

Remark 2.2 *In practice, the measurements provided by VMMs and PMUs might include bad data. In such cases, the estimation error will be higher than what is considered in the meter placement problem, simply because the measurement error is higher. However, the state-of-the-art state estimators usually perform a hypothesis test on the measurements for identifying and removing bad data. In addition, the metering network might face sensor failures due to various hardware or software causes. From a mathematical point of view, these effects are equivalent and can be captured in the robust meter placement problem as follows:*

$$\mathcal{A}^* = \arg \max_{|\mathcal{A}| \leq K} \min_{0 \leq l \leq L} \min_{|\mathcal{B}| \leq K_B} F_l(\mathcal{A} \backslash \mathcal{B}), \tag{2.48}$$

where $\mathcal{B}$ is the set of bad data (or failed sensors) and K_B is the maximum number of bad data. Even thought Algorithm 2 can be directly applied to this problem, the corresponding performance guarantee might become loose. Nonetheless, it is possible to modify the definition of $\bar{F}'$ to come up with a tighter performance guarantee, especially for small number of meters. We do not consider this case here and refer the interested reader to [76] for a full treatment of this approach.

2.5 Numerical Results and Discussions

In this section numerical results are provided that show the effectiveness of the submodular saturation algorithm (Algorithm 2) for meter placement in active distribution systems. In all the simulations, Algorithm 1 considers the worst case objective function among all configurations as a submodular function and greedily finds the meter places. Also, Algorithm 2 is employed with $\alpha = 1$ and without rounding the submodular functions. The voltage magnitude and the active and reactive power flows are assumed to be always available in the substation. In the case of PMU placement, one PMU is always assumed in the substation as the reference node.

The VMMs are assumed to measure the magnitudes of the voltages with a maximum error of 1%. Also, the PMUs are assumed to measure the phasor of the voltages with a maximum Total Vector Error (TVE) of 1%. Moreover, the active and reactive consumption powers at the nodes are found by aggregating the measurements of the smart meters. A maximum error of 10% for such measurements is considered which can model the low reporting rate of the smart meters compared with the requirements of the real-time applications. Note that in future smart grids the state estimation may be done in real-time but the reporting rate of the smart meters can be hourly. In some present distribution systems, the reporting rate of the smart meters is every few hours. The 10% error in the smart metering data is compliant with the maximum signal dynamics considered in [88] for non-stationary conditions. In real applications, one will have to consider the actual reporting rate of the smart meters to approximately adjust the measurement error of the smart meters. The measurement noises have been considered to be white and Gaussian with a standard deviation equal to one third of the maximum measurement error.

The results of the proposed algorithms are compared with that of the GA for three different test systems. In addition, the computational costs of the three algo-

rithms are compared in terms of the number of times that the objective function is evaluated for each configuration of the system. For GA, the number of populations and the number of generations are considered to be 200 and 500, respectively.

In all the following test cases, each system has one primary substation which feeds several secondary transformers via feeders. Accordingly, the substation measurements refer to the measurements performed at the primary substation of the system.

2.5.1 Meter Placement in a 33-node, 12.66 kV Active Distribution System

In this section a modified version of the 33-node, 12.66 kV distribution system presented in [89] is considered. For this system, five weekly meshed configurations are created by first opening all the tie lines and then closing one of the tie lines at a time. To make sure that these configurations satisfy the operational limits on nodal voltages the maximum loads of the test system are reduced by 30%. Note that this modification has to be done to the system as any practical configuration of a real distribution system should satisfy these operational constraints.

For the 33-node test system, the installation of up to 5 meters is considered. Table 2.1 lists the total estimation variances for VMM placement in the 33-node test system using Algorithm 1, Algorithm 2, and GA. The table suggests that Algorithm 2 outperforms Algorithm 1 in all cases. Moreover, in only one case the GA has been able to find a better solution than Algorithm 2. Also, Table 2.2 shows the total estimation variance for PMU placement in the 33-node test system. The Table shows that in all cases Algorithm 2 outperforms Algorithm 1 and GA.

Table 2.1: Worst-case Total Estimation Variance for VMM Placement in the 33-node Active Distribution System

K	Algorithm 1 ($\times 10^{-6}$)	Algorithm 2 ($\times 10^{-6}$)	GA ($\times 10^{-6}$)
1	**3.36**	**3.36**	3.65
2	**2.15**	**2.15**	2.25
3	1.17	**1.14**	1.46
4	0.93	0.90	**0.76**
5	0.69	**0.65**	**0.65**

Table 2.2: Worst-case Total Estimation Variance for PMU Placement in the 33-node Active Distribution System

K	Algorithm 1 ($\times 10^{-7}$)	Algorithm 2 ($\times 10^{-7}$)	GA ($\times 10^{-7}$)
1	**7.39**	**7.39**	10.13
2	**2.38**	**2.38**	2.41
3	**0.97**	**0.97**	1.57
4	0.36	**0.30**	0.38
5	0.21	**0.16**	0.21

Fig. 2.2 depicts the optimal location of five VMMs in the 33-node test system using Algorithm 1, Algorithm 2, and GA. Similarly, Fig. 2.3 shows the optimal location of five PMUs in the test system using Algorithm 1, Algorithm 2, and GA. Note that Fig. 2.2 and Fig. 2.3 merely show the layout of the 33-node test system and not its possible configurations.

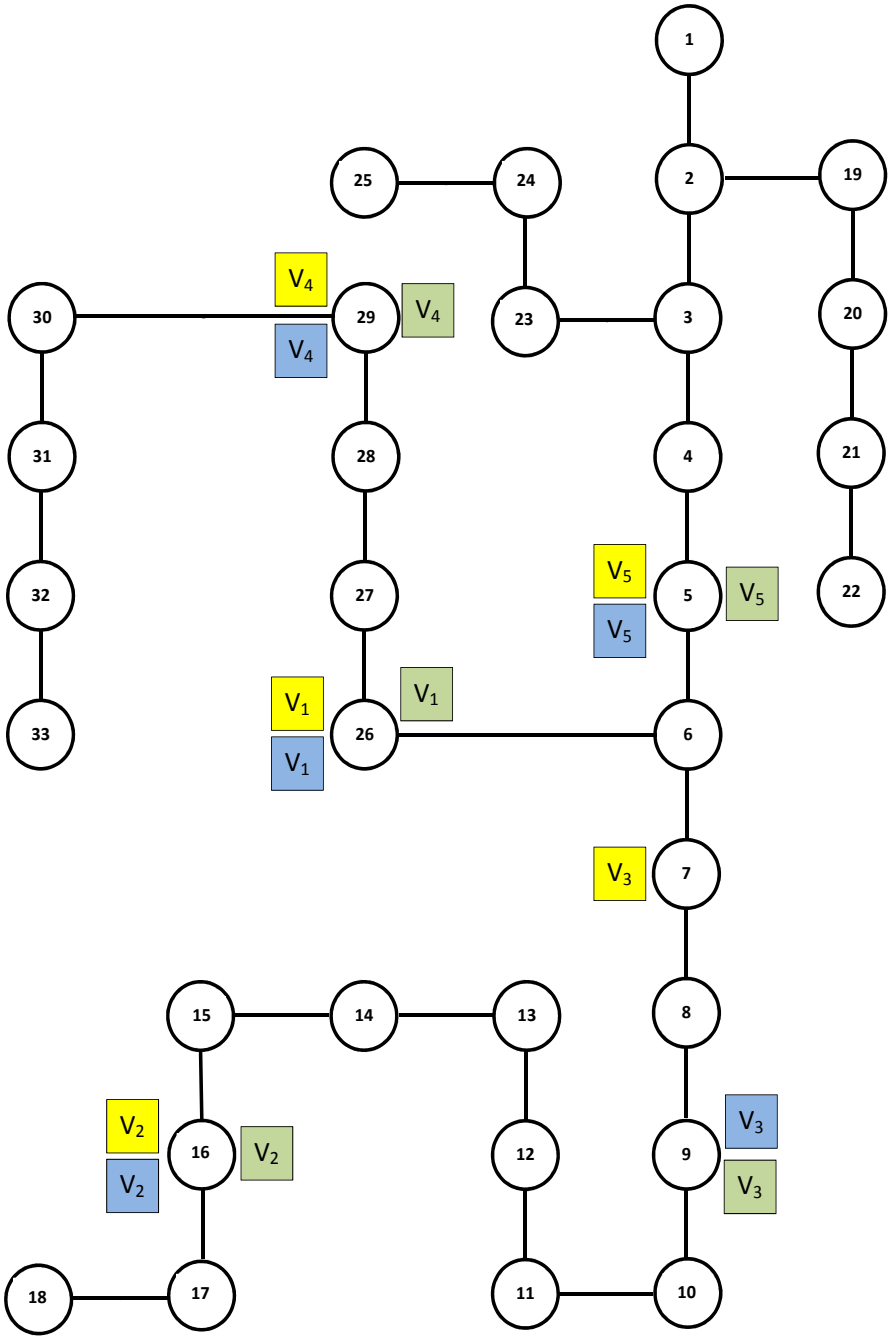

Figure 2.2: Optimal location of five VMMs in the 33-node test system using Algorithm 1 (yellow boxes), Algorithm 2 (blue boxes), and GA (green boxes).

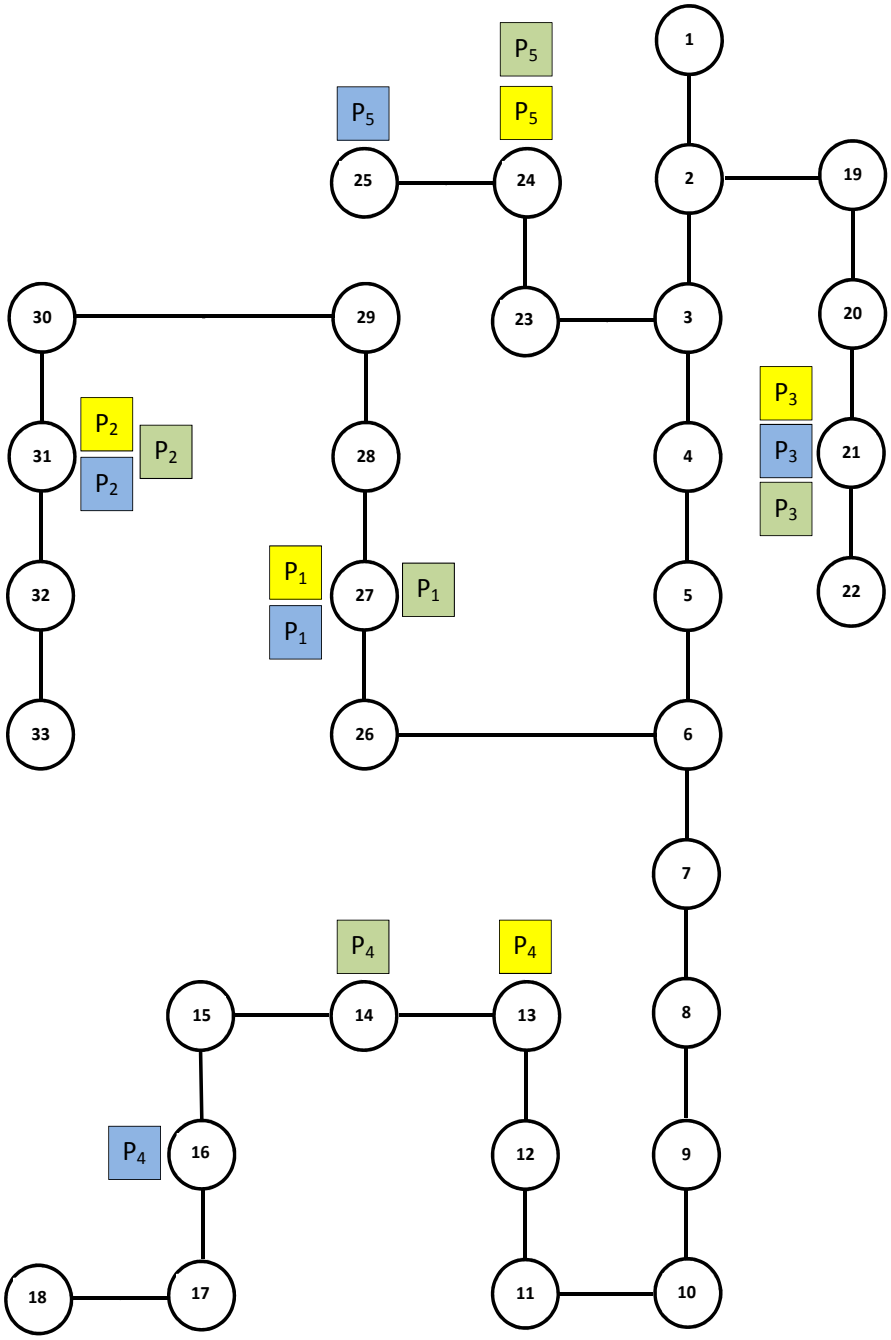

Figure 2.3: Optimal location of five PMUs in the 33-node test system using Algorithm 1 (yellow boxes), Algorithm 2 (blue boxes), and GA (green boxes).

2.5.2 Meter Placement in a 70-node, 11 kV Active Distribution System

In this section the robust meter placement problem for a modified version of an active 70-node, 11 kV distribution system [90] is considered. For this test system, 10 weekly meshed configurations are considered. These configurations are created as follows. First, all the tie branches are opened except branches $(9, 50)$, $(21, 27)$, and $(22, 67)$. The reason these three tie lines are kept closed is that, based on our simulations, they are crucial for keeping the minimum voltage of the system within operational constraints. Then, two pseudo-random tie switches are closed at a time. These two tie switches are selected from a large set of tie switches such that they provide a better minimum voltage in the system. Note that in real applications one would expect that those configurations be preferable as they meet the operational constraints and provide a better voltage profile. Finally, the maximum loads of the system are reduced by 20% such that all configurations of the system satisfy the operational constraints on nodal voltages.

For the 70-node test system, the robust placement of up to 9 meters is studied. Table 2.4 compares the performance of Algorithm 1, Algorithm 2, and GA for robust VMM placement in the system. The table shows that Algorithm 2 provides a better placement compared to Algorithm 1 and GA for all cases. Also, Table 2.5 demonstrates the results for PMU placement in the test system. The table suggests that Algorithm 2 results in the best placement for $K \leq 7$. For $K = 8, 9$, however, GA provides a better solution than Algorithm 1 and Algorithm 2.

Table 2.3: Worst-case Total Estimation Variance for VMM Placement in the 70-node Active Distribution System

K	Algorithm 1 ($\times 10^{-6}$)	Algorithm 2 ($\times 10^{-6}$)	GA ($\times 10^{-6}$)
1	**4.76**	**4.76**	4.78
2	**3.45**	**3.45**	3.49
3	**3.13**	**3.13**	3.28
4	2.92	**2.89**	3.10
5	2.83	**2.80**	3.00
6	2.77	**2.74**	2.90
7	2.72	**2.64**	2.83
8	2.62	**2.60**	2.75
9	2.45	**2.44**	2.62

Table 2.4: Worst-case Total Estimation Variance for PMU Placement in the 70-node Active Distribution System

K	Algorithm 1 ($\times 10^{-6}$)	Algorithm 2 ($\times 10^{-6}$)	GA ($\times 10^{-6}$)
1	**3.53**	**3.53**	3.58
2	**1.29**	**1.29**	1.42
3	**0.87**	**0.87**	0.99
4	**0.61**	**0.61**	0.71
5	0.46	**0.41**	0.55
6	0.40	**0.22**	0.51
7	0.37	**0.14**	0.21
8	0.13	0.11	**0.08**
9	0.08	0.08	**0.06**

Fig. 2.4 depicts the optimal location of 9 VMMs in the 70-node test system using Algorithm 1, Algorithm 2, and GA. Similarly, Fig. 2.5 shows the optimal location of 9 PMUs in the test system using Algorithm 1, Algorithm 2, and GA. Note that Fig. 2.4 and Fig. 2.5 merely show the layout of the 70-node test system and not its possible configurations.

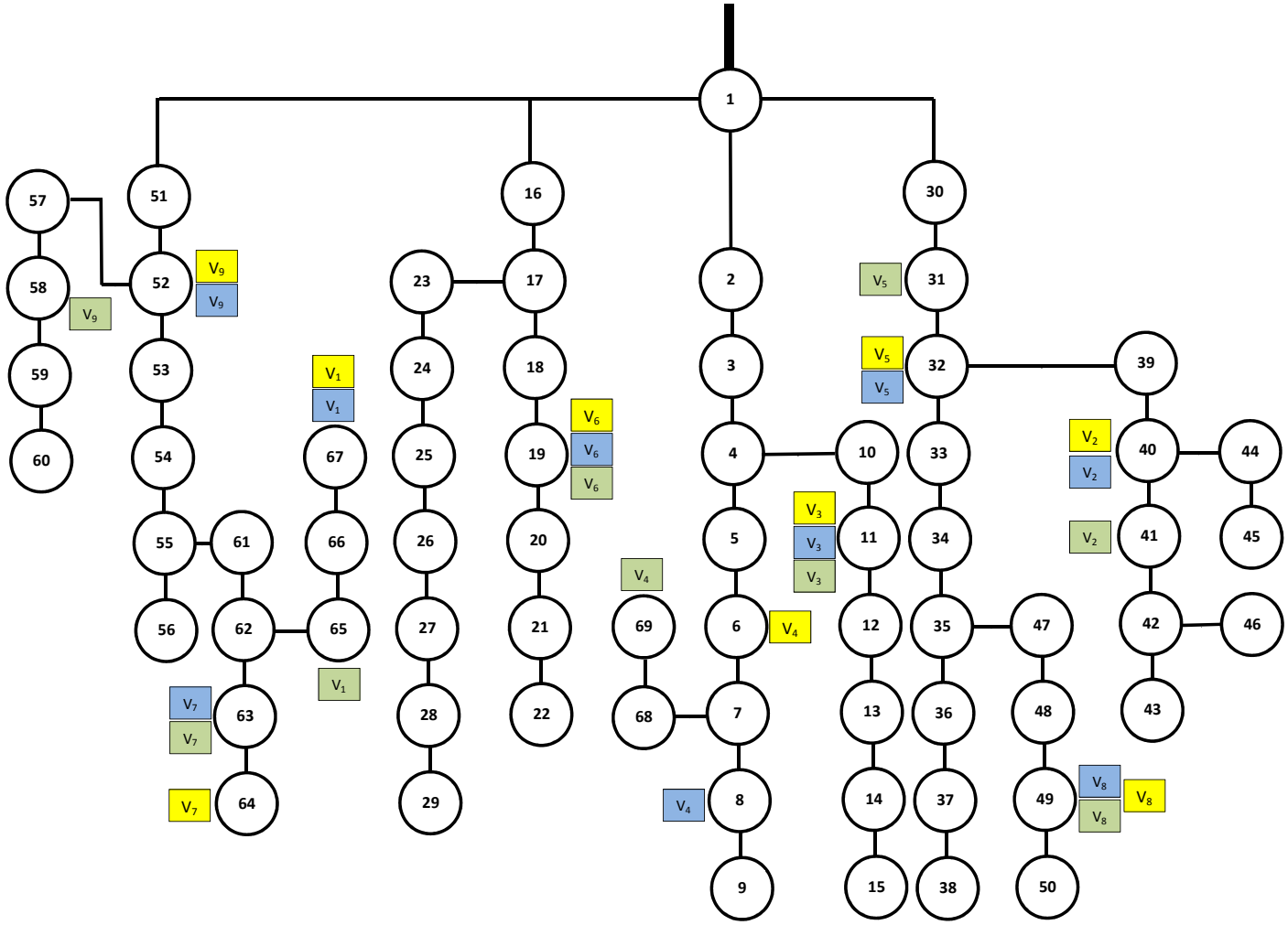

Figure 2.4: Optimal location of 9 VMMs in the 70-node test system using Algorithm 1 (yellow boxes), Algorithm 2 (blue boxes), and GA (green boxes).

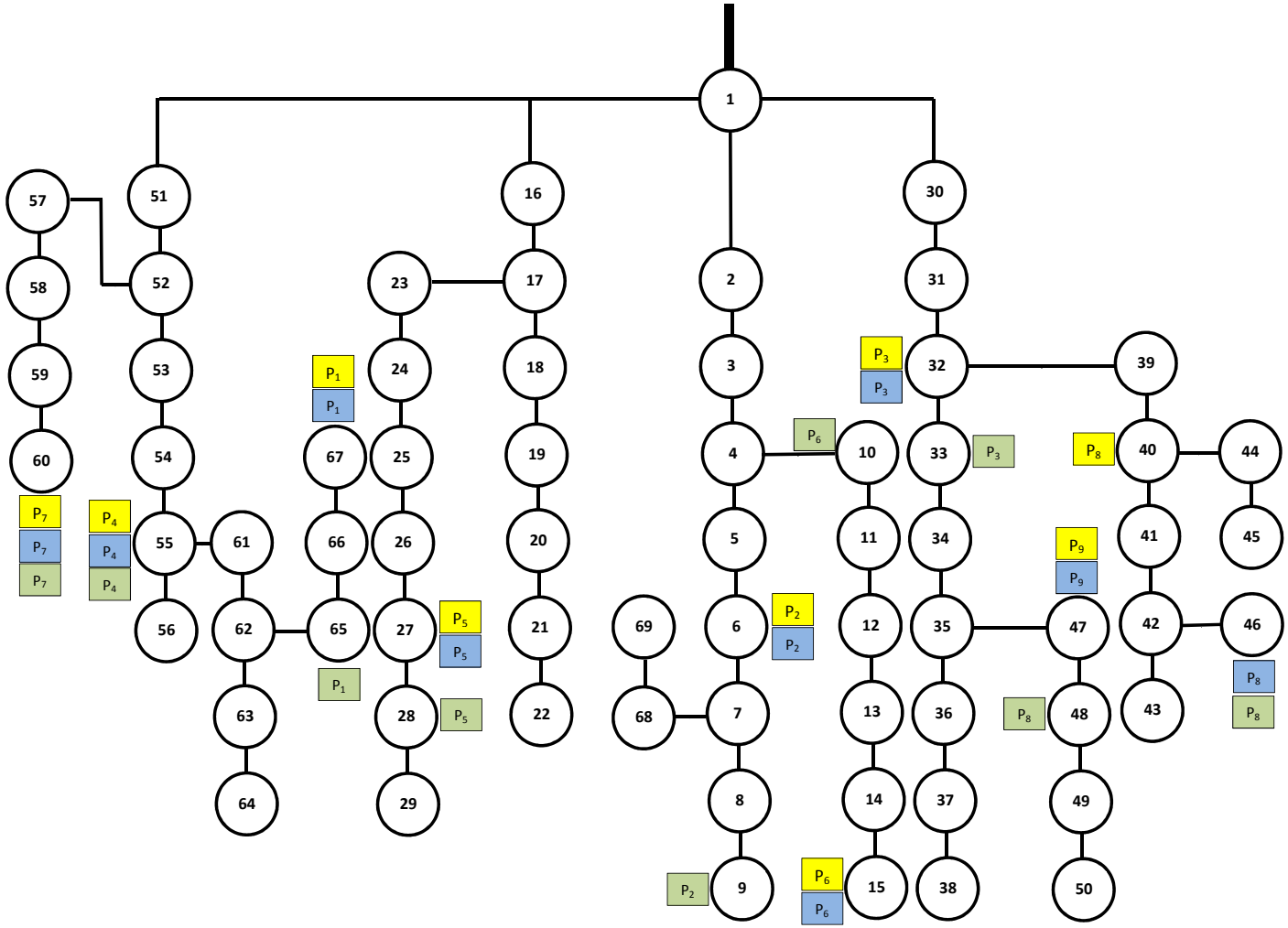

Figure 2.5: Optimal location of 9 PMUs in the 70-node test system using Algorithm 1 (yellow boxes), Algorithm 2 (blue boxes), and GA (green boxes).

2.5.3 Meter Placement in an 119-node, 11 kV Active Distribution System

In this section the problem of optimal meter placement for state estimation in a modified version of the 119-node, 11 kV distribution system presented in [91] is considered. For this system, first all the tie lines except for the two tie lines $(110, 118)$ and $(75, 88)$ are opened. Then, 30 weekly meshed configurations are created by closing three pseudo-random tie lines at a time. These three pseudo-random tie lines are obtained from a large set of random lines and by choosing those tie lines which result in a better minimum voltage along the feeder. Finally, the loads of the test system are reduced by 20% to make sure that all the configurations satisfy the operational constraints.

For the 119-node test system, the optimal placement of up to 9 meters has been studied. The results of the VMM placement using Algorithm 1, Algorithm 2, and GA are presented in Table 2.6. The table suggests that for five cases Algorithm 1 outperforms Algorithm 2, for two cases Algorithm 2 outperforms Algorithm 1, and for two cases the results are identical. Moreover, both algorithms outperform GA for all values of K. Also, Table 2.7 compares the performance of Algorithm 1, Algorithm 2, and GA for PMU placement in the test system. It is observed from the table that for all values of K Algorithm 2 outperforms Algorithm 1 and GA.

Table 2.5: Worst-case Total Estimation Variance for VMM Placement in the 119-node Active Distribution System

K	Algorithm 1 ($\times 10^{-6}$)	Algorithm 2 ($\times 10^{-6}$)	GA ($\times 10^{-6}$)
1	**13.44**	**13.44**	13.53
2	**10.50**	**10.50**	11.76
3	**8.83**	8.92	9.80
4	**7.78**	7.85	9.48
5	**6.73**	6.84	7.79
6	5.90	**5.63**	6.42
7	5.00	**4.91**	5.84
8	**4.19**	4.24	5.11
9	**3.82**	3.87	4.76

Table 2.6: Worst-case Total Estimation Variance for PMU Placement in the 119-node Active Distribution System

K	Algorithm 1 ($\times 10^{-6}$)	Algorithm 2 ($\times 10^{-6}$)	GA ($\times 10^{-6}$)
1	**11.42**	**11.42**	11.50
2	**6.30**	**6.30**	6.32
3	3.84	**3.76**	3.92
4	2.74	**2.65**	3.89
5	1.86	**1.79**	3.87
6	1.39	**1.17**	1.44
7	0.93	**0.75**	0.80
8	0.50	**0.41**	0.74
9	0.35	**0.33**	0.69

Fig. 2.6 illustrates the optimal location of 9 VMMs in the 119-node test system using Algorithm 1, Algorithm 2, and GA. Similarly, Fig. 2.7 shows the optimal location of 9 PMUs in the test system using Algorithm 1, Algorithm 2, and GA. Note that Fig. 2.6 and Fig. 2.7 merely show the layout of the 119-node test system and not its possible configurations.

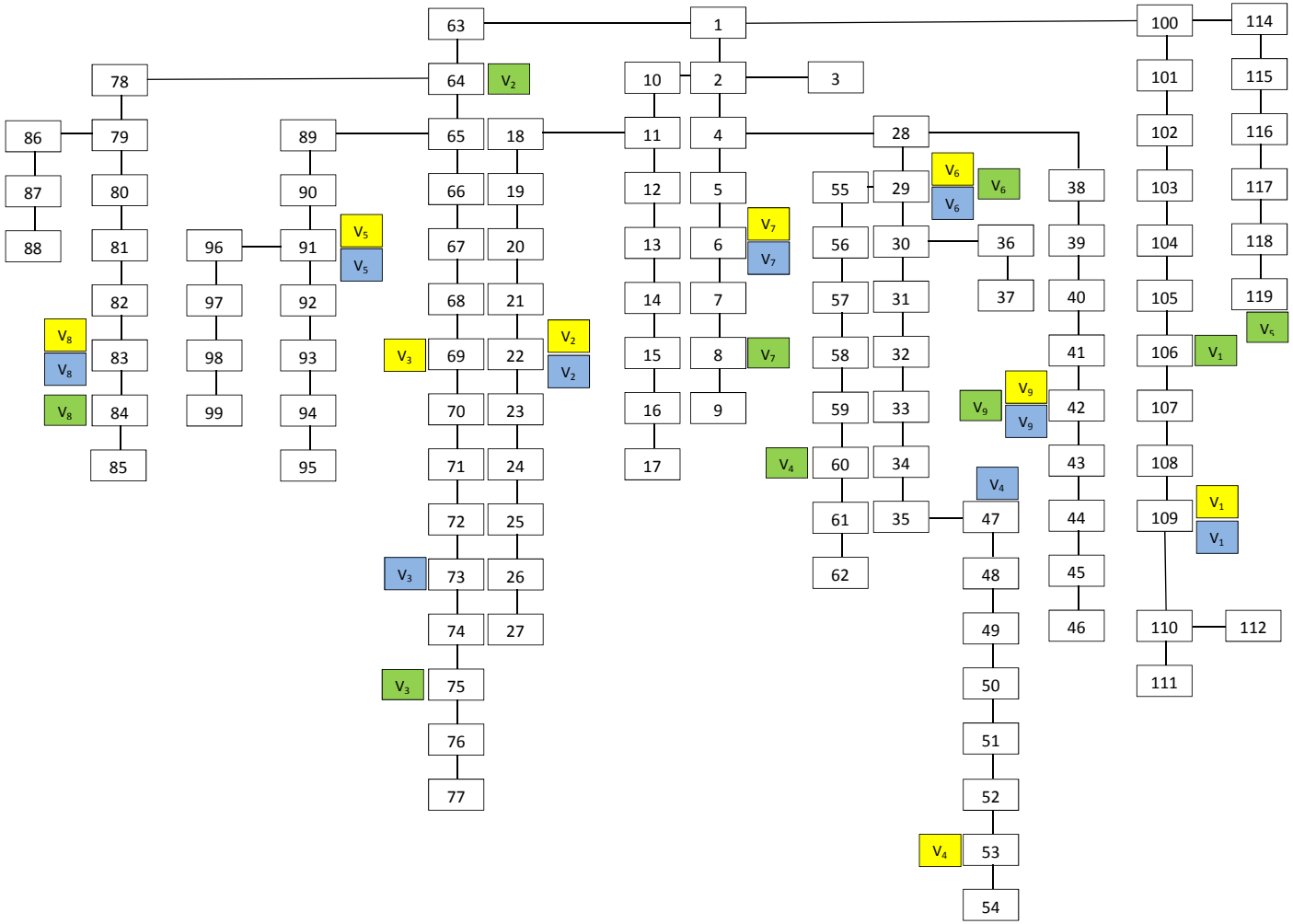

Figure 2.6: Optimal location of 9 VMMs in the 119-node test system using Algorithm 1 (yellow boxes), Algorithm 2 (blue boxes), and GA (green boxes).

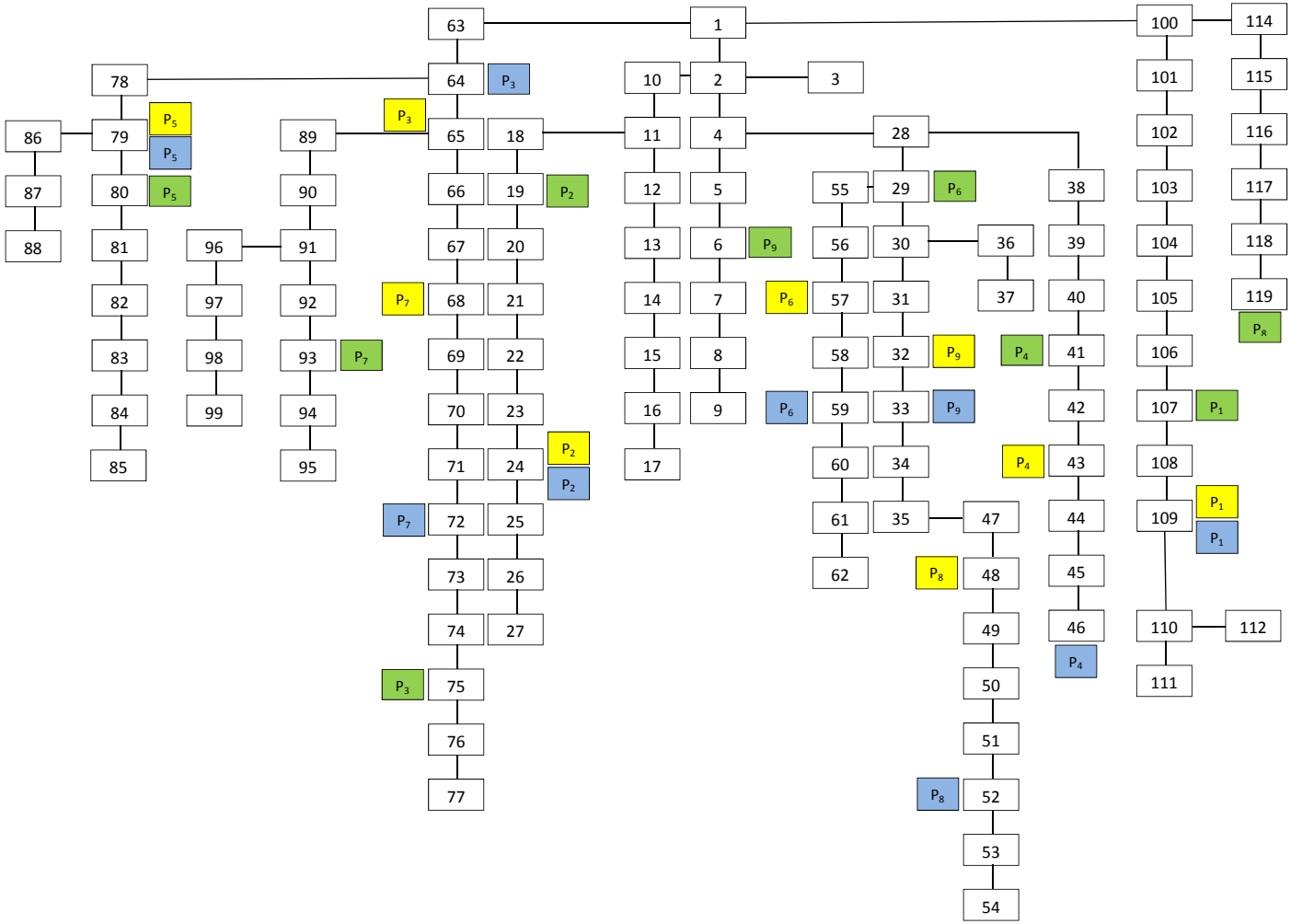

Figure 2.7: Optimal location of 9 PMUs in the 119-node test system using Algorithm 1 (yellow boxes), Algorithm 2 (blue boxes), and GA (green boxes).

2.5.4 Computational Cost

The number of objective function evaluations in Algorithm 1 is (slightly less than) KN per configuration. On the other hand, in the simulations conducted on all three test systems, Algorithm 2 always converged in less than 11 iterations (in the case of 33-node test system the algorithm often converged in 8 iterations). Therefore, the total number of function evaluations in Algorithm 2 is no more than $11KN$ per configuration. The interested reader is referred to [76] for a general upper bound on the number of function evaluations of Algorithm 2.

The number of function evaluations by GA is the number of populations times the number of generations which is equal to $200 \times 500 = 100000$ in our simulations. Therefore, Algorithm 1 always has the minimum computational cost. Moreover, based on the parameters used in our simulations and the size of the test systems, the number of function evaluations of Algorithm 2 is always less than $\frac{11\times10\times119}{200\times500} = 13\%$ of that of the GA.

To give an idea about the computational time of the proposed algorithms, the CPU time of the simulations are reported here. The simulations are performed on MATLAB using a computer with a processor of 3.4 GH and 4 GB of RAM. The CPU time for all the test systems were less than one minute for Algorithm 1, less than 4 minutes for Algorithm 2, and between 15 to 34 minutes for the GA.

2.5.5 Discussion

As shown in the numerical results over the three test systems, the submodular saturation algorithm outperforms the greedy algorithm in most cases and provides competitive results in other cases. These results are similar to the results reported in [76] where the submodular saturation algorithm outperforms the greedy algorithm for robust observation selection over various data sets.

The GA has several parameters to tune and its performance depends on these parameters. The submodular saturation algorithm, on the other hand, does not have any parameter to tune which makes it very favorable for an easy implementation. In many cases, the submodular saturation algorithm was capable of finding a better solution than GA even with a much less number of function evaluations. Therefore, the submodular saturation algorithm serves as a powerful tool for the meter placement problem in active distribution systems.

The meter placement problem in a reconfigurable distribution system is an NP-hard problem which does not admit any approximation guarantee [76]. Moreover, as shown in our numerical results, none of the algorithms beats others in all cases. Nonetheless, note that the meter placement problem is a design problem which has to be solved only once. Therefore, for a given test system and a given number of meters to be installed, one can compare the results of the submodular saturation algorithm with that of the greedy algorithm and GA to obtain the best placement.

2.6 Conclusion

In this chapter, we studied the problem of robust meter placement for state estimation in active distribution systems. The trace of the inverse of the FIM was chosen as criterion for the estimation accuracy. A robust meter placement algorithm, called submodular saturation algorithm, was proposed to optimize the worst case estimation accuracy among all possible configurations of the system. The results of the meter placement problem on three active distribution systems showed that the submodular saturation algorithm outperforms the greedy algorithm and the GA in most cases and provides competitive solutions in other cases. The numerical results presented show that a high level of accuracy in the state estimation task can be achieved with a much less number of PMUs than voltage magnitude

meters indicating the possible application of PMUs for state estimation in future smart grids.

Chapter 3

Distributed Storage Planning in Smart Distribution Grids

Distributed Storage Systems (DSS) are, conceptually, the storage units that can be installed on any node of the system independent of the location of the distributed generators. The DSS can play important roles in improving the performance of modern smart grids. These roles include coping with the inherent intermittence of non-dispatchable energy sources, enhancing the system resilience, reducing the possibility of energy curtailment, peak load shaving, energy price arbitrage, and power loss reduction. Toward achieving those goals in the most efficient way, it is crucial to find the best capacity, power rating, and location of DSS in the system. This chapter proposes a methodology for optimal DSS planning in smart distribution systems.

This chapter is organized as follows. Sec. 3.1 provides some review about the linearized power flow equations in distribution systems and a quadratic form for the loss function. Sec. 3.2 formulates the various financial gains due to installation of DSS in distribution systems. Sec. 3.3 presents a mixed-integer convex formulation of the problem of distributed storage planning in smart distribution systems. Sec. 3.4 provides the numerical results of the optimal DSS placement in a test system. Finally, Sec. 3.5 concludes the chapter.

3.1 Linearized Power Flow Equations and the Loss Function

Recall from Sec. 2.2.1 that the system voltages $\mathbf{v} = \mathbf{1} + \mathbf{e} + j\mathbf{f}$, can be found using linearized power flow equations in rectangular coordinates as:

$$\begin{bmatrix} \mathbf{p} \\ \mathbf{q} \end{bmatrix} - \begin{bmatrix} \mathbf{p}_{\mathrm{DG}} \\ \mathbf{q}_{\mathrm{DG}} \end{bmatrix} = \mathbf{A}^{-1} \begin{bmatrix} \mathbf{e} \\ \mathbf{f} \end{bmatrix} \tag{3.1}$$

where

$$\mathbf{A} = \begin{bmatrix} \tilde{\mathbf{G}} & -\tilde{\mathbf{B}} \\ -\tilde{\mathbf{B}} & -\tilde{\mathbf{G}} \end{bmatrix}^{-1}, \tag{3.2}$$

and $\tilde{\mathbf{G}}$ and $\tilde{\mathbf{B}}$ are, respectively, sub-matrices of the bus conductance and susceptance matrices corresponding to the non-slack nodes.

Using linearized power flow equations, the active power loss in the system can also be approximated as a quadratic function of power injections. To see this, let us first define the *net demand vector* $\mathbf{d}$ as:

$$\mathbf{d} = \begin{bmatrix} \mathbf{p} \\ \mathbf{q} \end{bmatrix} - \begin{bmatrix} \mathbf{p}_{\mathrm{DG}} \\ \mathbf{q}_{\mathrm{DG}} \end{bmatrix}. \tag{3.3}$$

Based on (3.3), the linearized equations (3.1) can be written in the following compact form:

$$\begin{bmatrix} \mathbf{e} \\ \mathbf{f} \end{bmatrix} = \mathbf{A}\mathbf{d}. \tag{3.4}$$

Using (3.4), one can show that the total active power loss in the system can be written as a quadratic function of the net demand vector. Particularly, if $L(\mathbf{d})$ is the total active power loss of the system as a function of the net demand vector,

then we have:

$$L(\mathbf{d}) = \frac{1}{2}\mathbf{d}'\mathbf{M}\mathbf{d}, \tag{3.5}$$

where

$$\mathbf{M} = 2\mathbf{A}' \begin{bmatrix} \tilde{\mathbf{G}} & \mathbf{0} \\ \mathbf{0} & \tilde{\mathbf{G}} \end{bmatrix} \mathbf{A}, \tag{3.6}$$

is a $2(N-1) \times 2(N-1)$ real matrix that depends merely on the bus conductance and bus susceptance matrices of the system. Note that since $\tilde{\mathbf{G}}$ is symmetric, $\mathbf{M}$ is symmetric too.

Eq. (3.5) can be established using the approach presented in [92]. For ease of notation define the augmented vectors $\hat{\mathbf{e}} = [0 \quad \mathbf{e}']'$, $\hat{\mathbf{f}} = [0 \quad \mathbf{f}']'$, and $\hat{\mathbf{p}} = [p_{\text{slack}}, p_2 - p_{\text{DG},2}, p_3 - p_{\text{DG},3}, \ldots, p_N - p_{\text{DG},N}]$. Also, let $\hat{\mathbf{i}}$ be the vector of current injections to the system. If the voltage of the slack node is 1 p.u., the active power loss in the system can be written as:

$$\begin{aligned}
L &= \mathbf{1}'\hat{\mathbf{p}} \\
&= \Re\{(\mathbf{1} + \hat{\mathbf{e}} + j\hat{\mathbf{f}})'\hat{\mathbf{i}}^*\} \\
&= \Re\{(\mathbf{1} + \hat{\mathbf{e}} + j\hat{\mathbf{f}})'[\mathbf{Y}(\mathbf{1} + \hat{\mathbf{e}} + j\hat{\mathbf{f}})]^*\} \\
&= \Re\{(\hat{\mathbf{e}} + j\hat{\mathbf{f}})'\mathbf{Y}^*(\hat{\mathbf{e}} - j\hat{\mathbf{f}})\} \qquad (3.7) \\
&= \Re\{(\hat{\mathbf{e}} + j\hat{\mathbf{f}})'(\mathbf{G} - j\mathbf{B})(\hat{\mathbf{e}} - j\hat{\mathbf{f}})\} \\
&= \hat{\mathbf{e}}'\mathbf{G}\hat{\mathbf{e}} + \hat{\mathbf{f}}'\mathbf{G}\hat{\mathbf{f}} \\
&= \mathbf{e}'\tilde{\mathbf{G}}\mathbf{e} + \mathbf{f}'\tilde{\mathbf{G}}\mathbf{f}, \qquad (3.8)
\end{aligned}$$

where (3.7) follows from the fact that $\mathbf{Y}^*\mathbf{1} = \mathbf{0}$ and $\mathbf{1}'\mathbf{Y}^* = \mathbf{0}$. This is because the shunt admittances are assumed to be zero. Note also that (3.8) follows directly from the definition of vectors $\hat{\mathbf{e}}$ and $\hat{\mathbf{f}}$ along with the partitioning of $\mathbf{G}$ as in (2.7).

Remark 3.1 *The shunt capacitors are assumed to be zero in the linearized power flow equations* (3.1)*. That is because the reactive power injected by shunt capacitors can be modeled as negative components in the reactive sub-vector of the net demand vector* $\mathbf{d}$*. As a result, in derivation of the quadratic form of the loss function in* (3.5)*, we considered* $\mathbf{Y}^*\mathbf{1} = \mathbf{0}$ *and* $\mathbf{1}'\mathbf{Y}^* = \mathbf{0}$*.*

Eq. (3.8) can be written in matrix form as:

$$L(\mathbf{e};\mathbf{f}) = \begin{bmatrix} \mathbf{e} \\ \mathbf{f} \end{bmatrix}' \begin{bmatrix} \tilde{\mathbf{G}} & \mathbf{0} \\ \mathbf{0} & \tilde{\mathbf{G}} \end{bmatrix} \begin{bmatrix} \mathbf{e} \\ \mathbf{f} \end{bmatrix}. \tag{3.9}$$

Eq. (3.5) then follows by substituting the the linearized power flow equations (3.4) into (3.9).

Using (3.5) and (3.6), it can be shown that the loss function $L(\mathbf{d})$ is convex in $\mathbf{d}$. Since $\nabla^2 L(\mathbf{d}) = \mathbf{M}$, the convexity of $L(\mathbf{d})$ can be established by demonstrating that $\mathbf{M}$ is positive semi-definite. To that end, first note that the system admittance matrix is positive semi-definite, that is $\mathbf{G} \succeq 0$. In [92], this has been shown using the fact that the active power loss in the system is non-negative for all values of the nodal voltages. Next, note that for a positive semi-definite matrix, all the principal submatrices have to be positive semi-definite. Therefore, it follows from the positive semi-definiteness of $\mathbf{G}$ that $\tilde{\mathbf{G}}$ is positive semi-definite, too. That is, for any $\boldsymbol{x} \in \mathbb{R}^{N-1}$, we have $\boldsymbol{x}'\tilde{\mathbf{G}}\boldsymbol{x} \geq 0$. Similarly, for any $\boldsymbol{x}$ and $\boldsymbol{y}$ belonging to $\mathbb{R}^{N-1}$ we have:

$$\begin{aligned} \begin{bmatrix} \boldsymbol{x} \\ \boldsymbol{y} \end{bmatrix}' \begin{bmatrix} \tilde{\mathbf{G}} & \mathbf{0} \\ \mathbf{0} & \tilde{\mathbf{G}} \end{bmatrix} \begin{bmatrix} \boldsymbol{x} \\ \boldsymbol{y} \end{bmatrix} &= \boldsymbol{x}'\tilde{\mathbf{G}}\boldsymbol{x} + \boldsymbol{y}'\tilde{\mathbf{G}}\boldsymbol{y} \\ &\geq 0. \end{aligned} \tag{3.10}$$

For any Hermitian, positive-definite matrix there exists a decomposition into the product of a lower triangular matrix and its conjugate transpose. This decomposition is called Cholesky decomposition or Cholesky factorization. Since $\tilde{\mathbf{G}}$ is symmetric and real, the following Cholesky decomposition exists:

$$\begin{bmatrix} \tilde{\mathbf{G}} & \mathbf{0} \\ \mathbf{0} & \tilde{\mathbf{G}} \end{bmatrix} = \mathbf{U}\mathbf{U}', \tag{3.11}$$

where $\mathbf{U}$ is a real, lower triangular matrix with positive diagonal entries. Therefore, for any $\mathbf{z} \in \mathbb{R}^{N-1}$, we have:

$$\begin{aligned} \mathbf{z}'\mathbf{M}\mathbf{z} &= 2\mathbf{z}'\mathbf{A}^T\mathbf{U}\mathbf{U}'\mathbf{A}\mathbf{z} \\ &= 2(\mathbf{U}'\mathbf{A}\mathbf{z})'(\mathbf{U}'\mathbf{A}\mathbf{z}) \\ &= 2\|\mathbf{U}'\mathbf{A}\mathbf{z}\|_2^2 \geq 0, \end{aligned} \tag{3.12}$$

which demonstrates that $\mathbf{M}$ is positive semi-definite.

To illustrate the effectiveness of the linearized power flow equations, we consider a modified version of the test system presented in [90]. For this system, inclined solar cells are considered on half of the nodes selected randomly. Moreover, two wind turbines are installed on the nodes 21 and 50 with power ratings of 400 kW and 800 kW, respectively. Real data of the loads, wind and solar generations are exploited for this illustration. Details about the test system and the real data used will be provided in Sec. 3.4. All the numbers reported here are obtained by simulating the system for 535 days, 24 hours each, with a total number of simulations equal to $535 \times 24 = 12840$. For each simulation, the error of the linearized power flow equations is computed in comparison with the Newton's AC Power Flow (ACPF) based on five different metrics. These metrics are Average Magnitude Error (AME)

in p.u., Average Angle Error (AAE) in degrees, Maximum Magnitude Error (MME) in p.u., Maximum Angle Error (MAE) in degrees, and Normalized Loss Error (NLE). In particular, these metrics are defined as follows:

$$\begin{aligned}
\text{AME} &= \frac{1}{N}\sum_{n=1}^{N}\Big||v_{n,\text{lin}}| - |v_{n,\text{ACPF}}|\Big| \\
\text{AAE} &= \frac{1}{N}\sum_{n=1}^{N}\Big|\angle v_{n,\text{lin}} - \angle v_{n,\text{ACPF}}\Big| \\
\text{MME} &= \max_{n}\Big||v_{n,\text{lin}}| - |v_{n,\text{ACPF}}|\Big| \\
\text{MAE} &= \max_{n}\Big|\angle v_{n,\text{lin}} - \angle v_{n,\text{ACPF}}\Big| \\
\text{NLE} &= \frac{\Big|L_{\text{lin}} - L_{\text{ACPF}}\Big|}{L_{\text{ACPF}}},
\end{aligned} \tag{3.13}$$

where the subscript *lin* indicates the solution of the linearized power flow equations. For the test system under study and using the real data of loads, wind, and solar generation, the AME and AAE indexes averaged over all simulations are 3.84×10^{-4} p.u. and 1.04×10^{-3} degrees, respectively. Also, the MME and MAE indexes averaged over all simulations turn out to be 1.45×10^{-3} p.u. and 9.31×10^{-3} degrees, respectively. Moreover, the NLE averaged over all simulations turns out to be 3.05%. These numbers show that the linearized power flow equations can provide good approximations in terms of nodal voltages and system power losses.

Fig. 3.1 illustrates the magnitudes and angles of the system voltages obtained from linearized equations and ACPF and by using real data of loads, wind, and solar power. The voltages plotted in this figure correspond to the peak hour of a typical day of light loading. As it can be seen from this figure, the voltages obtained from linearized power flow equations match that of the ACPF very well. Also, Fig. 3.2 depicts the magnitude and angles of the system voltages obtained using linearized

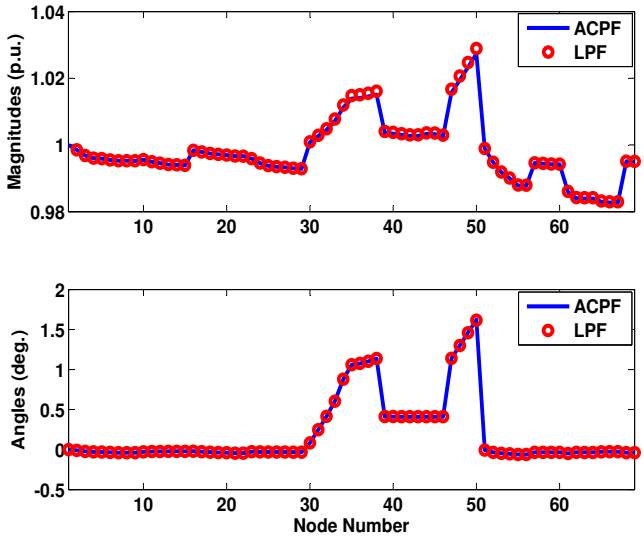

Figure 3.1: Magnitudes and angles of the nodal voltages in the test system obtained using linearized power flow equations and ACPF for the peak hour of a typical day with light loading.

power flow equations and ACPF for peak hour of a typical day of high loading. Although the linearized power flow equations introduce a higher error in this case, they still provide a good approximation compared with the ACPF.

3.2 Formulation of the Economic Gains of the Distributed Storage Systems

This section formulates the various economic gains of the DSS for smart distribution grids. Due to the stochasticity of the load, wind and solar generations, the expected economic gain of the SGO due to installation of storage units is considered. Similarly to [58] and [93], it is assumed that the storage units are charged and discharged once a day. Therefore, for each day there is one charging cycle corresponding to off-peak hours and one discharging cycle corresponding to peak hours.

In the proposed methodology for optimal DSS planning, the planning horizon

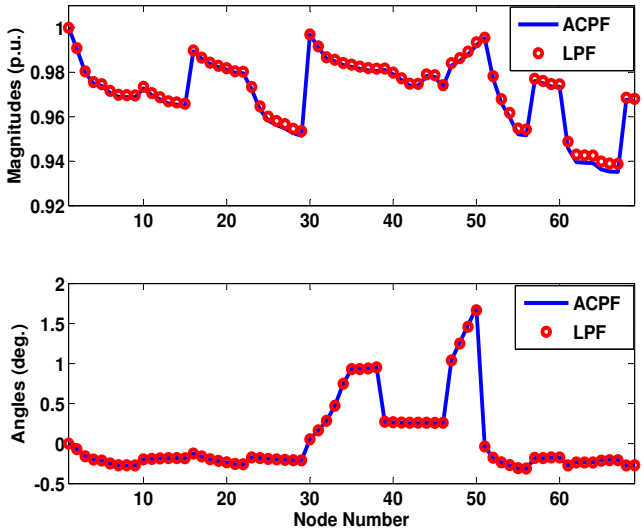

Figure 3.2: Magnitudes and angles of the nodal voltages in the test system obtained using linearized power flow equations and ACPF for the peak hour of a typical day with high loading.

consists of Y years and each year is divided into S segments. For hour h of segment s, let $\mathbf{p}_{s,h}^{\text{DSS}}$ be the vector of charging/discharging powers by the storage units installed in the system. Even though $\mathbf{p}_{s,h}^{\text{DSS}}$ is a $2(N-1) \times 1$ vector, throughout this chapter it is assumed that the DSS are operated in a way that they only absorb and inject active power. Therefore, it is implicitly assumed that the last $N-1$ elements of $\mathbf{p}_{s,h}^{\text{DSS}}$ are zero for all s and h. If a node is not equipped with a storage unit, the formulation trivially requires the active powers to be zero at all time. In general, the charging/discharging strategy of each storage unit can be optimized not only for each hour and each segment, but also for each year. However, we restrict ourselves to the case where the optimized strategy for each hour and segment remains the same for all years. That is because even though the load and renewable generations grow over years, the capacity of the DSS remains fixed for the whole planning horizon. Nonetheless, the proposed methodology can simply accommodate the case where the DSS strategy is optimized for each year, in addition to optimizing for each hour

and each segment. We will denote the operation strategy of the DSS in the sth segment of each year by

$$\boldsymbol{\pi}_s = \begin{bmatrix} \mathbf{p}_{s,1}^{\text{DSS}} \\ \mathbf{p}_{s,2}^{\text{DSS}} \\ \vdots \\ \mathbf{p}_{s,24}^{\text{DSS}} \end{bmatrix}. \tag{3.14}$$

Also, the matrix of DSS operation strategies for the whole planning horizon will be denoted by $\mathbf{\Pi} = [\boldsymbol{\pi}_1, \boldsymbol{\pi}_2, \ldots, \boldsymbol{\pi}_{\mathsf{S}}]$.

3.2.1 The Arbitrage Gain

To evaluate the arbitrage gain of the SGO due to installation of DSS, a Time of Use (ToU) pricing scheme is considered in this chapter. Let $\eta_{s,h}^{y}$ be the price of electricity per kWh at hour h of the sth segment of the yth year of the planning horizon. The average arbitrage gain in the yth year can be written as:

$$\Gamma_y^{\text{arb}}(\mathbf{\Pi}) = \frac{365}{\mathsf{S}} \sum_{s=1}^{\mathsf{S}} \left\{ \sum_{h \in \mathcal{H}_p} \eta_{s,h}^{y} \mathbf{1}' \mathbf{p}_{s,h}^{\text{DSS}} - \sum_{h \in \mathcal{H}_o} \eta_{s,h}^{y} \mathbf{1}' \mathbf{p}_{s,h}^{\text{DSS}} \right\}, \tag{3.15}$$

where $\mathcal{H}_p$ is the set of candidate discharging hours (peak hours) and

$$\mathcal{H}_o = \{1, 2, \ldots, 24\} \setminus \mathcal{H}_p$$

is the set of candidate charging hours (off-peak hours). Observe from (3.15) that the average arbitrage gain of the SGO is linear in $\mathbf{\Pi}$.

3.2.2 The Expected Reduction in Active Power Loss

In this section, the expected economic gain of the SGO due to reduction in the active power loss is formulated. The expected daily power loss of the system in the sth

segment of the yth year as a funciton of the DSS operation strategy can be written as:

$$\mathbb{E}\left\{\sum_{h=1}^{24} \mathrm{L}_{s,h}^{y}\left(\mathbf{p}_{s,h}^{\text{DSS}}\right)\right\} = \sum_{h\in\mathcal{H}_o} \mathbb{E}\left\{L\left(\mathbf{d}_{s,h}^{y} + \mathbf{p}_{s,h}^{\text{DSS}}\right)\right\} + \sum_{h\in\mathcal{H}_p} \mathbb{E}\left\{L\left(\mathbf{d}_{s,h}^{y} - \mathbf{p}_{s,h}^{\text{DSS}}\right)\right\}, \tag{3.16}$$

where the $L(\cdot)$ function is defined in (3.5) and $\mathbb{E}\{\cdot\}$ denotes the expectation operator. Here, $\mathbf{d}_{s,h}^{y}$ is the vector of stochastic net demands at hour h of the sth segment of the yth year. Expanding (3.16) using (3.5) and considering the ToU pricing scheme, the expected daily cost due to the active power loss in the sth segment of the yth year can be written as:

$$\begin{aligned}\mathbb{E}\left\{\sum_{h=1}^{24} \eta_{s,h}^{y}\mathrm{L}_{s,h}^{y}\left(\mathbf{p}_{s,h}^{\text{DSS}}\right)\right\} = \frac{1}{2}\sum_{h=1}^{24} \eta_{s,h}^{y}\left[\mathbf{p}_{s,h}^{\text{DSS}}\right]'\mathbf{M}\left[\mathbf{p}_{s,h}^{\text{DSS}}\right] + \sum_{h\in\mathcal{H}_o} \eta_{s,h}^{y}[\bar{\mathbf{d}}_{s,h}^{y}]'\mathbf{M}\ \mathbf{p}_{s,h}^{\text{DSS}} \\ - \sum_{h\in\mathcal{H}_p} \eta_{s,h}^{y}[\bar{\mathbf{d}}_{s,h}^{y}]'\mathbf{M}\ \mathbf{p}_{s,h}^{\text{DSS}} + \sum_{h=1}^{24} \eta_{s,h}^{y} c_{s,h}^{y},\end{aligned} \tag{3.17}$$

where $\bar{\mathbf{d}}_{s,h}^{y} = \mathbb{E}\left\{\mathbf{d}_{s,h}^{y}\right\}$, and

$$\begin{aligned} c_{s,h}^{y} &= \mathbb{E}\left\{\mathrm{L}_{s,h}^{y}\left(\mathbf{0}\right)\right\} \\ &= \frac{1}{2}\mathbb{E}\left\{[\mathbf{d}_{s,h}^{y}]'\ \mathbf{M}\ [\mathbf{d}_{s,h}^{y}]\right\}, \end{aligned} \tag{3.18}$$

is the expected hourly power loss in the sth segment of the yth year when no DSS is installed in the system.

Leveraging the LLN, it is possible to use the real data of the loads and renewable generations to approximate $\bar{\mathbf{d}}_{s,h}^{y}$ with the empirical mean which is an unbiased estimator. Let $d_{s,h}^{0}(l)$ be the lth random element of the net demand vector $\mathbf{d}_{s,h}^{0}$ at the first year. Also, assume that at the planning time a total number of K_s real data

points of the load and renewable generation is available for each hour of segment s. With slight abuse of notation, let $d^0_{s,h}(l,k)$ be the kth measured data corresponding to the lth element of the net demand vector at hour h and segment s. Then, based on LLN, $\bar{d}^0_{s,h}(l)$ can be approximated as:

$$\bar{d}^0_{s,h}(l) = \mathbb{E}\{d^0_{s,h}(l)\} \approx \frac{1}{K_s}\sum_{k=1}^{K_s} d^0_{s,h}(l,k). \tag{3.19}$$

In a similarly way, one can approximate the expected hourly power loss in the system when no DSS is installed. Note, however, that computation of $c^y_{s,h}$ is not necessary for the optimal DSS placement problem as will be explained soon. Nonetheless, the relevant details are provided here for completeness. Using real data of loads and renewable generation, the expected hourly power loss at the planning year can be approximated as:

$$\begin{aligned} c^0_{s,h} &= \frac{1}{2}\mathbb{E}\left\{[\mathbf{d}^0_{s,h}]'\ \mathbf{M}\ [\mathbf{d}^0_{s,h}]\right\} \\ &= \frac{1}{2}\sum_{l=1}^{2(N-1)}\sum_{r=1}^{2(N-1)} m_{l,r}\mathbb{E}\left\{d^0_{s,h}(l)d^0_{s,h}(r)\right\} \\ &\approx \frac{1}{2K_s}\sum_{l=1}^{2(N-1)}\sum_{r=1}^{2(N-1)}\sum_{k=1}^{K_s} m_{l,r}d^0_{s,h}(l,k)d^0_{s,h}(r,k) \end{aligned} \tag{3.20}$$

where $m_{l,r}$ is the (l,r) element of $\mathbf{M}$.

Computation of the above-mentioned expectations for the whole planning horizon requires the statistics of the vector of stochastic net demands in future years. This can be computed based on its current statistics as well as the anticipated growth rate of the load and renewable generations. Let the net demand data points at the planning time be decomposed as $d^0_{s,h}(l,k) = d^{0,\text{load}}_{s,h}(l,k) - d^{0,\text{DG}}_{s,h}(l,k)$, corresponding to the load and DGs. Assume a fixed annual growth rate of γ_{load} and

γ_{DG} for the the load and renewable generation, respectively. Then $\bar{\mathbf{d}}^{y}_{s,h}$ and $c^{y}_{s,h}$ for $y \geq 1$ can be computed by (3.19) and (3.20), respectively, with $d^{0}_{s,h}(l,k)$ replaced by $d^{y}_{s,h}(l,k) = [\gamma_{\mathrm{load}}]^{y} d^{0,\mathrm{load}}_{s,h}(l,k) - [\gamma_{\mathrm{DG}}]^{y} d^{0,\mathrm{DG}}_{s,h}(l,k)$.

Finally, the expected economic gain of SGO due to the reduction in the active power loss in the yth year of the planning horizon is given by:

$$\Gamma^{\mathrm{loss}}_{y}(\mathbf{\Pi}) = \frac{365}{\mathsf{S}} \sum_{s=1}^{\mathsf{S}} \sum_{h=1}^{24} \eta^{y}_{s,h} c^{y}_{s,h} - \mathbb{E}\left\{ \sum_{h=1}^{24} \eta^{y}_{s,h} \mathrm{L}^{y}_{s,h}\left(\mathbf{p}^{\mathrm{DSS}}_{s,h}\right) \right\}. \tag{3.21}$$

Observe from (3.21) and (3.17) that the terms corresponding to $c^{y}_{s,h}$ cancel out in $\Gamma^{\mathrm{loss}}_{y}$. Therefore, $\Gamma^{\mathrm{loss}}_{y}$ contains only quadratic and linear terms of $\mathbf{\Pi}$. This is indeed expected as $\Gamma^{\mathrm{loss}}_{y}(\mathbf{0})$ should be equal to zero. In other words, when no DSS is installed in the system, there will be no economic gain. Also note that the Hessian of $\Gamma^{\mathrm{loss}}_{y}(\mathbf{\Pi})$ with respect to $\mathbf{\Pi}$ is equal to $\frac{-1}{\mathsf{S}} \times \mathbf{diag}\{\eta^{y}_{1,1}\mathbf{M}, \eta^{y}_{2,1}\mathbf{M}, \ldots, \eta^{y}_{\mathsf{S},1}\mathbf{M}, \ldots, \eta^{y}_{\mathsf{S},24}\mathbf{M}\}$, which is negative semi-definite, because $\mathbf{M} \succeq 0$ and $\eta^{y}_{s,h} > 0, \forall h, \forall s, \forall y$. Therefore, $\Gamma^{\mathrm{loss}}_{y}(\mathbf{\Pi})$ is concave in $\mathbf{\Pi}$.

3.2.3 The Reduction in Expected Price of Renewable Energy Curtailed

Due to the intermittent nature of renewable energy sources, there may be times that the total generation of the renewable sources exceeds the total demand of the system. In such cases, the excess generation can flow to the sub-transmission system as long as the system constraints are satisfied. However, at times when the system constraints are about to be violated due to excess distributed generation, the SGO may have to curtail the renewable generation. Such a case, particularly, happens when high amounts of non-dispatchable generation causes over-voltage problems in the system. In contrast, if the system is equipped with DSS, they can be optimally

operated so as to improve the voltage profile and reduce the chance of over-voltage problems. As a result, in addition to the gains that the SGO obtains due to price arbitrage and reduction in the power loss, it may also benefit from reduction in the renewable energy spillage [25]. It is, however, difficult to explicitly formulate the expected economic value of the spilled energy as a function of the amount of DSS installed and their operation strategy. Instead, an indirect approach is taken in this chapter. Here, we regularize the objective function of the DSS placement with a virtual term associated with the improvement in the voltage profile. With this virtual benefit included in the objective function, the DSS placement routine will try to avoid the violation of voltage constraints. Therefore, the resulting DSS placement and strategy is expected to lower the amount of spilled energy. Once the storage units are optimally placed in the system and their operation strategy is optimized, the expected economic value of the spilled energy can be approximated through Monte Carlo simulations. To that end, a power flow method is performed for each hour of the available dataset to see if any of the constraints are violated in the system with and without DSS. If so, an optimal curtailment strategy will be used to find the minimum amount of renewable energy that needs to be curtailed, as will be explained later in this section. Finally, the expected gain in the price of energy curtailed will be approximated based on LLN. The average economic gain because of lower energy curtailment due to installation of DSS in year y will be denoted by $\Gamma_y^{\text{curt}}(\mathbf{\Pi})$.

To formulate the regularized objective function, first note that in distribution systems the imaginary part of the voltages are very small (the voltage angles are very small). Therefore, one can approximate the magnitude of the nodal voltages by their real parts. As a result, the total expected deviation in the real parts of the nodal voltages, with respect to the flat voltage profile, can serve as an index

for evaluation of the voltage profile. Now consider the following partitioning for the matrix $\mathbf{A}$ defined in (2.9):

$$\mathbf{A} = \begin{bmatrix} \mathbf{A_e} \\ \mathbf{A_f} \end{bmatrix}. \tag{3.22}$$

where $\mathbf{A_e}$ and $\mathbf{A_f}$ are $(N-1) \times 2(N-1)$ matrices corresponding to the real and imaginary parts, respectively. Let $\mathbf{e}^y_{s,h}(\mathbf{p}^{\text{DSS}}_{\mathbf{s,h}})$ be the vector of deviations in the real parts of the nodal voltages at hour h, segment s, and year y. Similarly to the way that the expected reduction in the power loss was computed in Sec. 3.2.2, the average improvement in the voltage profile during the planning horizon due to installation of DSS can be formulated as:

$$\begin{aligned}
\Gamma^{\text{vol}}(\mathbf{\Pi}) &= \frac{365}{\mathsf{SY}} \sum_{s,y} \mathbb{E}\left\{ \sum_{h=1}^{24} \left\|\mathbf{e}^y_{s,h}(\mathbf{0})\right\|^2 - \left\|\mathbf{e}^y_{s,h}(\mathbf{p}^{\text{DSS}}_{s,h})\right\|^2 \right\} \\
&= \frac{-1}{\mathsf{SY}} \sum_{s,y} \sum_{h=1}^{24} \left[\mathbf{p}^{\text{DSS}}_{s,h}\right]' \mathbf{A}'_{\mathbf{e}} \mathbf{A_e} \left[\mathbf{p}^{\text{DSS}}_{s,h}\right] + 2 \sum_{h \in \mathcal{H}_o} \left[\bar{\mathbf{d}}^y_{s,h}\right]' \mathbf{A}'_{\mathbf{e}} \mathbf{A_e} \left[\mathbf{p}^{\text{DSS}}_{s,h}\right] \\
&\qquad - 2 \sum_{h \in \mathcal{H}_p} [\bar{\mathbf{d}}^y_{s,h}]' \mathbf{A}'_{\mathbf{e}} \mathbf{A_e} \left[\mathbf{p}^{\text{DSS}}_{s,h}\right].
\end{aligned} \tag{3.23}$$

In (3.23), $\bar{\mathbf{d}}^y_{s,h}$ can be approximated using LLN as in (3.19). Observe that the Hessian of $\Gamma^{\text{vol}}(\mathbf{\Pi})$ with respect to $\mathbf{\Pi}$ is equal to $\frac{-2}{\mathsf{SY}} \times \mathbf{diag}\{\mathbf{A}'_{\mathbf{e}}\mathbf{A_e}, \mathbf{A}'_{\mathbf{e}}\mathbf{A_e}, \ldots, \mathbf{A}'_{\mathbf{e}}\mathbf{A_e}\}$ which is negative semi-definite, because $\mathbf{A}'_{\mathbf{e}}\mathbf{A_e} \succeq 0$ by structure. Therefore, $\Gamma^{\text{vol}}(\mathbf{\Pi})$ is concave in the operation strategy of the DSS.

Once the optimal DSS planning strategy is obtained for the system, the expected price of renewable energy curtailed will be computed for the system with and without DSS. Without loss of generality, assume that the wind turbines are candidates of energy curtailment as they are more likely to be utility-owned. Nonetheless, the formulation presented in this part can simply accommodate the curtailment of solar generation as well. Using linearized power flow equations, the optimal curtailment

strategy seeking the minimum power curtailment to satisfy the system constraints, can be formulated as:

$$\min \ \mathbf{1}'\mathbf{p}^{\text{curt}} \tag{3.24}$$

subject to.

$$\mathbf{0} \leq \mathbf{p}^{\text{curt}} \leq \mathbf{p}^{\text{wind}} \tag{3.25}$$

$$\mathbf{v}^{min} \leq \mathbf{A_e}(\mathbf{d} + \mathbf{p}^{\text{curt}}) \leq \mathbf{v}^{max} \tag{3.26}$$

$$|I_l(\mathbf{p}^{\text{curt}})|^2 \leq |I_l^{\max}|^2, \qquad l = 1, 2, \ldots, L, \tag{3.27}$$

where $\mathbf{p}^{\text{curt}}$ is the vector of curtailed powers and $\mathbf{p}^{\text{wind}}$ is the vector of power generations by wind turbines. Also, $\mathbf{v}^{min}$ and $\mathbf{v}^{max}$ are the vector of minimum and maximum allowable voltage limits, respectively. Here, $\mathbf{d}$ is the vector of forecast total demand of the nodes for the next hour. In (3.27), $|I_l|$ is the magnitude of the current flowing in branch l, $I_l^{\max}$ is the ampacity of branch l, and L is the total number of branches in the system. It is possible to leverage the linearized power flow equations to approximate the magnitude of the currents as follows:

$$|I_l(\mathbf{p}^{\text{curt}})|^2 = (\mathbf{d} + \mathbf{p}^{\text{curt}})'\mathbf{T}_l(\mathbf{d} + \mathbf{p}^{\text{curt}}), \tag{3.28}$$

where $\mathbf{T}_l$ is a positive semi-definite matrix. Therefore, (3.27) is indeed a convex constraint in $\mathbf{p}^{\text{curt}}$. Since the constraints (3.25) and (3.26) are also convex, problem (3.24) is convex. Note, however, that due to the inherent approximation of the linearized power flow equations, the solution of (3.24) is a rough estimate of the curtailed powers. To find an accurate solution, one can solve (3.24) for coarse tuning the curtailed powers and then do grid search along with ACPF to fine tune the results.

To derive the quadratic form of (3.28) for the magnitude of the currents, let $\boldsymbol{i} = \boldsymbol{i}_{\text{re}} + j\boldsymbol{i}_{\text{im}}$ be the vector of currents in the branches of the system. Also, let $\mathbf{Y}_{\text{br}}$ be the branch admittance matrix of the system. Then the vector of branch currents corresponding to the total demand of $\mathbf{d} + \mathbf{p}^{\text{curt}}$ is given by:

$$\begin{aligned}
\boldsymbol{I} &= \mathbf{Y}_{\text{br}}(\mathbf{1} + \hat{\mathbf{e}} + j\hat{\mathbf{f}}) \\
&= \mathbf{Y}_{\text{br}}(\hat{\mathbf{e}} + j\hat{\mathbf{f}}) && (3.29) \\
&= \tilde{\mathbf{Y}}_{\text{br}}(\mathbf{e} + j\mathbf{f}) \\
&= (\tilde{\mathbf{G}}_{\text{br}}\mathbf{e} - \tilde{\mathbf{B}}_{\text{br}}\mathbf{f}) + j(\tilde{\mathbf{G}}_{\text{br}}\mathbf{f} + \tilde{\mathbf{B}}_{\text{br}}\mathbf{e}) \\
&= \big[(\tilde{\mathbf{G}}_{\text{br}}\mathbf{A}_{\mathbf{e}} - \tilde{\mathbf{B}}_{\text{br}}\mathbf{A}_{\mathbf{f}}) + j(\tilde{\mathbf{G}}_{\text{br}}\mathbf{A}_{\mathbf{f}} + \tilde{\mathbf{B}}_{\text{br}}\mathbf{A}_{\mathbf{e}})\big](\mathbf{d} + \mathbf{p}^{\text{curt}}) \\
&= \mathbf{T}^{\text{re}}(\mathbf{d} + \mathbf{p}^{\text{curt}}) + j\mathbf{T}^{\text{im}}(\mathbf{d} + \mathbf{p}^{\text{curt}}), && (3.30)
\end{aligned}$$

where again $\hat{\mathbf{e}}$ and $\hat{\mathbf{f}}$ are the augmented voltage deviation vectors and $\mathbf{T}^{\text{re}}$ and $\mathbf{T}^{\text{im}}$ are defined as follows:

$$\mathbf{T}^{\text{re}} = \tilde{\mathbf{G}}_{\text{br}}\mathbf{A}_{\mathbf{e}} - \tilde{\mathbf{B}}_{\text{br}}\mathbf{A}_{\mathbf{f}}, \tag{3.31}$$

$$\mathbf{T}^{\text{im}} = \tilde{\mathbf{G}}_{\text{br}}\mathbf{A}_{\mathbf{f}} + \tilde{\mathbf{B}}_{\text{br}}\mathbf{A}_{\mathbf{e}}. \tag{3.32}$$

Also, $\tilde{\mathbf{Y}}_{\text{br}} = \tilde{\mathbf{G}}_{\text{br}} + j\tilde{\mathbf{B}}_{\text{br}}$ is the branch admittance matrix with the first column removed. Moreover, (3.29) stems from the fact that $\mathbf{Y}_{\text{br}}\mathbf{1} = \mathbf{0}$. Let $\mathbf{t}'_{\text{re},l}$ and $\mathbf{t}'_{\text{im},l}$ be the lth row of $\mathbf{T}^{\text{re}}$ and $\mathbf{T}^{\text{im}}$, respectively. Then, the magnitude of the currents in the branches of the system as a function of the curtailment vector $\mathbf{p}^{\text{curt}}$ will be

given by:

$$
\begin{aligned}
|I_l(\mathbf{p}^{\text{curt}})|^2 &= \left(\mathbf{t}'_{\text{re},l}(\mathbf{d}+\mathbf{p}^{\text{curt}})\right)^2 + \left(\mathbf{t}'_{\text{im},l}(\mathbf{d}+\mathbf{p}^{\text{curt}})\right)^2 \\
&= (\mathbf{d}+\mathbf{p}^{\text{curt}})'\mathbf{t}_{\text{re},l}\mathbf{t}'_{\text{re},l}(\mathbf{d}+\mathbf{p}^{\text{curt}}) + (\mathbf{d}+\mathbf{p}^{\text{curt}})'\mathbf{t}_{\text{im},l}\mathbf{t}'_{\text{im},l}(\mathbf{d}+\mathbf{p}^{\text{curt}}) \\
&= (\mathbf{d}+\mathbf{p}^{\text{curt}})'\mathbf{T}_l(\mathbf{d}+\mathbf{p}^{\text{curt}}),
\end{aligned} \tag{3.33}
$$

where

$$
\mathbf{T}_l = \mathbf{t}_{\text{re},l}\mathbf{t}'_{\text{re},l} + \mathbf{t}_{\text{im},l}\mathbf{t}'_{\text{im},l}. \tag{3.34}
$$

Note that the matrices $\mathbf{t}_{\text{re},l}\mathbf{t}'_{\text{re},l}$ and $\mathbf{t}_{\text{im},l}\mathbf{t}'_{\text{im},l}$ are positive semi-definite by structure. Therefore, $\mathbf{T}_l$ is positive semi-definite, too.

3.2.4 The Improvement in the System Resilience

In this section the economic value of the DSS in terms of improving the system resilience is formulated.

Let $\mathcal{H}_o(h) \in \mathcal{H}_o$ be the set of off-peak hours from the beginning of the off-peak period up to the hour h. Similarly, let $\mathcal{H}_p(h) \in \mathcal{H}_p$ be the set of peak hours from the beginning of the peak period up to the hour h. Also, let $0 < \beta_{ch} < 1$ and $0 < \beta_{dis} < 1$ be the charging and discharging efficiencies of the DSS technology used, respectively. Hence, $\beta_{rt} = \beta_{ch}\beta_{dis} < 1$ is the round-trip efficiency of the storage units. Denote the total energy that the DSS can supply to the grid in segment s and at the end of hour h by $\mathcal{E}_{s,h}(\mathbf{\Pi})$. Since $\mathcal{E}_{s,h}$ is equal to the total energy stored in the storage units times β_{dis}, one can write:

$$
\mathcal{E}_{s,h} = \begin{cases} \beta_{rt} \sum_{h' \in \mathcal{H}_o(h)} \mathbf{1}'\mathbf{p}^{\text{DSS}}_{s,h'}, & h \in \mathcal{H}_o \\ \\ \beta_{rt} \sum_{h' \in \mathcal{H}_o} \mathbf{1}'\mathbf{p}^{\text{DSS}}_{s,h'} - \sum_{h' \in \mathcal{H}_p(h)} \mathbf{1}'\mathbf{p}^{\text{DSS}}_{s,h'}, & h \in \mathcal{H}_p \end{cases}
$$

Upon imposing appropriate charging/discharging constraints, as will be done in Sec. 3.3, $\mathcal{E}_{s,h}$ is guaranteed to be non-negative. In the event that the primary supply of the system is interrupted, the distribution system may be operated as an islanded microgrid [27, 94, 95]. In such a case, the local DGs as well as the energy stored in the DSS can supply the loads of the system for a limited time. The non-critical loads of the system may need to be shed depending on the availability of the energy by local sources [96]. Therefore, $\mathcal{E}_{s,h}$ can be viewed as the additional amount of load that can be preserved each time the supply from the primary source has failed. In distribution systems, the System Average Interruption Frequency Index (SAIFI) measures the average number of power interruptions a customer experiences during one year. Let $\bar{\mu}_y$ be the expected interruption cost per 1 kWh of energy in year y of the planning horizon. In practice, the interruption cost per unit kWh is a function of the interruption duration as well [97]. However, one can use the Customer Average Interruption Duration Index (CAIDI) to find an approximate value for the expected interruption cost. Let $\xi_{s,h}$ be the fraction of the interruptions that occur at hour h during segment s of each year, see [97]. The average economic value of the DSS in terms of enhancing the resilience of the system can be approximated as:

$$\Gamma_y^{\text{res}}(\mathbf{\Pi}) = \bar{\mu}_y \times \text{SAIFI} \times \sum_h \sum_s \xi_{s,h} \mathcal{E}_{s,h}. \tag{3.35}$$

Note that $\Gamma_y^{\text{res}}(\mathbf{\Pi})$ is linear in $\mathcal{E}_{s,h}$ and, hence, in $\mathbf{\Pi}$.

3.2.5 The Economic Gain of the System Upgrade Deferral

Due to the constant load growth in distribution systems, the system will require an upgrade in the feeder ampacities and substation capacity at some point in the future. However, if DSS are installed in the system, they can be employed to shave the load at peak hours and thereby defer the required upgrade of the system [31, 32].

In order to defer the upgrade of the system, the objective function of the DSS placement can include a term to shave the peak load in the system. To that end, form the expected total active power drawn from the substation during peak hours as:

$$P_{s,h}^{\text{peak}}(\mathbf{\Pi}) = \mathbb{E}\{[\mathbf{1}' \;\; \mathbf{0}'](\mathbf{d}_{s,h}^{\mathsf{Y}} - \mathbf{p}_{s,h}^{\text{DSS}})\}, \qquad \forall s, h \in \mathcal{H}_p, \tag{3.36}$$

where $\mathbf{1}$ and $\mathbf{0}$ are of size $(N-1) \times 1$. The optimization routine will try to lower the maximum of $P_h^{\text{peak}}(\mathbf{\Pi})$ over peak hours as will be explained in the next section. Note that the expected total load in (3.36) has been computed for the last year of the planning horizon because the last year is supposed to have the maximum demand.

Once the DSS is optimally planned in the system, the economic gain of deferring the system upgrade due to installation of DSS will be computed. As per common practice of distribution system planning, the system constraints have to be satisfied for all combinations of the load and distributed generation. To evaluate the latest possible time for the system upgrade, the histograms of the available real data are examined to find the maximum values of the load and minimum values of the distributed generation based a predetermined confidence interval. These extremums are then scaled based on the given annual growth for the load and distributed generation (see Sec. 3.2.2) to estimate the extremums of all the years of the planning horizon. Then, for each year of the planning horizon a power flow is run according to the the extreme loading and generation to find the required ampacity of the feeders and substations. Then, the upgrade requirements of the feeders and substation of the system are calculated for the system with and without DSS [31]. Finally, the average yearly difference in the system upgrade cost for the yth year, denoted by $\Gamma_y^{\text{up}}(\mathbf{\Pi})$, is computed.

3.3 The Optimal Distributed Storage Planning Problem

This section aims at formulating the optimal DSS planning problem in smart distribution grids. To that end, the *regularized* expected discounted gain of the SGO due to installation of DSS is defined as:

$$\Gamma'(\mathbf{\Pi}) = \omega_1 \Gamma^{\text{vol}}(\mathbf{\Pi}) - \omega_2 \Delta + \sum_{y=1}^{\mathsf{Y}} \lambda^y \Big\{ \Gamma_y^{\text{arb}}(\mathbf{\Pi}) + \Gamma_y^{\text{loss}}(\mathbf{\Pi}) + \Gamma_y^{\text{res}}(\mathbf{\Pi}) \Big\}, \tag{3.37}$$

where $\omega_1, \omega_2 > 0$ are two regularization factors and Δ is an auxiliary variable used for shaving the peak load as will be explained shortly (see (3.43)). Also, $0 < \lambda < 1$ is the discount factor. If the interest rate is int and a uniform inflation rate of inf is assumed for the energy price and the interruption cost, then $\lambda = (1 + \mathsf{inf})/(1 + \mathsf{int})$. The regularization parameters ω_1 and ω_2 will be tuned based on simulations to yield the best trade-off between the investment cost and the economic gain of the DSS. Note that based on the formulations presented in Sec. 3.2, $\Gamma'(\mathbf{\Pi})$ is concave in $\mathbf{\Pi}$.

In order to formulate the investment cost of the DSS, let $\mathbf{b} = [b_2, b_3, \ldots, b_N]'$ be the capacity of the installed storage units in kWh. Also, let κ_1 \$/kWh be the unit cost of the DSS technology used and κ_2 \$/kW be the associated power electronics and O&M costs. Then, the initial investment cost of DSS in the system is equal to $\kappa_1 \mathbf{1}'\mathbf{b} + \kappa_2 \mathbf{1}'\mathbf{r}$, where $\mathbf{r} = [r_2, r_3, \ldots, r_n]'$ is the vector of rated powers of the storage units. Now, assume that the planning horizon is greater than the lifetime of the DSS with a factor of K, i.e., $\mathsf{Y} = \mathsf{K} \times \mathsf{Y}_{\text{DSS}}$, where Y_{DSS} is the DSS lifetime in years. Then, the storage units need to be replaced in the system K times. Therefore, the

discounted investment cost of storage units will be given by:

$$\Omega(\mathbf{b}, \mathbf{r}) = \left(\kappa_1 \sum_{\mathsf{k}=0}^{\mathsf{K}-1} \lambda^{\mathsf{k}\mathsf{Y}_{\mathrm{DSS}}} \right) \times \mathbf{1}'\mathbf{b} + \kappa_2 \mathbf{1}'\mathbf{r}. \tag{3.38}$$

Observe from (3.38) that $\Omega(\mathbf{b}, \mathbf{r})$ is linear in $\mathbf{b}$ and $\mathbf{r}$.

The optimal DSS planning aiming at maximizing the economic gain minus the investment cost can now be cast as the following optimization problem:

$$\max_{\mathbf{b},\mathbf{r},\mathbf{\Pi}} \ \Gamma'(\mathbf{\Pi}) - \Omega(\mathbf{b}, \mathbf{r}) \tag{3.39}$$

subject to a series of constraints as follows.

- *The power rating of the storage units.* The absorbed and injected power by the storage units is limited by the inverter's power rating, that is:

$$\mathbf{0} \leq \mathbf{p}_{s,h}^{\mathrm{DSS}} \leq \mathbf{r}, \qquad \forall s, h. \tag{3.40}$$

- *The charging/discharging capacity of the storage units.*

  Let γ_{DOD} be the Depth of Discharge (DOD) of the storage units. The parameter γ_{DOD} along with β_{ch} and β_{dis} determines how much energy is needed to charge a storage unit of a given capacity during off-peak hours. The first time that a storage unit of size b_n is connected to node n, a total energy of $(1-\gamma_{\mathrm{DOD}})b_n$ kWh is absorbed which remains in the unit and never discharges. Next, an amount of up to $\gamma_{\mathrm{DOD}} b_n$ kWh is absorbed from the grid during the next charging cycle. Therefore, for charging cycles (off-peak hours) one can

write:

$$\beta_{ch} \sum_{h \in \mathcal{H}_o} \mathbf{p}_{s,h}^{\text{DSS}} = \gamma_{\text{DOD}} \mathbf{b}, \qquad \forall s. \tag{3.41}$$

Similarly, at peak hours when storage units get discharged, the total energy absorbed by the units during off-peak hours times the discharging efficiency will be equal to the total energy injected to the grid. That is,

$$\begin{aligned} \sum_{h \in \mathcal{H}_p} \mathbf{p}_{s,h}^{\text{DSS}} &= \beta_{dis} \beta_{ch} \sum_{h \in \mathcal{H}_o} \mathbf{p}_{s,h}^{\text{DSS}} \\ &= \beta_{rt} \sum_{h \in \mathcal{H}_o} \mathbf{p}_{s,h}^{\text{DSS}}, \qquad \forall s. \end{aligned} \tag{3.42}$$

Since the values of the charging and discharging powers are assumed to be non-negative in our formulation, the constraints (3.41) and (3.42) require that the charging/discharging power of each node be zero if no storage unit is installed on the node. Also note that our formulation assumes that the storage units are charged during off-peak hours and discharged during peak hours. That is, the charging and discharging pattern of the storage units is only once a day. This assumption ensures a longer lifetime for the storage units and has been made extensively in the literature, see, e.g., [58, 93].

Note that in practice the peak and off-peak hours may differ for different segments of the year. Similarly, the solar radiation pattern may change in different segments. In such cases, the formulations provided in this chapter can be easily modified to optimize the charging and discharging strategies of different segments by considering separate peak and off-peak hours for each segment.

- *The maximum peak load.* The parameter Δ in (3.37) serves to represent the

maximum peak load over peak hours. Hence, the following set of linear constraints has to be added to the optimal DSS placement problem:

$$P_{s,h}^{\text{peak}}(\mathbf{\Pi}) \leq \Delta, \qquad \forall s, h \in \mathcal{H}_p \tag{3.43}$$

where $P_{s,h}^{\text{peak}}(\mathbf{\Pi})$ is defined in (3.36).

- *The allowable capacity of DSS that can be installed on each node.*

  The installed capacity of the DSS for each node has to be non-negative. Due to possible physical limitations, the maximum capacity at each node may also be limited. These constraints can be written as follows:

$$\mathbf{0} \leq \mathbf{b} \leq \mathbf{b}^{\max}, \tag{3.44}$$

  where $\mathbf{b}^{\max}$ is the vector of maximum installable storage capacity in the system.

Once the optimal DSS planning problem (3.39) is solved, the total discounted economic gain of the SGO will be computed as:

$$\Gamma(\mathbf{\Pi}) = \sum_{y=1}^{\mathsf{Y}} \lambda^y \Big\{ \Gamma_y^{\text{arb}}(\mathbf{\Pi}) + \Gamma_y^{\text{loss}}(\mathbf{\Pi}) + \Gamma_y^{\text{res}}(\mathbf{\Pi}) + \Gamma_y^{\text{curt}}(\mathbf{\Pi}) + \Gamma_y^{\text{up}}(\mathbf{\Pi}) \Big\}. \tag{3.45}$$

Note that the explicit formulation of $\Gamma_y^{\text{curt}}(\mathbf{\Pi})$ and $\Gamma_y^{\text{up}}(\mathbf{\Pi})$ in terms of $\mathbf{\Pi}$ is intractable and, hence, the regularized expected discounted gain $\Gamma'(\mathbf{\Pi})$ is considered for optimal DSS planning instead of $\Gamma(\mathbf{\Pi})$.

3.4 Numerical Results

This section provides the numerical results of the optimal DSS planning methodology on a modified version of the distribution test system presented in [90].

3.4.1 The Setting of the Simulations

The modified test system is radial (all tie line switches are open) with four feeders where node 1 is considered as the slack node. For this system, inclined solar cells are considered on 34 randomly selected nodes of the grid. The nodes equipped with solar cells are 3, 4, 6, 8, 10, 13, 17, 19, 20, 22, 23, 30, 31, 32, 33, 35, 36, 37, 40, 44, 45, 46, 49, 51, 53, 55, 57, 58, 61, 62, 63, 65, 67, 68. A total rated power of 1000 kW is considered for the solar cells in this test system. This total rated power is allocated to the solar cell-equipped nodes proportionally to their secondary transformer power rating. Based on the time series of the real data from smart meters and solar cells from July 2009 to December 2010, the total energy provided by the solar cells is calculated to be 7.9% of the total energy demand of the system. In addition, two wind turbines are installed on the nodes 21 and 50 with power ratings of 400 kW and 800 kW, respectively. Based on the time series of demands measured by smart meters and the generation by wind turbines, the total energy provided by the wind turbines turns out to be 29.7% of the total energy demand of the system from July 2009 to December 2010.

In our simulations, the Advanced Metering Infrastructure (AMI) data released by the Commission for Energy Regulation (CER) [98] is utilized to model the loads. The dataset provided by CER is from the Electricity Customer Behaviour Trail study and has been collected from 5000 smart meters in Ireland from July 14, 2009 to December 31, 2010. This dataset was received by the author from Irish Social Science Data Archive (ISSDA) [99]. The reactive power demands are modeled by assuming

a constant power factor for the nodes. A growth of 5% [50] in the demands of the nodes is considered over the planning horizon. The time series of wind generation and solar generation are obtained from [100] and [101], respectively.

The type of DSS used is Lead-Acid (LA) due to its lower installation and replacement costs [102]. The DSS are assumed to come in 100 kW-100 kWh units with charging and discharging efficiency of $\beta_{ch} = \beta_{dis} = 0.85$. The DOD of the storage units is assumed to be $\gamma_{\text{DOD}} = 0.75$. The DSS costs are 305 \$/kWh for storage units and replacements, 175 \$/kW for the inverter, and 15 \$/kW for annual maintenance. The planning horizon is assumed to be twice as the lifetime of the DSS and each year is divided into 12 segments. The maximum installable storage unit on each node is considered to be 500 kWh.

The price of energy is considered to be 8.29 ¢/kWh for off-peak hours and 12.43 ¢/kWh for peak hours. The interest rate and the inflation rates are assumed 5% and 1%, respectively. Also, μ is considered 15 \$/kWh based on the survey reported in [97] and SAIFI is 1.5. These values are typical values but in practice may be different for different cases.

The system upgrade includes upgrading the distribution system feeders and substation. In addition, similarly to [32], it is assumed that a 20 km transmission line between the distribution substation and the HV/MV primary substation needs to be upgraded too. An average length of 150 meters per branch is assumed for the distribution feeders in accordance with the IEEE distribution test systems [103]. The upgrade costs of lines, feeders and substations are obtained from [104].

The simulations are conducted using MATPOWER [105] and the optimization problems are solved using the package CVX: Software for Disciplined Convex Programming, version 2.1 [106] bundled with Mosek, version 7.1.

3.4.2 Results

The optimal DSS planning methodology on the system under study results in the installation of a storage unit of size 200 kWh with an inverter power rating of 100 kW. The optimal location of this unit is node 29 which is on feeder 2. Fig. 3.3 illustrates the test system under study with the optimal location of the storage unit. The locations of the two wind turbines are also shown in Fig. 3.3. In this figure, the nodes equipped with solar cells are indicated with shadow.

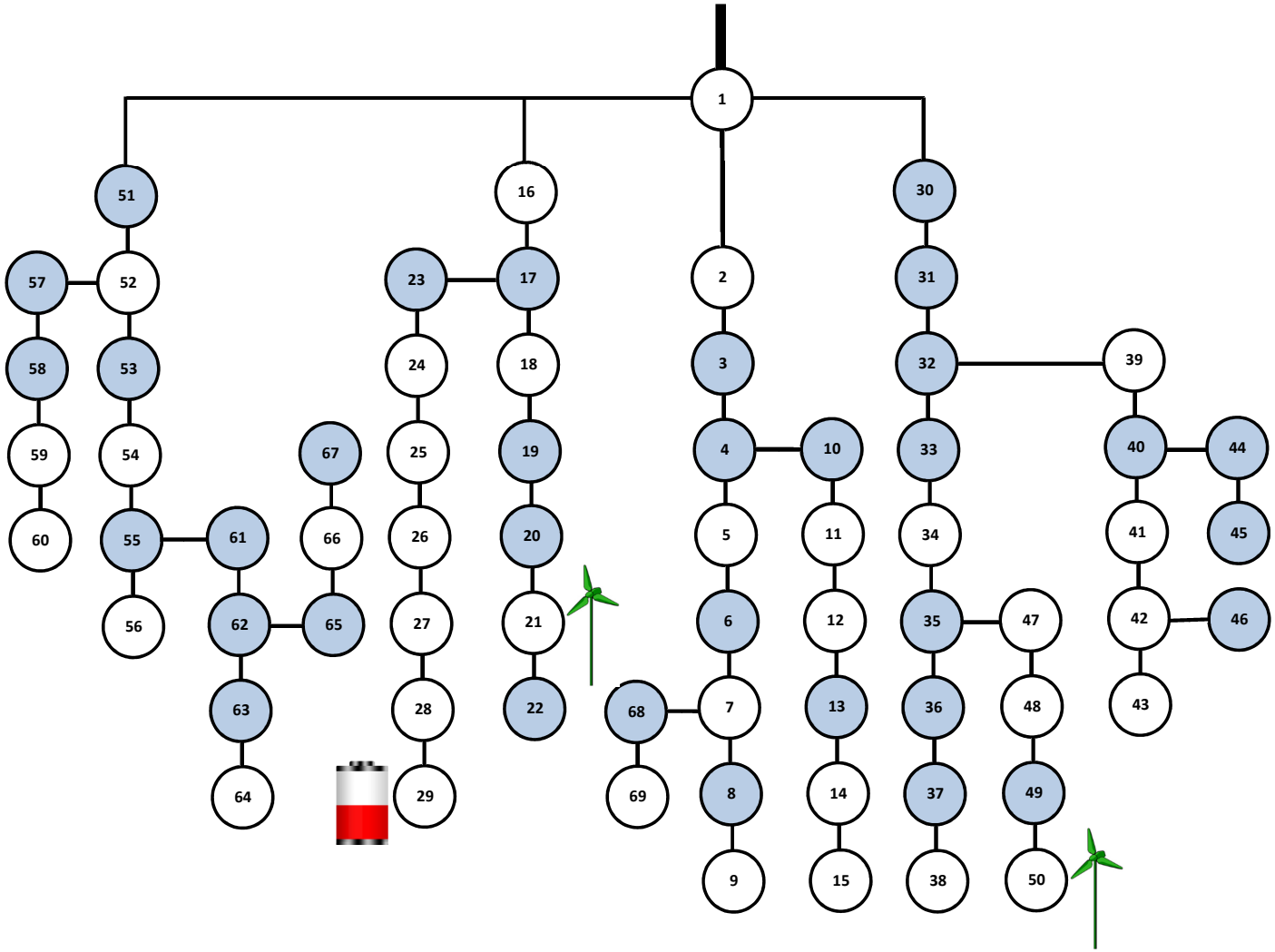

Figure 3.3: The modified test system with wind turbines and solar cells and the storage unit optimally located on node 29.

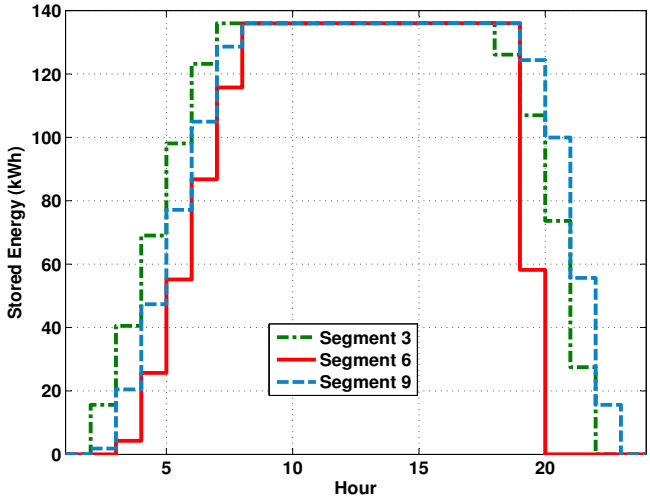

Figure 3.4: The optimal charging and discharging strategy of the installed storage unit for three different segments of the year.

Fig. 3.4 depicts the optimal charging and discharging strategy of the storage unit for three different segments of the year. Note that the optimal charging and discharging pattern in Fig. 3.4 shows the energy stored in the unit in addition to the amount that is always there due to DoD.

The total investment cost for this storage unit will be $\$141,310$ which includes the following:

- Initial investment cost: $\$78,500$
- Replacement cost: $\$43,006$
- Total discounted maintenance cost: $\$19,804$

With the optimal DSS placement in the system, the SGO is expected to obtain the following gains during the entire planning horizon:

- Expected discounted arbitrage gain: $\$6,135$
- Expected discounted gain due to reduction in the system losses: $\$1,946$

- Expected discounted economic value of system resilience enhancement: $\$25,038$
- Expected discounted gain due to reduction in the renewable energy curtailment: $\$235$
- Total economic gain due to deferring the upgrade of the system: $\$193,540$

The gain in the deferral of the system upgrade comes from a gain of $\$31,290$ in feeder 2 upgrade deferral, a gain of $\$133,500$ in the transmission line upgrade deferral, and a gain of $\$28,750$ in the substation upgrade deferral. Based on these numbers, the total discounted gain that the SGO obtains due to installation of DSS will be $\$226,894$. Given that the total investment and maintenance cost of DSS installation is $\$141,310$, we conclude that energy storage in this system results in a total discounted saving of $\$85,584$.

It is worth mentioning that the proposed DSS placement routine found a single storage unit to be installed in this test system. The reason why the optimal solution in this system consists of just one store unit is because of the integrality of the capacity and power rating of the units. If the integrality constraint is relaxed in the problem formulation, the optimal solution will be different. Nonetheless, for practical applications, the storage units are expected to come in predefined sizes and the integrality constraint should be preserved.

We finish this chapter by emphasizing that a detailed and case-specific analysis should be carried out to evaluate the actual economic gain of DSS in any distribution system. The test system studied in this chapter represents a case in which DSS installation is an economically justified investment for the SGO. However, depending on how close the system is to requiring an upgrade, the situation may change, possibly rendering the DSS installation uneconomical. Nonetheless, the trade-off between investment costs and the return the SGO obtains is expected to change in

the future in favor of DSS. That is because as more companies enter the bluishness and energy storage efficiency improves, the cost of storing energy per kWh reduces.

3.5 Conclusion

This chapter presented a methodology for optimal planning of DSS in smart distribution grids. The problem of optimizing the expected economic gain of the system operator was formulated as a mixed-integer convex program. In particular, the optimal planning problem incorporated the arbitrage gain, the reduction in the active power loss, the reduction in the non-dispatchable energy curtailment, the improvement in the system resilience, and the financial gain due to deferring the system upgrade to future years. Numerical results using real data of smart meters and renewable energy sources on a typical distribution system was presented which demonstrated the effectiveness of using DSS in future smart grids.

Chapter 4

Volt-VAR Optimization in Active Smart Grids

Due to the high variability of non-dispatchable energy sources in active smart grids, the Volt-VAR Optimization (VVO) problem will be a very important operational task of the SGO. Fig. 4.1 illustrates the schematic of an active smart grid with various equipment that can be used for VVO, including DSS, capacitor banks, ULTCs, and feeder reconfiguration.

This chapter presents a comprehensive formulation of the VVO problem in active smart grids considering wind turbines, DSS, capacitor banks, ULTCs, and feeder

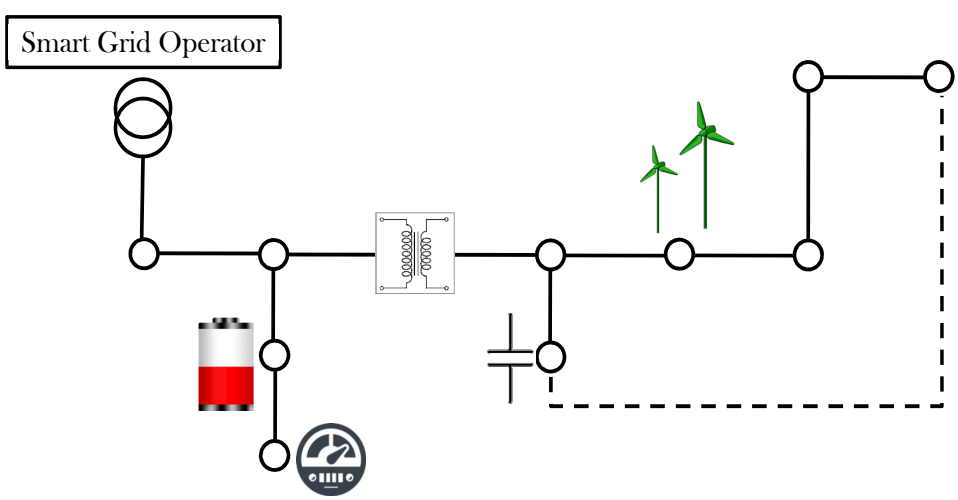

Figure 4.1: Schematic of an active smart grid with distributed wind turbines and various VVO equipment.

reconfiguration [107]. The VVO problem is formulated as a mixed-integer, quadratic program to be solved using branch-and-bound methods. In order to formulate the expected power loss of the system, the stochasticity of the wind power generation is addressed using a first-order Markov Chain (MC) model [77]. Simulation results on a 33-node, 12.66 kV reconfigurable smart grid using real data from wind turbines and smart meters are presented and discussed. Various test cases are considered in the simulations to compare the impact of different VVO equipment on the system loss and voltage profile.

The load model considered in this chapter is a constant load model. Although the VVO problem is related to the voltage-dependence of the loads, in many cases this information is not available to the system operator. As an approximation, the use of a constant load model enables us to formulate the problem of VVO as a mixed-integer, quadratic program which can be solved efficiently using existing softwares.

This chapter is organized as follows. Sec. 4.1 provides some preliminaries about the power flow equations in radial distribution systems as well as an MC model for wind power generation. Sec. 4.2 presents the formulation of the VVO problem considering DSS, capacitor banks, ULTCs, and network reconfiguration. Sec. 4.3 provides the numerical results on a reconfigurable test system and by using real data from smart meters and wind turbines. Finally, Sec. 4.4 concludes the chapter.

4.1 Preliminaries

This section reviews the DistFlow equations of radial distribution systems [8, 81] and extends them to accommodate the DGs and bi-directional flow of power. Also, an MC model for wind power generation based on [77] is reviewed.

Consider a radial distribution system with N nodes and let $v_n = |v_n|e^{j\theta_n}, n =$

$1, 2, \ldots, N$ be the voltage phasor of the nth node, where $j = \sqrt{-1}$. Let $s_n = p_n + jq_n$ denote the complex power demand of a generic node n. Similarly, let $s_n^G = p_n^G + jq_n^G$ be the complex power generation of node n. For any radial configuration of the system, let $\mathcal{L}$ be the set of all lines which connect two nodes of the system together. Note that $\mathcal{L}$ uniquely specifies the configuration of the system and, therefore, we denote the configuration of the system by $\mathcal{L}$. With some abuse of notation, we also use $(n, m) \in \mathcal{L}$ to specify that node n is connected to node m in configuration $\mathcal{L}$. In addition, let $\mathcal{N}_n^{\mathcal{L}}$ be the set of all nodes which are connected to node n via a line in $\mathcal{L}$. Also, let $\mathcal{S}_{\text{sub}}$ be the set of substations in the system.

Throughout the chapter, it is assumed that the renewable sources provide only active power. Likewise, it is assumed that the DSS only store and supply active power, and reactive power demands will be compensated by capacitors as needed. Nevertheless, the formulations can be easily modified to account for the possibility of reactive power injection by DSS. In such a case, an appropriate joint constraint on the active and reactive power injection capability of the DSS should be considered. Such a constraint is non-linear in general but can be easily replaced by a set of approximated linear constrains [58].

4.1.1 DistFlow Equations

Suppose that node n is connected to node m in a radial configuration via line $l \in \mathcal{L}$ with impedance $z_l = r_l + jx_l$. For any instant of time, let $s_{nm} = p_{nm} + jq_{nm}$ be the complex power that flows from node n towards node m. Also, let $s_{mn} = p_{mn} + jq_{mn}$

denote the complex power that flows from node m towards node n. Then we have:

$$\begin{aligned} s_{nm} + s_{mn} &= z_l \frac{|s_{nm}|^2}{|v_n|^2} \\ &= z_l \frac{|s_{mn}|^2}{|v_m|^2} \end{aligned} \tag{4.1}$$

$$v_m = v_n - z_l \frac{s_{nm}^*}{v_n^*}. \tag{4.2}$$

Separating the active and reactive parts in (4.1) and the voltage magnitudes in (4.2), yields:

$$\begin{aligned} p_{nm} + p_{mn} &= r_l \frac{p_{nm}^2 + q_{nm}^2}{|v_n|^2} \\ &= r_l \frac{p_{mn}^2 + q_{mn}^2}{|v_m|^2} \end{aligned} \tag{4.3}$$

$$\begin{aligned} q_{nm} + q_{mn} &= x_l \frac{p_{nm}^2 + q_{nm}^2}{|v_n|^2} \\ &= x_l \frac{p_{mn}^2 + q_{mn}^2}{|v_m|^2} \end{aligned} \tag{4.4}$$

$$|v_m|^2 = |v_n|^2 - 2(r_l p_{nm} + x_l q_{nm}) + (r_l^2 + x_l^2) \frac{p_{nm}^2 + q_{nm}^2}{|v_n|^2}. \tag{4.5}$$

Equations (4.3)-(4.5) together with the following generation-demand equations

$$p_n^G - p_n = \sum_{m \in \mathcal{N}_n^{\mathcal{L}}} p_{nm} \tag{4.6}$$

$$q_n^G - q_n = \sum_{m \in \mathcal{N}_n^{\mathcal{L}}} q_{nm} \tag{4.7}$$

are called the *DistFlow* equations and provide a full AC power flow model for a radial distribution system. Note that these equations are slightly different from the DistFlow equations in [11] and [8] in that they support bi-directional flow of power which is required for radial systems with distributed generations. Accordingly, the active and reactive powers that flow from one node to another can take both positive and negative values.

4.1.2 Markov Chain Model of Wind Power Generation

The wind power generation can be modeled as a first-order homogeneous MC as proposed in [77]. To that end, the range of the power generation by the wind turbine is divided into S intervals, each denoted by a state level $x_i, i = 1, 2, \ldots, S$. Here, x_i is the mean power generated by the wind turbine when the power generation is in the ith interval. Next, a transition probability $0 \leq \theta_{ij} \leq 1$ is assigned to the event that the wind power generation goes from state i at hour h to the state j at hour $h + 1$. These probabilities form the transition probability matrix $\mathbf{T} = [\theta_{ij}]$. The matrix $\mathbf{T}$ is a stochastic matrix satisfying $\mathbf{T1} = \mathbf{1}$, where $\mathbf{1}$ denotes a vector with all elements equal to one.

Let $\boldsymbol{\pi}(h) = [\pi_1(h), \pi_2(h), \ldots, \pi_S(h)]'$ be the state probability vector at hour h. Then, based on the Chapman-Kolmogorov equation, the probability of being in each state at hour $h + \tau$ will be $\boldsymbol{\pi}(h + \tau) = (\mathbf{T}')^{\tau} \boldsymbol{\pi}(h)$. In practice, the realization of the wind power generation is observed at the beginning of the optimization process. Therefore, all the elements of $\boldsymbol{\pi}(0)$ but one are equal to zero. The initial state probability vector $\boldsymbol{\pi}(0)$ is used to obtain subsequent state probability vectors.

The entries of the matrix $\mathbf{T}$ can be estimated from real data using a Maximum-Likelihood (ML) approach. Let $W = (W_1, W_2, \ldots, W_K)$ be the wind MC and $w = (w_1, w_2, \ldots, w_K)$ be the chain of K wind generation samples in the available dataset.

It follows from the Markovianity of W that:

$$\Pr.(W = w) = \Pr.(W_1 = w_1) \times \prod_{k=2}^{K} \Pr.(W_k = w_k, W_{k-1} = w_{k-1}) \tag{4.8}$$

$$= \Pr.(W_1 = w_1) \times \prod_{i=1}^{S} \prod_{j=1}^{S} \theta_{ij}^{n_{ij}}, \tag{4.9}$$

where Pr.() denotes the probability and n_{ij} is the number of times that the MC goes from state i to state j in the available dataset. Based on (4.9), the log-likelihood function can be written as:

$$\log \Pr.(W = w) = \log \Pr.(W_1 = w_1) + \sum_{i=1}^{S} \sum_{j=1}^{S} n_{ij} \log \theta_{ij}. \tag{4.10}$$

Now since we have:

$$\sum_{j} \theta_{ij} = 1, \qquad i = 1, 2, \ldots, S, \tag{4.11}$$

the Lagrangian can be formed as:

$$\mathsf{L}(\mathbf{T}) = \log \Pr.(W_1 = w_1) + \sum_{i=1}^{S} \sum_{j=1}^{S} n_{ij} \log \theta_{ij} - \sum_{i} \lambda_i \left(1 - \sum_{j} \theta_{ij} \right), \tag{4.12}$$

where λ_i is the ith Lagrange multiplier. Taking the derivative with respect to θ_{ij} for each i and setting it equal to zero yields:

$$\frac{n_{i1}}{\theta_{i1}} = \frac{n_{i2}}{\theta_{i2}} = \cdots = \frac{n_{iS}}{\theta_{iS}} = \lambda_i, \qquad i = 1, 2, \ldots, S. \tag{4.13}$$

It follows from (4.13) that θ_{ij} is proportional to n_{ij} for each i, which together with

(4.11), gives the following expression for the ML estimate:

$$\hat{\theta}_{ij} = \frac{n_{ij}}{\sum_j n_{ij}}. \tag{4.14}$$

Remark 4.1 *It is to be noted that for all practical purposes for a day-ahead VVO scheme, one needs to update the look-ahead state probability vectors ever day. That is because the convergence of the state probability vector of the wind MC is very slow. To demonstrate this in a mathematically rigorous way, some background on MCs is briefly provided here. An MC is called* irreducible *if every state i can reach every other state j in a finite amount of time. Intuitively, we expect the wind power MC to be irreducible as starting from any generation state can lead to any other state in a finite amount of time. For an irreducible MC defined on a finite state space, there exits a stationary state probability vector $\boldsymbol{\pi}_\infty$ which is the normalized right eigenvector of $\mathbf{T}'$. In other words, $\boldsymbol{\pi}_\infty$ is the unique solution of the following fixed-point equation:*

$$\boldsymbol{\pi} = \mathbf{T}'\boldsymbol{\pi}, \tag{4.15}$$

$$\mathbf{1}'\boldsymbol{\pi} = 1. \tag{4.16}$$

An MC is called regular *if there exists a fixed amount of time within which every state can reach every other state. Again, intuitively the wind power MC is expected to be regular. In fact, the regularity of the wind MC yields its irreducibility. A regular MC forgets its initial condition geometrically fast in the Second Largest Eigenvalue Modulus (SLEM) of $\mathbf{T}$. The SLEM is also upper-bounded by the Dobrushin coefficient which is defined as:*

$$\mathsf{r} = \frac{1}{2}\max_{i,j}\sum_{l=1}^{S}|\theta_{il} - \theta_{jl}|. \tag{4.17}$$

Based on our dataset of the wind power generation, the SLEM of $\mathbf{T}$ *turns out to be* 0.9766 *which is very close to* 1*. Also,* r *turns out to be equal to* 1 *which renders the Dobrushin upper-bound trivial. Therefore, for small time horizons which are typical for operational optimizations of smart grids, the non-asymptotic state probability vectors need to be computed and used. The stationary probability vector, however, can be used for long horizons that are typical of planning problems.*

Unlike wind power generation, the loads of the system usually have daily patterns that can be forecast with acceptable accuracy based on season, day of the week, time of the day, and weather conditions. Therefore, similarly to [50, 63, 108–110], typical load patterns obtained using smart meter measurements are employed for day-ahead VVO in this research. In particular, the load pattern of each node is simply obtained by computing the average load of the node over a history of a prescribed length, e.g., one month. Once the day-ahead schedule of the system equipments are obtained based on typical load patterns, finer adjustments can be made in real time based on the actual measurements of the loads [108, 111].

4.2 Formulation of the Volt-VAR Optimization Problem

This section formulates the VVO problem in active smart grids considering wind generation, DSS, ULTCs, capacitors, and feeder reconfiguration. Note that the formulation presented here provides a mathematical tool for VVO in smart grids. However, one should be aware that, in practice, the continuous use of tap changers and shunt capacitors increases their maintenance cost.

4.2.1 The Objective Function of the VVO Problem

In this chapter, the objective function of the VVO problem is considered to be the expected active power loss in the system. Based on the DistFlow equations, the total active power loss in the system at hour h is given by:

$$\text{Loss}(h) = \sum_{(n,m)\in\mathcal{L}} r_l \frac{p_{nm}^2(h) + q_{nm}^2(h)}{|v_n(h)|^2}. \tag{4.18}$$

Approximating the nodal voltages by 1 p.u. in the right-hand side of (4.3), the total active power loss in the system at hour h will be given by the following quadratic form:

$$\text{Loss}(h) \approx \sum_{(n,m)\in\mathcal{L}} r_l \left(p_{nm}^2(h) + q_{nm}^2(h)\right). \tag{4.19}$$

The active power loss in the system at each hour is a random variable due to the stochasticity of the wind power generation. Therefore, the VVO problem should try to minimize the expected active power loss in the system as:

$$\min \mathbb{E}\left\{\frac{1}{H}\sum_{h=1}^{H} \text{Loss}(h)\right\}, \tag{4.20}$$

where $\mathbb{E}\{\cdot\}$ is the expectation operator. Also, H is the horizon of the VVO problem which, in the case of a day-ahead approach, equals 24. One can employ the MC model of the wind power generation to compute the expectation in (4.20) as follows:

$$\mathbb{E}\left\{\frac{1}{H}\sum_{h=1}^{H} \text{Loss}(h)\right\} = \frac{1}{H}\sum_{i=1}^{S}\sum_{h=1}^{H} \pi_i(h)\ \text{Loss}(h;i), \tag{4.21}$$

where $\text{Loss}(h;i)$ is the total power loss at hour h assuming that the wind power generation is in the ith state. It is seen from (4.19) and (4.21) that the objective function of the VVO problem is quadratic and convex.

4.2.2 Power Flow Equations, Distributed Storage Systems, Capacitors, and ULTCs

The VVO problem needs to be solved subject to a series of constraints. Below, the constraints corresponding to power flow equations as well as the operation of DSS, capacitors, and ULTCs are formulated.

A full set of AC power flow equations can be described by (4.3)-(4.5) along with the generation-demand equations. To include the charging and discharging strategies of the storage units as well as the reactive power injection of capacitors, the generation-demand equations (4.6)-(4.7) have to be modified as follows:

$$p_n^G(h) - p_n(h) - p_n^{\mathrm{DSS}}(h) = \sum_{m \in \mathcal{N}_n^{\mathcal{L}}} p_{nm}(h), \qquad h \in \mathcal{H}_o,\ \forall n, \tag{4.22}$$

$$p_n^G(h) - p_n(h) + p_n^{\mathrm{DSS}}(h) = \sum_{m \in \mathcal{N}_n^{\mathcal{L}}} p_{nm}(h), \qquad h \in \mathcal{H}_p,\ \forall n, \tag{4.23}$$

$$q_n^G(h) - q_n(h) = \sum_{m \in \mathcal{N}_n^{\mathcal{L}}} q_{nm}(h), \qquad h \in \mathcal{H}_o \cup \mathcal{H}_p,\ \forall n. \tag{4.24}$$

In this formulation, $p_n^{\mathrm{DSS}}(h)$ is the amount of average power that the storage unit installed on node n stores from or supplies to the grid at hour h. Also, $q_n^G(h)$ is the amount of reactive power generation of the capacitor installed on node n at hour h. Moreover, $\mathcal{H}_p$ and $\mathcal{H}_o$ denote the set of peak and off-peak hours, respectively.

The constraints corresponding to the rated power limit of the storage units during charging and discharging periods can be written as:

$$\mathbf{0}_N \leq \mathbf{p}^{\mathrm{DSS}}(h) \leq \mathbf{p}^{\mathrm{DSS},max}, \quad \forall h, \tag{4.25}$$

where $\mathbf{0}_N$ is an all-zero vector of length N. Also,

$$\mathbf{p}^{\text{DSS}}(h) = [p_1^{\text{DSS}}(h), p_2^{\text{DSS}}(h), \ldots, p_N^{\text{DSS}}(h)]'$$

is the vector of power storage and injections of the storage units at hour h, and

$$\mathbf{p}^{\text{DSS},max} = [p_1^{\text{DSS},max}, p_2^{\text{DSS},max}, \ldots, p_N^{\text{DSS},max}]'$$

is the vector of power ratings of the storage units. If a node n is not equipped with a storage unit, then its power rating is set to zero, that is:

$$p_n^{\text{DSS},max} = 0, \quad n \notin \mathcal{S}_{\text{DSS}}, \tag{4.26}$$

where $\mathcal{S}_{\text{DSS}}$ is the set of nodes equipped with DSS.

The constraints corresponding to the capacity of the storage units can be formulated as:

$$\sum_{h \in \mathcal{H}_o} \mathbf{p}^{\text{DSS}}(h) = \frac{\gamma_{\text{DOD}}}{\beta_{ch}} \mathbf{b}, \tag{4.27}$$

$$\sum_{h \in \mathcal{H}_p} \mathbf{p}^{\text{DSS}}(h) = \beta_{dis} \gamma_{\text{DOD}} \mathbf{b}, \tag{4.28}$$

where $\mathbf{b} = [b_1, b_2, \ldots, b_n]'$ in kWh is the vector of DSS capacities installed in the system. If a node n is not equipped with DSS, then $b_n = 0$. Also, γ_{DOD} is the DOD of the storage units and $0 < \beta_{ch} < 1$ and $0 < \beta_{dis} < 1$ are the charging and discharging efficiencies of the DSS technology, respectively. Hence, $\beta_{ch}\beta_{dis}$ is the round-trip efficiency of the storage units. The derivation of (4.27) and (4.28) is provided in Sec. 3.3.

The shunt capacitors can inject reactive power into the feeder. This reactive

power is modeled as:

$$q_n^G(h) = c_n(h) q_n^{cap}, \qquad n \in \mathcal{S}_{\text{cap}}, \tag{4.29}$$

$$c_n(h) \in \{0, 1, 2, \ldots, c_n^{max}\}, \qquad \forall h. \tag{4.30}$$

where q_n^{cap} is the reactive power injection by a unit module of the capacitor bank installed on node n and $c_n(h)$ is the number of modules connected at hour h. Also, $\mathcal{S}_{\text{cap}}$ is the set of nodes equipped with a shunt capacitor and c_n^{max} is the maximum number of modules available in the capacitor bank installed on node n.

A ULTC that is installed on the branch connecting node n to node m with branch impedance of z_l can be modeled as follows [72, 112]. An ideal transformer is modeled between node n and an auxiliary node m', in series with the impedance z_l between node m' and node m. Therefore, the ULTC operation can be formulated as:

$$|v_m|^2 = |v_{m'}|^2 - 2(r_l p_{m'm} + x_l q_{m'm}) + (r_l^2 + x_l^2) \frac{p_{m'm}^2 + q_{m'm}^2}{|v_{m'}|^2}. \tag{4.31}$$

$$|v_{m'}(h)| = (1 + \gamma\delta)|v_n(h)|, \tag{4.32}$$

where γ is the ULTC tap position and δ is the tap step size. For instance, if the transformer ratio is between $1 - a$ and $1 + a$ with step size δ, then

$$\gamma \in \left\{ \gamma_i = i \middle| i = -\frac{a}{\delta}, -\frac{a}{\delta} + 1, \ldots, \frac{a}{\delta} - 1, \frac{a}{\delta} \right\}. \tag{4.33}$$

For the sake of simplicity, no explicit index has been used for the ULTC tap position and step size to indicate the corresponding node numbers.

Finally, the operational constraints on the nodal voltages and feeder ampacities

should be formulated. The nodal voltages should be bounded as:

$$\mathbf{v}^{min} \leq |\mathbf{v}(h)| \leq \mathbf{v}^{max}, \quad \forall h, \tag{4.34}$$

where $\mathbf{v}(h) = [|v_1(h)|, |v_2(h)|, \ldots, |v_N(h)|]'$ is the vector of nodal voltage magnitudes at hour h. Also,

$$\mathbf{v}^{min} = [v_1^{min}, v_2^{min}, \ldots, v_N^{min}]',$$
$$\mathbf{v}^{max} = [v_1^{max}, v_2^{max}, \ldots, v_N^{max}]',$$

are the vector of minimum and maximum allowable voltage magnitudes, respectively. The limits on feeder ampacities can be written as:

$$p_{nm}^2(h) + q_{nm}^2(h) \leq |s_{nm}^{max}|^2, \ (m,n) \in \mathcal{L}, \ \forall h \tag{4.35}$$

$$p_{mn}^2(h) + q_{mn}^2(h) \leq |s_{nm}^{max}|^2, \ (n,m) \in \mathcal{L}, \ \forall h \tag{4.36}$$

where $|s_{nm}^{max}|$ is the maximum apparent power that can flow in the line which connects node n to node m.

4.2.3 Feeder Reconfiguration

Modern smart grids are equipped with remotely-controllable tie-line switches for topological reconfiguration. This section formulates the role of feeder reconfiguration on the VVO problem. It is assumed that the reconfiguration routine is performed once in 24 hours, i.e., in a day-ahead fashion.

To formulate the constraints corresponding to feeder reconfiguration, the extended formulation of [11] is exploited which accommodates the existence of DGs and bi-directional flow of power. Let $\mathcal{L}_\infty$ be the layout of the network, i.e. the con-

figuration of the system when all the tie-line switches are closed. Denote by $|\mathcal{L}_\infty|$ the cardinality of $\mathcal{L}_\infty$. Define $|\mathcal{L}_\infty|$ binary variables $y_{nm} \in \{0, 1\}$ associated with each line between any two nodes in the final radial configuration as:

$$y_{nm} = \begin{cases} 1, & \text{if node } n \text{ is connected to node } m \\ \\ 0, & \text{otherwise} \end{cases} \tag{4.37}$$

and stack them in $\mathbf{y}$. Using these notations, the constraints corresponding to the reconfiguration routine can be formulated as follows. For any $n \in \{1, 2, \ldots, N\}$, $(n, m) \in \mathcal{L}_\infty$, the generation-demand equations (4.22)-(4.24) in a reconfigurable distribution system should be augmented with the following constraints:

$$-Dy_{nm} \leq p_{nm}(h) \leq Dy_{nm}, \qquad \forall h \tag{4.38}$$

$$-Dy_{nm} \leq q_{nm}(h) \leq Dy_{nm}, \qquad \forall h \tag{4.39}$$

$$-Dy_{nm} \leq p_{mn}(h) \leq Dy_{nm}, \qquad \forall h \tag{4.40}$$

$$-Dy_{nm} \leq q_{mn}(h) \leq Dy_{nm}, \qquad \forall h \tag{4.41}$$

where $D \gg 1$ is a large disjunctive constant.

The radiality constraint can be imposed by requiring that the resulting configuration should be loop-free and connected. As explained in [13], for distribution systems with DGs this can be achieved by introducing a set of fictitious loads on the nodes that can be fed only from the substation. Let k_n be the fictitious load on node n. Also, let k_{nm} be the fictitious power that flows from node n towards node m. Then, the following set of linear constraints are equivalent to the radiality of the

system.

$$\mathbf{1}'\mathbf{y} = N - 1, \tag{4.42}$$

$$k_n = \sum_{m \in \mathcal{N}_n^{\mathcal{L}_\infty}} k_{nm}, \quad \forall n, (n,m) \in \mathcal{L}_\infty, \tag{4.43}$$

$$-Dy_{nm} \leq k_{nm} \leq Dy_{nm}, \tag{4.44}$$

where $\mathbf{1}$ is an all-one vector. Note that it is required to impose the radiality constraint for only one hour. Therefore, k_m and k_{nm} do not depend on h.

In addition, it is possible to limit the number of switching actions during the reconfiguration procedure to prevent excessive costs. Let $\bar{\mathbf{y}}$ denote the status of the switches in the current configuration of the system. Also, let $\boldsymbol{\alpha}$ be an auxiliary vector. Then, the following set of linear constraints limits the number of switching actions to ρ:

$$\mathbf{y} - \bar{\mathbf{y}} \leq \boldsymbol{\alpha}, \tag{4.45}$$

$$\bar{\mathbf{y}} - \mathbf{y} \leq \boldsymbol{\alpha}, \tag{4.46}$$

$$\mathbf{1}'\boldsymbol{\alpha} \leq \rho, \tag{4.47}$$

$$\boldsymbol{\alpha} \leq \mathbf{1}. \tag{4.48}$$

Note that for the system to remain connected, opening one switch requires closing another switch. Therefore, ρ should be an even number in (4.47).

Finally, if a branch of the system is not equipped with remotely controllable switches, its connection is forced to remain unchanged. That is,

$$y_{nm} = \bar{y}_{nm}, \qquad (n,m) \notin \mathcal{S}_{\text{tie}} \tag{4.49}$$

where $\mathcal{S}_{\text{tie}}$ is the set of branches equipped with a remotely controllable switch.

4.2.4 Convexification of the VVO Problem

The VVO problem derived above is non-convex due to some non-linearities in the power flow equations, the multiplication of variables in the right-hand side of (4.32), and the integrality constraints (4.30) and (4.33). However, it is possible to make approximations to the power flow equations [11] to come up with a mixed-integer convex optimization problem. To that end, we will need to consider the square of the voltage magnitudes as independent optimization variables. Also, the multiplication of variables in (4.32) can be replaced by alternative convex constraints as will be discussed next.

Although mixed-integer convex optimization problems are NP-hard, the relaxed version of those problems is convex and, hence, they can often be solved in a reasonable time. In practice, mixed-integer convex programs are solved using a combination of a convex optimization technique and an exhaustive search algorithm, such as branch-and-bound methods. Two main characteristics that makes solving mixed-integer convex programs particularly easier are the following. First, when performing the exhaustive search over integer variables along a tree, some branches of the tree can be shown (through solving a relaxed problem) not to include the optimal solution. Therefore, there is no need to follow those branches. Second, if an optimal solution is found before searching all combinations of the integer variables, it may be possible to prove that this solution is optimal through solving a relaxed problem. This is in contrast with non-convex integer programs, where even if the optimal solution is obtained before searching all the combinations, there is no way to prove that this solution is actually optimal.

To convexify the VVO problem, first, constraint (4.32) is replaced by a series

of linear constraints using the approach presented in [112]. Since the square of the voltage magnitudes are considered as the optimization variables, (4.32) should be written as:

$$|v_{m'}(h)|^2 = (1+\gamma\delta)^2|v_n(h)|^2, \tag{4.50}$$

and

$$(1+\gamma\delta)^2 = 1 + 2\delta\gamma + \delta^2\gamma^2. \tag{4.51}$$

The integer variable γ can be expanded using a series of binary variables $\kappa_i \in \{0,1\}$ as:

$$\gamma = \sum_{i=-\frac{a}{\delta}}^{\frac{a}{\delta}} \kappa_i\gamma_i, \tag{4.52}$$

$$\sum_{i=-\frac{a}{\delta}}^{\frac{a}{\delta}} \kappa_i = 1. \tag{4.53}$$

Similarly,

$$\gamma^2 = \sum_{i=-\frac{a}{\delta}}^{\frac{a}{\delta}} \kappa_i\gamma_i^2. \tag{4.54}$$

Therefore, one can rewrite (4.50) as:

$$|v_{m'}(h)|^2 = |v_n(h)|^2 + 2\delta\sum_i \gamma_i|\tilde{v}_{n,i}(h)|^2 + \delta^2\sum_i \gamma_i^2|\tilde{v}_{n,i}(h)|^2, \tag{4.55}$$

where

$$|\tilde{v}_{n,i}(h)|^2 = \kappa_i|v_n(h)|^2, \quad i = -\frac{a}{\delta},\ldots,\frac{a}{\delta}. \tag{4.56}$$

Constraint (4.55) is linear in $|v_m(h)|^2$, $|v_n(h)|^2$, and the $\frac{2a}{\delta}+1$ variables $|\tilde{v}_{n,i}(h)|^2$. Constraints (4.56) which are multiplications of a binary variable and a bounded continuous variable can each be replaced by the following linear constraints [108,

112]:

$$|v_n(h)|^2 - (1-\kappa_i)(v_2^{max})^2 \leq |\tilde{v}_{n,i}(h)|^2, \tag{4.57}$$

$$|\tilde{v}_{n,i}(h)|^2 \leq |v_n(h)|^2 - (1-\kappa_i)(v_2^{min})^2, \tag{4.58}$$

$$\kappa_i(v_2^{min})^2 \leq |\tilde{v}_{n,i}(h)|^2 \leq \kappa_i(v_2^{max})^2, \tag{4.59}$$

If κ_i is zero, (4.59) forces $|\tilde{v}_{n,i}(h)|^2$ to be zero and (4.57) and (4.58) become redundant (same as voltage magnitude constraints (4.34)). If κ_i is one, (4.57) and (4.58) force $|\tilde{v}_{n,i}(h)|^2$ to be equal to $|v_n(h)|^2$ and (4.59) becomes redundant.

To come up with a mixed-integer convex approximation of the VVO problem, it remains to convexify the power flow equations (4.3)-(4.5). Note that $r_l(p_{nm}^2 + q_{nm}^2)/|v_n|^2$ and $x_l(p_{nm}^2 + q_{nm}^2)/|v_n|^2$ are, respectively, the active and reactive power loss on the line l which connects node n to node m. Therefore, by ignoring the power loss on the lines, the power flow equations (4.3)-(4.4) assume the following linear form:

$$p_{nm}(h) + p_{mn}(h) = 0, \qquad \forall h, (n,m) \in \mathcal{L} \tag{4.60}$$

$$q_{nm}(h) + q_{mn}(h) = 0, \qquad \forall h, (n,m) \in \mathcal{L}. \tag{4.61}$$

Moreover, since r_l and x_l have small values in real distribution systems, one can drop the third term in the right-hand side of (4.5). That is, (4.5) can be approximated with the following constraint:

$$|v_m(h)|^2 = |v_n(h)|^2 - 2\big(r_l p_{nm}(h) + x_l q_{nm}(h)\big), \qquad \forall h, (n,m) \in \mathcal{L}. \tag{4.62}$$

Notice that if $|v_n|^2$ is considered as an independent variable of the optimization then (4.62) is a linear constraint.

The VVO problem (4.20) subject to (4.60)-(4.62), (4.22)-(4.30), (4.34)-(4.36), (4.38)-(4.49), (4.55), and (4.57)-(4.59) is a mixed-integer quadratic problem and optimizes the joint operation of the DSS, shunt capacitors, ULTCs, and remotely controllable reconfiguration switches for power loss minimization.

4.3 Case Studies and Numerical Results

In this section, the presented VVO methodology is tested on an active distribution system and several cases with different VVO equipment availability are compared.

4.3.1 The Setting of the Simulations

The VVO problem for loss minimization is considered for a 33-node, 12.66 kV [89] active distribution system depicted in Fig. 4.2. In Fig. 4.2, the branches equipped with remotely controllable switches are shown with dotted lines. In the presented simulations, the AMI data released by the Commission for Energy Regulation (CER) [98] is utilized to model the loads. The author received this dataset from Irish Social Science Data Archive (ISSDA) [99]. The reactive power demands are modelled by assuming a constant power factor for the nodes. The horizon of the VVO problem is considered to be 24 hours corresponding to a day-ahead scenario.

A wind turbine of a rated power of 1000 kW is installed on node 14. The time series of wind generation is obtained from [100]. The rated capacity of the wind turbine is divided into 10 states for MC modeling. Based on the real data of the wind turbine, the mean power generation in the states (i.e., the state levels) is 53.96 kW, 147.16 kW, 246.9 kW, 347.47 kW, 446.96 kW, 549.96 kW, 648.19 kW, 745.16 kW, 848.05 kW, 948.07 kW, respectively.

Two storage units of capacities 200 kWh and 300 kWh are installed on the nodes 14 and 15, respectively. The power rating of both units is assumed to be 100 kW.

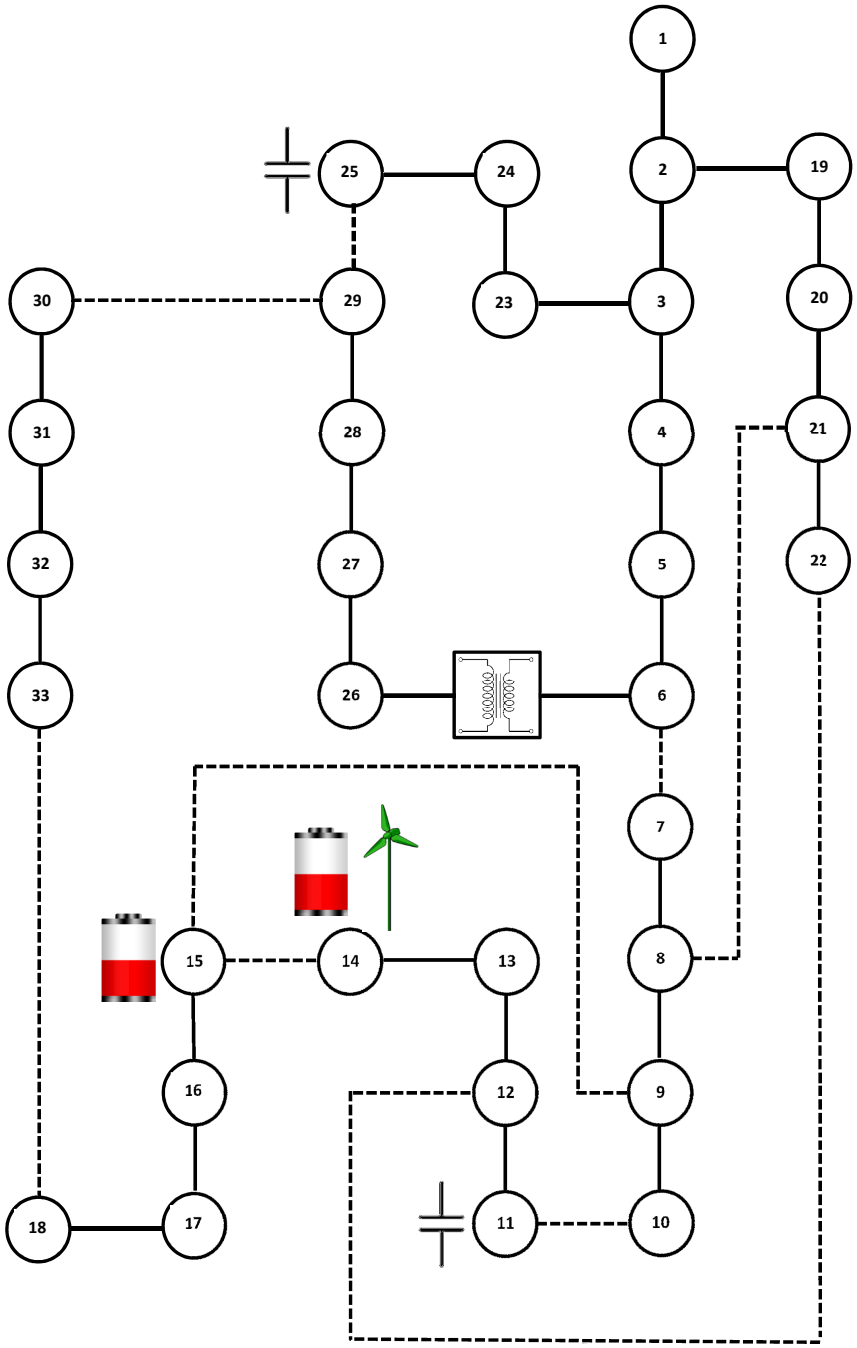

Figure 4.2: The 33-node active smart grid with a wind turbine, DSS, and VVO equipment.

The specifications of the DSS are obtained from [113] and [50] and are as follows. The charging and discharging efficiency of the storage units is $\beta_{ch} = \beta_{dis} = 0.85$. The DOD of the storage units is assumed to be $\gamma_{\text{DOD}} = 0.75$.

Two shunt capacitors are installed on the nodes 11 and 25. The reactive power rating of the the capacitors are assumed to be 400 kvar consisting of 4 modules of size 100 kvar. A ULTC with the ratio in the range of $0.9 \sim 1.1$ and with tap step sizes of 0.01 is installed between nodes 6 and 26. The branches equipped with remotely controllable tie line switches are the normally-open branches $(8, 21)$, $(9, 15)$, $(12, 22)$, $(18, 33)$, $(25, 29)$ as well as branches $(6, 7)$, $(10, 11)$, $(14, 15)$, $(29, 30)$. The maximum number of switching actions per day is considered to be $\rho = 6$ which is equivalent to opening 3 switches and closing 3 other switches. The minimum and maximum voltage limits for all nodes is considered to be 0.94 p.u. and 1.06 p.u., respectively. The disjunctive parameter considered for the reconfiguration routine is equal to 100.

The VVO technique presented in the chapter is conducted on the system under study for $N_{\text{day}} = 30$ days and the average results are reported. Typical load patterns obtained by averaging over a history of one month are used for optimization. Also, the MC model of the wind power generation is used during the optimization. Once the optimized operation of the VVO equipment is obtained, the system is tested with the actual loads and wind power generation of the next day to compute the nodal voltages and the active power losses. In addition to the average active power loss of the system, four more metrics of quality are also reported. These metrics are the average peak load of the system, the average minimum voltage in the feeder, the average maximum voltage in the feeder, and the average voltage spread in the feeder. The average voltage spread in the feeder is computed to measure the voltage

deviation in the system and is defined as:

$$\text{Voltage Spread} = \frac{1}{N_{\text{day}} H} \sum_{i=1}^{N_{\text{day}}} \sum_{h=1}^{H} \left[v_{\max}(h) - v_{\min}(h) \right], \tag{4.63}$$

where

$$v_{\max}(h) = \max_{n} |v_n(h)|, \tag{4.64}$$

$$v_{\min}(h) = \min_{n} |v_n(h)|. \tag{4.65}$$

All simulations are done using MATPOWER [105] and the optimization problems are solved using the package CVX: Software for Disciplined Convex Programming, version 2.1 [106] bundled with Mosek, version 7.1.

4.3.2 Results

As explained in Sec. 4.1, a linearized version of DistFlow equations is employed in this chapter which allows for bi-directional flow of power in a radial system. To first examine the accuracy of the linearized DistFlow equations, a study is conducted on the system. Unlike the VVO optimization procedure, it is assumed in this study that the actual load and wind power generation is available for solving the power flow equations. This study in conducted in the default configuration of the system without shunt capacitors and DSS. The position of the ULTC is fixed at a ratio of 1.05. The simulations are done for 30 days, 24 hour each, and the results are compared with that of the Newton's AC power flow method. The results of this study show that the average difference in the voltage magnitudes between the linearized extended DistFlow equations and the Newton's method is 3.35×10^{-4} p.u.. Moreover, the average maximum nodal error of the linearized extended DistFlow equations turns out to be 5.36×10^{-4} p.u.. Also, the average error and the average

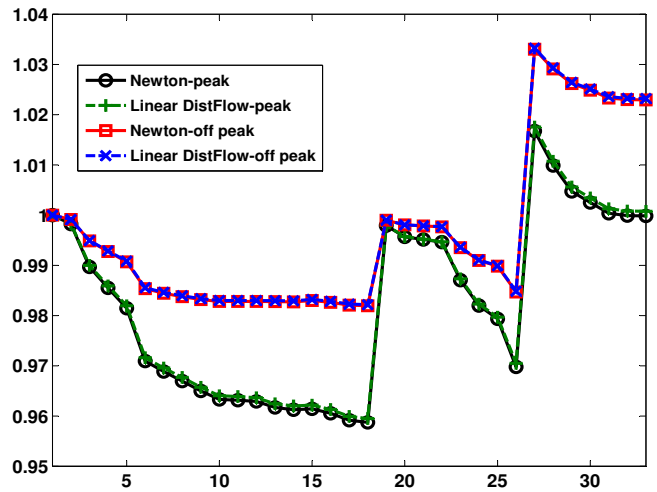

Figure 4.3: Voltage profile of the system on a typical day at a peak and an off-peak hour. Newton's AC power flow versus linearized extended DistFlow equations.

maximum error under peak load are 5.39×10^{-4} p.u. and 8.55×10^{-4} p.u., respectively. In addition, the average error in the active power loss computed using the linearized DistFlow equations turns out to be 1.56 kW or 3.3%. Fig. 4.3. depicts the voltage profile of the system for a typical day and for a peak and an off-peak hour. The figure contrasts the voltage profile obtained by the linearized extended DistFlow equations and that of the Newton's method.

Table 4.1 presents the performance of the optimal VVO solution obtained under various case studies. In particular, 9 cases, including a default test case, are simulated. The default test case corresponds to the test system without any VVO equipment while the remaining 8 cases have different VVO equipment. Specifically, the following list of VVO equipment is considered for the test cases studied:

- Case 1: ULTC
- Case 2: Reconfiguration switches
- Case 3: Capacitors

- Case 4: Capacitors and storage units
- Case 5: ULTC and reconfiguration switches
- Case 6: ULTC, reconfiguration switches, and storage units
- Case 7: ULTC, reconfiguration switches, and capacitors
- Case 8: ULTC, reconfiguration switches, capacitors, and storage units

Also included in Table 4.1 is the differences between the optimized system compared with the default test system in terms of the five metrics of quality. A negative sign in the row of comparisons indicates that optimizing the objective function (i.e., expected active power losses) in the system worsens that particular metric of quality.

Table 4.1: Performance of the Optimal VVO Solution Under Different Settings

	Losses		Peak Load		Minimum Voltage		Maximum Voltage		Voltage Spread	
	Value (kW)	Reduced by (%)	Value (kW)	Reduced by (%)	Value (p.u.)	Increased by (p.u.)	Value (p.u.)	Reduced by (p.u.)	Value (p.u.)	Reduced by (p.u.)
Default	37.94	-	2.256	-	0.951	-	1	-	0.036	-
Case 1	37.29	1.72	2.255	0.05	0.955	0.004	1.031	−0.031	0.047	−0.011
Case 2	31.30	17.51	2.241	0.64	0.958	0.007	1.001	−0.001	0.030	0.006
Case 3	30.47	19.69	2.241	0.64	0.953	0.002	1.002	−0.002	0.032	0.004
Case 4	30.15	20.52	2.169	3.85	0.954	0.003	1.001	−0.001	0.031	0.005
Case 5	30.66	19.19	2.240	0.69	0.967	0.016	1.033	−0.033	0.046	−0.010
Case 6	30.55	19.47	2.174	3.61	0.969	0.018	1.027	−0.027	0.040	−0.004
Case 7	26.97	28.91	2.233	1	0.975	0.024	1.033	−0.033	0.041	−0.005
Case 8	25.69	32.27	2.165	4.02	0.966	0.015	1.007	−0.007	0.023	0.013

Table 4.1 suggests that optimal capacitor switching and feeder reconfiguration can result in maximal improvements in the active power loss of the system. The results also show that optimal control of DSS marginally improves on the system losses as it decreases the peak load in the system. While feeder reconfiguration and optimal capacitor control can reduce the peak load of the system, the greatest reduction in the peak load comes from optimal DSS scheduling. In terms of minimum voltage of the feeder, the table shows that feeder reconfiguration in conjunction with ULTC can play a very important role. This impact on increasing the minimum voltage of the feeder becomes more significant if shunt capacitors are also employed for VVO in the system. Although the improvement in the minimum voltage reduces if all the equipment in the system are jointly controlled for power loss minimization, the average maximum voltage and the voltage spread improve significantly in return. Particularly, if reconfiguration switches, the ULTC, and shunt capacitors are jointly controlled in the system, the voltage spread in the feeder is 0.041 p.u.. If the storage units are also employed for VVO, the voltage spread reduces to 0.013 p.u. which is in agreement with a much better maximum voltage in this case. All in all, we conclude that the DSS can improve the peak load and the voltage profile of the system significantly.

To visualize the results presented in Table 4.1, different performance metrics are illustrated in the following figures. Fig. 4.4 presents the reduction in the active power losses in percentage points, Fig. 4.5 shows the reduction in the peak load in percentage points, Fig. 4.6 illustrates the increase in the minimum voltage of the system in p.u., Fig. 4.7 depicts the decrease in the maximum voltage of the system in p.u., and Fig. 4.8 shows the decrease in the maximum voltage of the system in p.u..

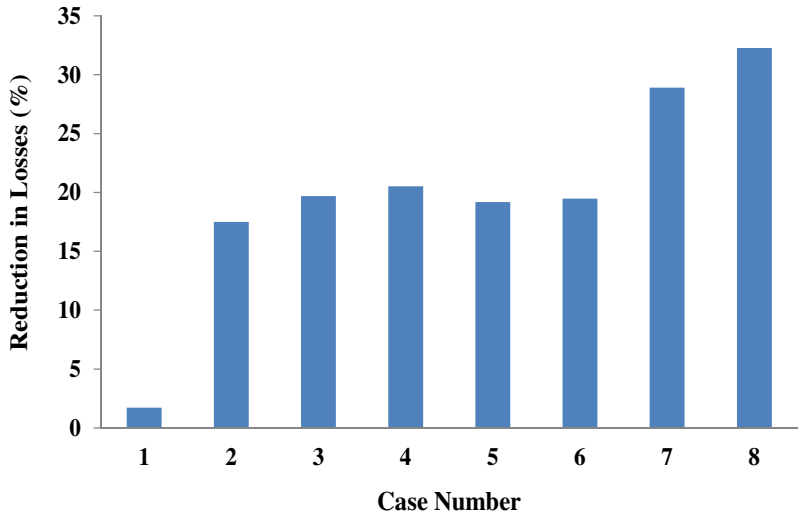

Figure 4.4: The reduction in active power losses (%) after optimal VVO for various test cases.

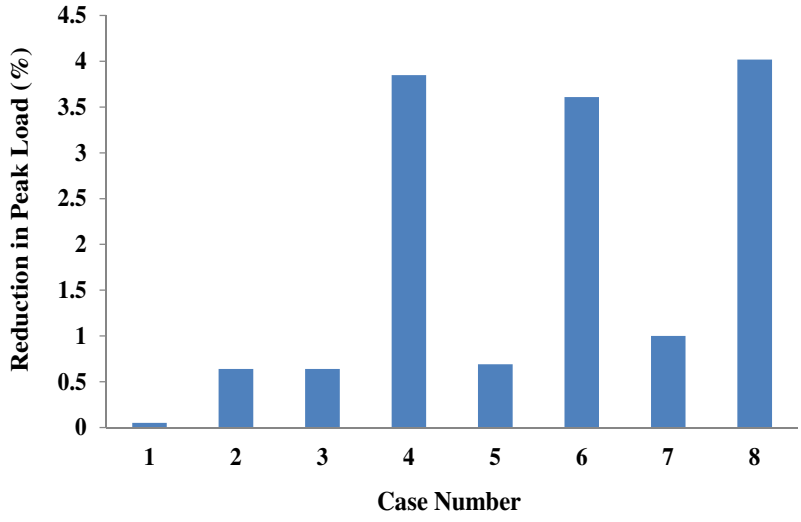

Figure 4.5: The reduction in the peak load (%) after optimal VVO for various test cases.

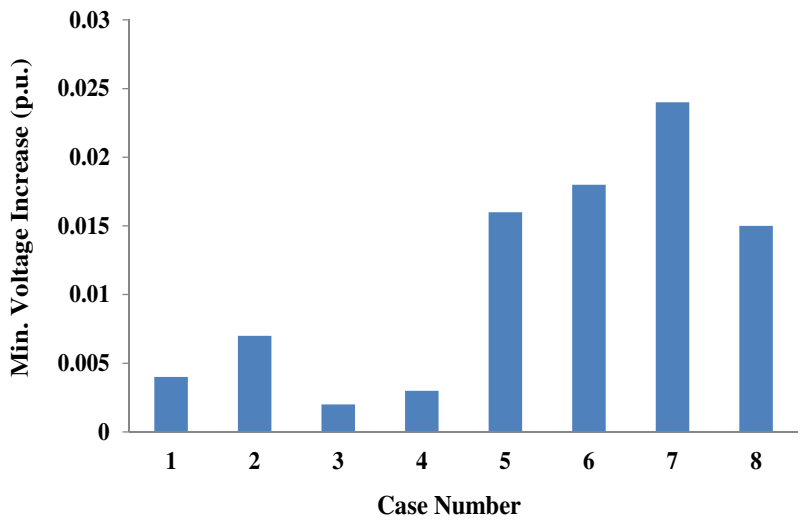

Figure 4.6: The increase in the minimum voltage of the system (p.u.) after optimal VVO for various test cases.

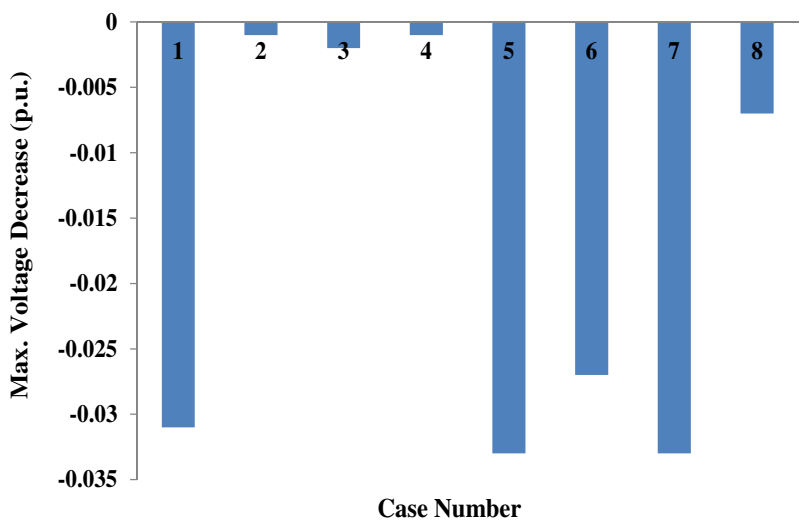

Figure 4.7: The decrease in the maximum voltage of the system (p.u.) after optimal VVO for various test cases.

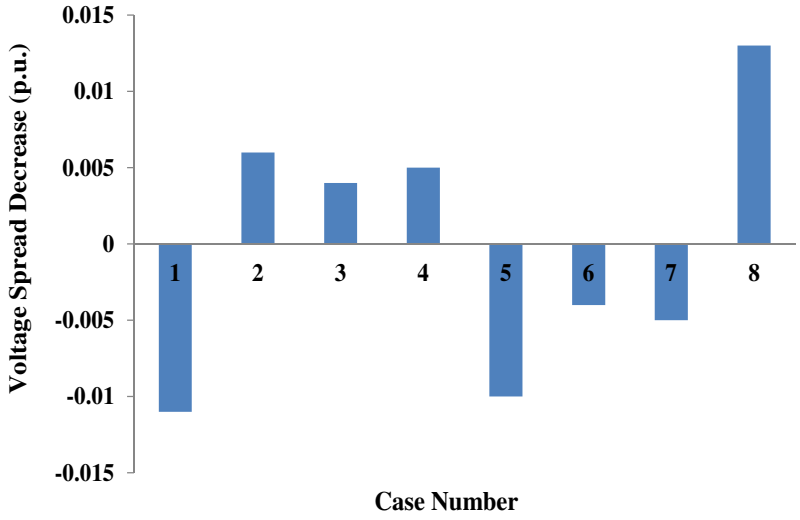

Figure 4.8: The decrease in the voltage spread of the system (p.u.) after optimal VVO for various test cases.

Fig. 4.9 illustrates the voltage profile of the system under peak load of a typical day. Two test cases have been removed from the figure to make other curves more visible. Clearly, use of any VVO equipment in a day-ahead fashion has resulted in an improved voltage profile. Also, as expected, the smoothest voltage profile corresponds to the case where all VVO equipment are jointly operated in an optimal fashion.

4.4 Conclusion

In smart grids with high penetration of renewable energy sources, the voltages of the system are subject to sever fluctuations. This is mostly because of the high variability of non-dispatchable wind generation. Therefore, the operational task of VVO is of great importance in systems with considerable wind power penetration.

In this chapter, the optimal VVO problem aiming at minimizing the expected active power loss was formulated and solved. The VVO problem was formulated

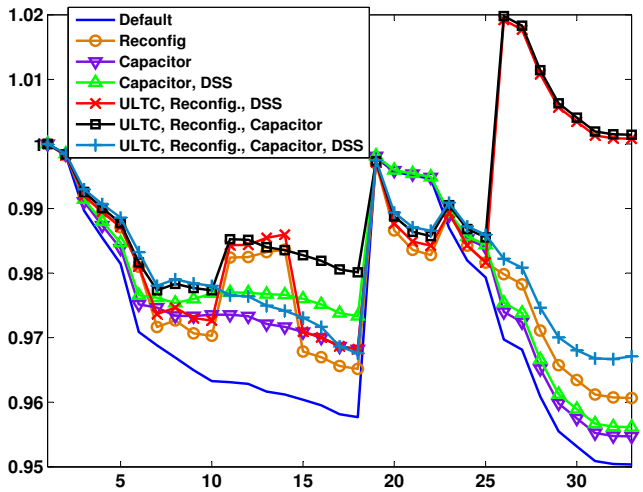

Figure 4.9: Voltage profile of the system under different VVO test cases. The voltage profile is of a typical day at peak hour.

using mixed-integer convex programming to be solved using existing branch-and-bound methods. The methodology presented in the chapter is comprehensive in that it jointly formulates the operation of shunt capacitors, storage units, reconfiguration switches, and ULTCs. The stochasticity of wind power generation was also addressed using a Markov chain model. Numerical results on an active smart grid and using real data from smart meters and wind turbines was presented and discussed. The results indicated the significance of shunt capacitors and feeder reconfiguration in active power loss minimization and the importance of DSS in alleviating the peak load and improving the voltage profile of the system.

Chapter 5

Conclusions and Future Research

This section provides the conclusions and some possible directions for future research about active smart grids.

Smart grids are the next-generation distribution systems that that are more visible due to advanced metering infrastructures and more controllable due to the two-way communication between the SGO and the demand side. The widespread use of renewable energy sources, energy storage systems, and remotely controllable reconfiguration switches will enable the future smart grids to be operated in a much more active fashion. The active nature of smart distribution systems will require a more accurate monitoring and a more sophisticated planning and operation.

In the present thesis, various aspects of active smart grids was studied and mathematical formulations and algorithmic solutions was presented to be used by the SGO. In particular, three major problems was considered which included robust meter placement for state estimation and situational awareness in reconfigurable smart grids, optimal planning of energy storage systems for smart distribution grids, and VVO for active smart grids. The main focus of the thesis was to mathematically formulate different planning and operational problems in such a way that can be solved efficiently for real smart grids. The methodologies presented in the thesis were validated on sample test systems using real data of smart meters and renewable

energy sources.

It was shown in this thesis that the energy storage systems can have considerable impacts on the planning and operation of future smart grids. In fact, the usage of energy storage systems can improve the voltage quality and alleviate the peak load of the system. The peak load alleviation of the distribution systems can in turn allow the system operator to defer the upgrade of the system which readily translates into noticeable financial gains. The peak load of the system can also be further improved by reducing the losses. The reduction in the system losses can be achieved through a VVO scheme which optimally operates the system equipment such as ULTCs, capacitor banks, and reconfiguration switches.

The work presented in this thesis can be extended in various aspects. In what follows we propose a few possible directions for future research about active smart grids.

- It was assumed in this thesis that the location of the DGs are already determined in the system. The joint placement of DGs and DSS in the system can be a topic of future research for systems in which the DGs are yet to be localized.

- A major advantage of storing the energy within the grid is to improve the resilience of the system. To estimate the improvement in the system resilience more accurately, the criticality and the inter-dependence of the of the loads should be taken into account. To model the inter-dependence of the critical loads in the system, the Infrastructure Inter-dependence Simulator (I2Sim) platform [114] can be employed. Therefore, another possible line of research is to integrate the I2Sim platform into the optimal DSS planning procedure. Use of I2Sim also enables the SGO to operate the DSS in the system in such a way that the reliability of critical infrastructure is enhanced.

- In future smart grids, the customers (especially the private owners of critical loads) may be willing to pay more for an improved reliability level. A possible line of research could be to investigate how the cost-benefit trade-off of DSS installation is affected in systems with such reliability-oriented customers. An enabler of such a paradigm can be a customer specific energy pricing in future smart grids.

- A unique feature of smart grids is a two-way communication between the SGO and the grid. It would be interesting to investigate the impact of cyber attacks and communication errors on the real time operation of smart grids. This impact can be sever particularly if the reliability of the critical infrastructure of the system is involved. To that end, the inter-dependence of the energy distribution and the communications sub-systems of the smart grid needs to be modeled.

Bibliography

[1] Nikos Hatziargyriou, Hiroshi Asano, Reza Iravani, and Chris Marnay. Microgrids. *IEEE power and energy magazine*, 5(4):78–94, 2007.

[2] Alberto Borghetti, Carlo Alberto Nucci, Mario Paolone, Gaetano Ciappi, and Aurelio Solari. Synchronized phasors monitoring during the islanding maneuver of an active distribution network. *IEEE Trans. Smart Grid*, 2(1):82–91, 2011.

[3] Mohammad Reza Dorostkar-Ghamsari, Mahmud Fotuhi-Firuzabad, Matti Lehtonen, and Amir Safdarian. Value of distribution network reconfiguration in presence of renewable energy resources. *IEEE Trans. on Power Syst.*, 31(3):1879–1888, 2016.

[4] Shuheng Chen, Weihao Hu, and Zhe Chen. Comprehensive cost minimization in distribution networks using segmented-time feeder reconfiguration and reactive power control of distributed generators. *IEEE Trans. on Power Syst.*, 31(2):983–993, 2016.

[5] Florin Capitanescu, Luis F Ochoa, Harag Margossian, and Nikos D Hatziargyriou. Assessing the potential of network reconfiguration to improve distributed generation hosting capacity in active distribution systems. *IEEE Trans. Power Syst.*, 30(1):346–356, 2015.

[6] Zhechao Li, Saeed Jazebi, and Francisco De Leon. Determination of the opti-

mal switching frequency for distribution system reconfiguration. *IEEE Trans. on Power Delivery, to appear.*

[7] Robert P Broadwater, Asif H Khan, Hesham E Shaalan, and Robert E Lee. Time varying load analysis to reduce distribution losses through reconfiguration. *IEEE Trans. on Power Delivery*, 8(1):294–300, 1993.

[8] Mesut E Baran and Felix F Wu. Network reconfiguration in distribution systems for loss reduction and load balancing. *IEEE Trans. Power Del.*, 4(2):1401–1407, 1989.

[9] Abdollah Kavousi-Fard and Taher Niknam. Optimal distribution feeder reconfiguration for reliability improvement considering uncertainty. *IEEE Trans. Power Del.*, 29(3):1344–1353, 2014.

[10] Adi Botea, Jussi Rintanen, and Debdeep Banerjee. Optimal reconfiguration for supply restoration with informed A* search. *IEEE Trans. Smart Grid*, 3(2):583–593, 2012.

[11] Joshua A Taylor and Franz S Hover. Convex models of distribution system reconfiguration. *IEEE Trans. Power Syst.*, 27(3):1407–1413, 2012.

[12] R Srinivasa Rao, Kumudhini Ravindra, K Satish, and SVL Narasimham. Power loss minimization in distribution system using network reconfiguration in the presence of distributed generation. *IEEE Trans. Power Syst.*, 28(1):317–325, 2013.

[13] Marina Lavorato, John F Franco, Marcos J Rider, and Ruben Romero. Imposing radiality constraints in distribution system optimization problems. *IEEE Trans. Power Syst.*, 27(1):172–180, 2012.

[14] PR Bijwe and Viswanadha GK Raju. Fuzzy distribution power flow for weakly meshed systems. *IEEE Trans. Power Syst.*, 21(4):1645–1652, 2006.

[15] Arturo Losi and Mario Russo. Object-oriented load flow for radial and weakly meshed distribution networks. *IEEE Trans. Power Syst.*, 18(4):1265–1274, 2003.

[16] Catalina Gómez-Quiles, Antonio Gómez-Exposito, and Antonio de la Villa Jaén. State estimation for smart distribution substations. *IEEE Trans. Smart Grid*, 3(2):986–995, 2012.

[17] Ravindra Singh, Bikash C Pal, and Richard B Vinter. Measurement placement in distribution system state estimation. *IEEE Trans. Power Syst.*, 24(2):668–675, 2009.

[18] Ravindra Singh, Bikash C Pal, Rabih A Jabr, and Richard B Vinter. Meter placement for distribution system state estimation: an ordinal optimization approach. *IEEE Trans. Power Syst.*, 26(4):2328–2335, 2011.

[19] Arun G Phadke and John Samuel Thorp. *Synchronized phasor measurements and their applications.* Springer, 2008.

[20] Daniel A Haughton and Gerald Thomas Heydt. A linear state estimation formulation for smart distribution systems. *IEEE Trans. Power Syst.*, 28(2):1187–1195, 2013.

[21] Andrea Carta, Nicola Locci, and Carlo Muscas. GPS-based system for the measurement of synchronized harmonic phasors. *IEEE Trans. Instrum. Meas.*, 58(3):586–593, 2009.

[22] Andrea Carta, Nicola Locci, and Carlo Muscas. A PMU for the measurement

of synchronized harmonic phasors in three-phase distribution networks. *IEEE Trans. Instrum. Meas.*, 58(10):3723–3730, 2009.

[23] J Ren, SS Venkata, and E Sortomme. An accurate synchrophasor based fault location method for emerging distribution systems. *IEEE Trans. Power Del.*, 29(1):297–298, 2014.

[24] Antonio Moreno-Munoz, Victor Pallares-Lopez, Juan Jose Gonzalez de la Rosa, Rafael Real-Calvo, Miguel Gonzalez-Redondo, and Isabel María Moreno-García. Embedding synchronized measurement technology for smart grid development. *IEEE Trans. Ind. Informat.*, 9(1):52–61, 2013.

[25] Yasser Moustafa Atwa and EF El-Saadany. Optimal allocation of ESS in distribution systems with a high penetration of wind energy. *IEEE Trans. Power Syst.*, 25(4):1815–1822, 2010.

[26] Farid Katiraei, Reza Iravani, Nikos Hatziargyriou, and Aris Dimeas. Microgrids management. *IEEE Power and Energy Magazine*, 6(3):54–65, 2008.

[27] J Lopes, CL Moreira, and AG Madureira. Defining control strategies for microgrids islanded operation. *IEEE Trans. Power Syst.*, 21(2):916–924, 2006.

[28] Jong-Yul Kim, Jin-Hong Jeon, Seul-Ki Kim, Changhee Cho, June Ho Park, Hak-Man Kim, and Kee-Young Nam. Cooperative control strategy of energy storage system and microsources for stabilizing the microgrid during islanded operation. *IEEE Trans. Power Electron.*, 25(12):3037–3048, 2010.

[29] Cuong P Nguyen and Alexander J Flueck. Agent based restoration with distributed energy storage support in smart grids. *IEEE Trans. Smart Grid*, 3(2):1029–1038, 2012.

[30] Tao Jiang, Yang Cao, Liang Yu, and Zhiqiang Wang. Load shaping strategy based on energy storage and dynamic pricing in smart grid. *IEEE Trans. Smart Grid*, 5(6):2868–2876, 2014.

[31] Ahmed SA Awad, Tarek HM El-Fouly, and Magdy Salama. Optimal ESS allocation for load management application. *IEEE Trans. on Power Syst.*, 30(1):327–336, 2015.

[32] Alexdandre Oudalov, Daniel Chartouni, Christian Ohler, and G_ Linhofer. Value analysis of battery energy storage applications in power systems. In *Power Systems Conference and Exposition, 2006. PSCE'06. 2006 IEEE PES*, pages 2206–2211. IEEE, 2006.

[33] Konstantina Christakou, Dan-Cristian Tomozei, Maryam Bahramipanah, J-Y Le Boudec, and Mario Paolone. Primary voltage control in active distribution networks via broadcast signals: the case of distributed storage. *IEEE Trans. Smart Grid*, 5(5):2314–2325, 2014.

[34] Pengfei Wang, Daniel H Liang, Jialiang Yi, Pádraig F Lyons, Peter J Davison, and Philip Charles Taylor. Integrating electrical energy storage into coordinated voltage control schemes for distribution networks. *IEEE Trans. Smart Grid*, 5(2):1018–1032, 2014.

[35] Bradford P Roberts and Chet Sandberg. The role of energy storage in development of smart grids. *Proc. IEEE*, 99(6):1139–1144, 2011.

[36] Cody Hill, Matthew Clayton Such, Dongmei Chen, Juan Gonzalez, W Mack Grady, et al. Battery energy storage for enabling integration of distributed solar power generation. *IEEE Trans. Smart Grid*, 3(2):850–857, 2012.

[37] Salman Kahrobaee, Sohrab Asgarpoor, and Wei Qiao. Optimum sizing of distributed generation and storage capacity in smart households. *IEEE Trans. Smart Grid*, 4(4):1791–1801, 2013.

[38] Ali Nourai, Ram Sastry, and Thomas Walker. A vision & strategy for deployment of energy storage in electric utilities. In *Power and Energy Society General Meeting, 2010 IEEE*, pages 1–4. IEEE, 2010.

[39] Sayed Masoud Hashemi, Jacob Ostergaard, and Guangya Yang. A scenario-based approach for energy storage capacity determination in LV grids with high PV penetration. *IEEE Trans. Smart Grid*, 5(3):1514–1522, 2014.

[40] Paolo Attilio Pegoraro and Sara Sulis. Robustness-oriented meter placement for distribution system state estimation in presence of network parameter uncertainty. *IEEE Trans. Instrum. Meas.*, 62(5):954–962, 2013.

[41] Junqi Liu, Junjie Tang, Ferdinanda Ponci, Antonello Monti, Carlo Muscas, and Paolo Attilio Pegoraro. Trade-offs in PMU deployment for state estimation in active distribution grids. *IEEE Trans. Smart Grid*, 3(2):915–924, 2012.

[42] Junqi Liu, Ferdinanda Ponci, Antonello Monti, Carlo Muscas, Paolo Attilio Pegoraro, and Sara Sulis. Optimal meter placement for robust measurement systems in active distribution grids. *IEEE Trans. Instrum. Meas.*, 63(5):1096–1105, 2014.

[43] Gerardo Sánchez-Ayala, Julio Romero Aguerc, David Elizondo, et al. Current trends on applications of PMUs in distribution systems. In *Innovative Smart Grid Technologies (ISGT)*, pages 1–6. IEEE, 2013.

[44] A P Sakis Meliopoulos and Fan Zhang. Multiphase power flow and state esti-

mation for power distribution systems. *IEEE Trans. Power Syst.*, 11(2):939–946, 1996.

[45] Gerald Thomas Heydt. The next generation of power distribution systems. *IEEE Trans. Smart Grid*, 1(3):225–235, 2010.

[46] Marco Pau, Paolo Attilio Pegoraro, and Sara Sulis. Efficient branch-current-based distribution system state estimation including synchronized measurements. *IEEE Trans. Instrum. Meas.*, 62(9):2419–2429, 2013.

[47] R Singh, BC Pal, and RA Jabr. Choice of estimator for distribution system state estimation. *IET Gener. Transmiss. Distrib.*, 3(7):666–678, 2009.

[48] A P Sakis Meliopoulos et al. Smart grid technologies for autonomous operation and control. *IEEE Trans. Smart Grid*, 2(1):1–10, 2011.

[49] Antonio Gómez-Expósito, Ali Abur, Antonio de la Villa Jaén, and Catalina Gómez-Quiles. A multilevel state estimation paradigm for smart grids. *Proc. IEEE*, 99(6):952–976, 2011.

[50] Guido Carpinelli, Gianni Celli, Susanna Mocci, Fabio Mottola, Fabrizio Pilo, and Daniela Proto. Optimal integration of distributed energy storage devices in smart grids. *IEEE Trans. Smart Grid*, 4(2):985–995, 2013.

[51] Christos Thrampoulidis, Subhonmesh Bose, and Babak Hassibi. Optimal placement of distributed energy storage in power networks. *IEEE Trans. on Automatic Control*, 61(2):416–429, 2016.

[52] Mahmoud Ghofrani, A Arabali, M Etezadi-Amoli, and MS Fadali. Energy storage application for performance enhancement of wind integration. *IEEE Trans. on Power Syst.*, 28(4):4803–4811, 2013.

[53] Adarsh Nagarajan and Raja Ayyanar. Design and strategy for the deployment of energy storage systems in a distribution feeder with penetration of renewable resources. *IEEE Trans. on Sustainable Energy*, 6(3):1085–1092, 2015.

[54] Qifeng Li, Raja Ayyanar, and Vijay Vittal. Convex optimization for DES planning and operation in radial distribution systems with high penetration of photovoltaic resources. *IEEE Trans. on Sustainable Energy*, 7(3):985–995, 2016.

[55] Joydeep Mitra. Reliability-based sizing of backup storage. *IEEE Trans. on Power Syst.*, 25(2):1198–1199, 2010.

[56] AF Crossland, D Jones, and NS Wade. Planning the location and rating of distributed energy storage in LV networks using a genetic algorithm with simulated annealing. *International Journal of Electrical Power & Energy Systems*, 59:103–110, 2014.

[57] Jeroen Tant, Frederik Geth, Daan Six, Peter Tant, and Johan Driesen. Multi-objective battery storage to improve PV integration in residential distribution grids. *IEEE Trans. Sustain. Energy*, 4(1):182–191, 2013.

[58] Mostafa Nick, Rachid Cherkaoui, and Mario Paolone. Optimal allocation of dispersed energy storage systems in active distribution networks for energy balance and grid support. *IEEE Trans. Power Syst.*, 29(5):2300–2310, 2014.

[59] Ahmed S Awad, Tarek HM EL-Fouly, Magdy M Salama, et al. Optimal ESS allocation and load shedding for improving distribution system reliability. *IEEE Trans. Smart Grid*, 5(5):2339–2349, 2014.

[60] Mahdi Sedghi, Ali Ahmadian, and Masoud Aliakbar-Golkar. Optimal storage

planning in active distribution network considering uncertainty of wind power distributed generation. *IEEE Trans. Power Syst.*, 31(1):304–316, 2016.

[61] Peng Xiong and Chanan Singh. Optimal planning of storage in power systems integrated with wind power generation. *IEEE Trans. on Sustainable Energy*, 7(1):232–240, 2016.

[62] Ahmed SA Awad, Tarek HM El-Fouly, and Magdy Salama. Optimal ESS allocation for benefit maximization in distribution networks. *IEEE Trans. on Smart Grid, to appear.*

[63] Antonio Padilha-Feltrin, Darwin Alexis Quijano Rodezno, and José Roberto Sanches Mantovani. Volt-VAR multiobjective optimization to peak-load relief and energy efficiency in distribution networks. *IEEE Trans. on Power Delivery*, 30(2):618–626, 2015.

[64] Siddharth Deshmukh, Balasubramaniam Natarajan, and Anil Pahwa. State estimation and voltage/VAR control in distribution network with intermittent measurements. *IEEE Trans. on Smart Grid*, 5(1):200–209, 2014.

[65] Rabih A Jabr and Izudin Džafić. Sensitivity-based discrete coordinate-descent for volt/var control in distribution networks. *IEEE Trans. on Power Syst., to appear*, 2016.

[66] Zhaoyu Wang, Jianhui Wang, Bokan Chen, Miroslav M Begovic, and Yanyi He. MPC-based voltage/var optimization for distribution circuits with distributed generators and exponential load models. *IEEE Trans. on Smart Grid*, 5(5):2412–2420, 2014.

[67] Johanna Barr and Ritwik Majumder. Integration of distributed generation

in the Volt/VAR management system for active distribution networks. *IEEE Trans. on Smart Grid*, 6(2):576–586, 2015.

[68] I Roytelman, BK Wee, and RL Lugtu. Volt/var control algorithm for modern distribution management system. *IEEE Trans. on Power Syst.*, 10(3):1454–1460, 1995.

[69] Siddharth Deshmukh, Balasubramaniam Natarajan, and Anil Pahwa. Voltage/VAR control in distribution networks via reactive power injection through distributed generators. *IEEE Trans. on Smart Grid*, 3(3):1226–1234, 2012.

[70] Taher Niknam, Mohsen Zare, and Jamshid Aghaei. Scenario-based multiobjective volt/var control in distribution networks including renewable energy sources. *IEEE Trans. on Power Delivery*, 27(4):2004–2019, 2012.

[71] Florin Capitanescu, Ilya Bilibin, and Esther Romero Ramos. A comprehensive centralized approach for voltage constraints management in active distribution grid. *IEEE Trans. on Power Syst.*, 29(2):933–942, 2014.

[72] Zhuang Tian, Wenchuan Wu, Boming Zhang, and Anjan Bose. Mixed-integer second-order cone programing model for VAR optimisation and network reconfiguration in active distribution networks. *IET Generation, Transmission & Distribution*, 10(8):1938–1946, 2016.

[73] Pengfei Wang, Daniel H Liang, Jialiang Yi, Pádraig F Lyons, Peter J Davison, and Philip C Taylor. Integrating electrical energy storage into coordinated voltage control schemes for distribution networks. *IEEE Trans. on Smart Grid*, 5(2):1018–1032, 2014.

[74] Qiao Li, Rohit Negi, and Marija D Ilic. Phasor measurement units placement

for power system state estimation: A greedy approach. In *IEEE Power and Energy Society General Meeting 2011*, pages 1–8. IEEE, 2011.

[75] George L Nemhauser, Laurence A Wolsey, and Marshall L Fisher. An analysis of approximations for maximizing submodular set functions-I. *Math. Program.*, 14(1):265–294, 1978.

[76] Andreas Krause, H Brendan McMahan, Carlos Guestrin, and Anupam Gupta. Robust submodular observation selection. *J. Mach. Learn. Res.*, 9(12), 2008.

[77] George Papaefthymiou and Bernd Klockl. MCMC for wind power simulation. *IEEE Trans. on Energy Conversion*, 23(1):234–240, 2008.

[78] Saverio Bolognani and Sandro Zampieri. On the existence and linear approximation of the power flow solution in power distribution networks. *IEEE Trans. on Power Syst.*, 31(1):163–172, 2016.

[79] Ross Baldick. DC power flow in rectangular coordinates. *DIMACS Workshop on Energy Infrastructure: Designing for Stability and Resilience.*

[80] Sairaj V Dhople, Swaroop S Guggilam, and Yu Christine Chen. Linear approximations to AC power flow in rectangular coordinates. *arXiv preprint:1512.06903*, 2015.

[81] Mesut E Baran and Felix F Wu. Optimal sizing of capacitors placed on a radial distribution system. *IEEE Trans. Power Del.*, 4(1):735–743, 1989.

[82] Mohammad Ghasemi Damavandi, Vikram Krishnamurthy, and José R. Martí. Robust meter placement for state estimation in active distribution systems. *IEEE Trans. Smart Grid*, 6(4):1972–1982, July 2015.

[83] Farhad Ghassemi and Vikram Krishnamurthy. Separable approximation for solving the sensor subset selection problem. *IEEE Trans. Aerosp. Electron. Syst.*, 47(1):557–568, 2011.

[84] Ali Abur and Antonio Gomez Exposito. *Power system state estimation: theory and implementation.* CRC Press, 2004.

[85] Uriel Feige. A threshold of $\ln n$ for approximating set cover. *J. ACM (JACM)*, 45(4):634–652, 1998.

[86] Laurence A Wolsey. An analysis of the greedy algorithm for the submodular set covering problem. *Combinatorica*, 2(4):385–393, 1982.

[87] Andreas Krause, Ajit Singh, and Carlos Guestrin. Near-optimal sensor placements in gaussian processes: Theory, efficient algorithms and empirical studies. *J. Mach. Learn. Res.*, 9:235–284, 2008.

[88] *IEEE Standard for Synchrophasor Measurements for Power Systems.* IEEE Std C37.118.1-2011 (Revision of IEEE Std C37.118-2005).

[89] Mesut E Baran and Felix F Wu. Network reconfiguration in distribution systems for loss reduction and load balancing. *IEEE Trans. Power Del.*, 4(2):1401–1407, 1989.

[90] Debapriya Das. A fuzzy multiobjective approach for network reconfiguration of distribution systems. *IEEE Trans. Power Del.*, 21(1):202–209, 2006.

[91] Dong Zhang, Zhengcai Fu, and Liuchun Zhang. An improved TS algorithm for loss-minimum reconfiguration in large-scale distribution systems. *Elect. Power Syst. Res.*, 77(5):685–694, 2007.

[92] Sebastian De la Torre and Francisco D Galiana. On the convexity of the system loss function. *IEEE Trans. Power Syst.*, 20(4):2061–2069, 2005.

[93] Aouss Gabash and Pu Li. Flexible optimal operation of battery storage systems for energy supply networks. *IEEE Trans. Power Syst.*, 28(3):2788–2797, 2013.

[94] Faridaddin Katiraei, Mohammad Reza Iravani, and Peter W Lehn. Microgrid autonomous operation during and subsequent to islanding process. *IEEE Trans. on Power Del.*, 20(1):248–257, 2005.

[95] Robert H Lasseter and Paolo Paigi. Microgrid: a conceptual solution. In *Power Electronics Specialists Conference, 2004. PESC 04. 2004 IEEE 35th Annual*, volume 6, pages 4285–4290. IEEE, 2004.

[96] Amin Khodaei. Resiliency-oriented microgrid optimal scheduling. *IEEE Trans. on Smart Grid*, 5(4):1584–1591, 2014.

[97] Michael Sullivan, Josh Schellenberg, and Marshall Blundell. Updated value of service reliability estimates for electric utility customers in the united states. Technical report, Ernest Orlando Lawrence Berkeley National Laboratory, Berkeley, CA (US), 2015.

[98] Commission for Energy Regulation (CER), Customer Behaviour Trials (CBTs), http://www.cer.ie/electricity-gas/smart-metering/, last visited September 15, 2016.

[99] Irish Social Science Data Archive, CER Smart Metering Project, http://www.ucd.ie/issda/data/commissionforenergyregulationcer/, data received August 12, 2014.

[100] EirGrid, http://www.eirgrid.com/operations/systemperformancedata/, data retrieved April 6, 2015.

[101] Solar Radiation Data, http://www.soda-is.com/eng/services/, data retrieved March 19, 2015.

[102] Piyasak Poonpun, Ward T Jewell, et al. Analysis of the cost per kilowatt hour to store electricity. *IEEE Trans. on Energy Conversion*, 23(2):529–534, 2008.

[103] IEEE PES Distribution System Analysis Subcommittee's Distribution Test Feeder Working Group. Distribution test feeders.

[104] Simon Wong, Kankar Bhattacharya, and J David Fuller. Electric power distribution system design and planning in a deregulated environment. *IET generation, transmission & distribution*, 3(12):1061, 2009.

[105] Ray D Zimmerman. MATPOWER: A MATLAB power system simulation package.

[106] Michael Grant, Stephen Boyd, and Yinyu Ye. CVX: Matlab software for disciplined convex programming, 2008.

[107] Mohammad Ghasemi Damavandi, Vikram Krishnamurthy, and José R. Martí. A comprehensive methodology for Volt-VAR optimization in active smart grids. *arXiv preprint:1609.08697*, 2016.

[108] Hamed Ahmadi, José R Martí, and Hermann W Dommel. A framework for volt-VAR optimization in distribution systems. *IEEE Trans. on Smart Grid*, 6(3):1473–1483, 2015.

[109] Zhaoyu Wang, Hao Chen, Jianhui Wang, and Miroslav Begovic. Inverter-less

hybrid voltage/var control for distribution circuits with photovoltaic generators. *IEEE Trans. on Smart Grid*, 5(6):2718–2728, 2014.

[110] Zechun Hu, Xifan Wang, Haozhong Chen, and GA Taylor. Volt/VAr control in distribution systems using a time-interval based approach. *IEE Proceedings-Generation, Transmission and Distribution*, 150(5):548–554, 2003.

[111] Abheejeet Mohapatra, Pradeep R Bijwe, and Bijaya K Panigrahi. An efficient hybrid approach for volt/var control in distribution systems. *IEEE Trans. on Power Delivery*, 29(4):1780–1788, 2014.

[112] Leonardo H Macedo, John F Franco, Marcos J Rider, and Rubén Romero. Optimal operation of distribution networks considering energy storage devices. *IEEE Trans. on Smart Grid*, 6(6):2825–2836, 2015.

[113] KC Divya and Jacob Østergaard. Battery energy storage technology for power systems- An overview. *Elect. Power Syst. Res.*, 79(4):511–520, 2009.

[114] Hafiz Abdur Rahman, Mazana Armstrong, DeTao Mao, and José R Martí. I2sim: a matrix-partition based framework for critical infrastructure interdependencies simulation. *Electric Power Conference, 2008. EPEC 2008. IEEE Canada*, pages 1–8, 2008.